UNIVERSIDAD COMPLUTENSE DE MADRID

FACULTAD DE CIENCIAS FÍSICAS
Departamento de Astrofísica y Ciencias de la Atmósfera

TESIS DOCTORAL

The Stratospheric ENSO Pathway: flavors and asymmetry

La Vía Estratosférica de ENSO: tipos y asimetría

MEMORIA PARA OPTAR AL GRADO DE DOCTOR
PRESENTADA POR

Maddalen Iza San Juan

Directora
Natalia Calvo Fernández

Madrid, 2017

Agradecimientos

Una etapa se acaba y nuevos caminos se abren, pero la experiencia ganada y lo aprendido durante estos años se quedan.

Ante todo, y sobre todo, gracias Natalia por confiar en mí y en mí trabajo, por apoyarme durante todos estos años y darme ánimos para continuar en los peores momentos. Gracias por todo el trabajo que has hecho para que esta tesis salga adelante.

Elisa, thank you for hosting me in Hamburg so warmly and teaching me so much, every meeting with you was a speed-up lesson! I hope all the work we did together during those stays is reflected in this thesis.

Ricardo, gracias por cuidar de todos nosotros, detectar nuestras flaquezas y aplicarnos el paliativo adecuado. David, tu generosidad es inabarcable, siempre disponible y siempre certero. Me considero afortunada por haber aprendido a vuestro lado.

Gracias también a los demás compañeros del grupo, a aquellos que me ayudasteis en mis tímidos inicios y a aquellos que me habéis conocido y soportado al final. Pero, principalmente, a quien ha recorrido este camino conmigo, gracias Froila por ser la persona que eres, no podría haber tenido mejor compañera de viaje.

Antza denez erabaki garrantzitsuak norberak bere hizkuntzan hartu behar ditu, era berean, esker garrantzitsuenak euskeraz idatzi nahi ditut. Eskerrik asko ama, aita. Lan hau etxean txikitatik ikasitakoaren ondorioa da, ikasteko grina eta lanerako konstantzia. Kattalin, beti ondoan, askotan etortzen zait burura duela urte asko eskritorioan jarri zenuen kartel hura, gogoratzen? Eskerrik asko.

Baita ere eskerrak nere bizitzatik igaro den pertsona garrantzitsuari. Eskerrik asko Xabi, urte guzti horietan zure laguntza ezinbestekoa izan zen, ongi dakizunez zu gabe ez nintzatekeen inoiz honaino iritsiko.

Azkenik, nere ondoan daukaten pertsonari. Gracias Antonio, primero por tu amistad y después por todo el cariño y las interminables conversaciones. Espero que me sigas llevando a la bahía.

En definitiva, gracias a todas aquellas personas que de un modo u otro han dulcificado este, a veces amargo, camino.

Mila esker!

Ama eta aita,
dena eman diguzuelako

Contents

Resumen

Introducción

ENSO (El Niño-Southern Oscillation) es el principal modo de variabilidad interanual en los trópicos y muestra relevantes teleconexiones en los extratrópicos del hemisferio norte (HN) (Horel and Wallace 1981). Durante la fase cálida de ENSO, El Niño, su señal en la troposfera tropical se propaga hacia extratrópicos mediante ondas de Rossby (ej., García-Herrera et al. 2006), propiciando además un aumento de la actividad ascendente de las ondas hacia la estratosfera. (ej., Manzini et al. 2006). En consecuencia, el vórtice polar se debilita y la circulación meridiana media se intensifica generando anomalías cálidas en el polo, que se propagan hacia la troposfera, afectando el clima de las regiones del norte del Atlántico y Europa (NAE) (Ineson and Scaife 2009; Cagnazzo and Manzini 2009; Bell et al. 2009).

Sin embargo, la respuesta estratosférica a un distinto tipo de El Niño, más centrado en el Pacífico (CP) que El Niño canónico en el este del Pacífico (EP), aún no está clara. Estudios previos han mostrado conclusiones contradictorias sobre el parecido de CP El Niño con EP El Niño en el HN y los resultados parecen depender del número de casos analizados y la definición utilizada (Garfinkel et al. 2013). La vía estratosférica para la fase fría de ENSO, La Niña, es también incierta, dado que en los registros observacionales su enfriamiento estratosférico parece ser débil o no significativo (Free and Seidel 2009; Mitchell et al. 2011). Por ello, se cree que La Niña es menos efectiva que El Niño en la respuesta estratosférica (ej., Manzini et al. 2006). De hecho, los patrones El Niño y La Niña no son simétricos en sus anomalías de temperatura superficial del mar (ATSM) (An and Jin 2004), aunque se desconoce si la asimetría en el Pacífico tropical puede ser trasladada a la vía estratosférica. Además, otras fuentes de variabilidad, como los Calentamientos Súbitos

Estratosféricos (CSEs) y la Oscilación Cuasi-Bienal (OCB) interactúan no linealmente con ENSO modulando el vórtice polar.

Objetivos

En esta tesis se pretende:

1. Reevaluar la vía estratosférica de La Niña en el HN en datos de reanálisis. Analizar la sensibilidad de la señal estratosférica de La Niña a las distintas definiciones existentes con distintos umbrales. Explorar la influencia de los CSEs y la OCB en la respuesta estratosférica a La Niña.
2. Reexaminar la señal estratosférica de EP y CP El Niño en el HN y establecer si las respuestas son distinguibles o no, teniendo en cuenta el posible impacto de los CSEs y la posible sensibilidad de la señal de CP El Niño al índice utilizado y el tamaño del composite.
3. Investigar la existencia de una variabilidad en la muestra en la asimetría entre El Niño y La Niña en las ATSM, utilizando un gran número de simulaciones numéricas. Evaluar si la asimetría en el forzamiento de las ATSM es el principal modulador de la asimetría entre El Niño y La Niña en las teleconexiones de la vía estratosférica en el HN.

Datos y Métodos

Para seleccionar los eventos observados de ENSO utilizamos el índice de NCEP/CPC, basado en ERSSTv4, y los datos HadISST. En el estudio de La Niña usamos datos del reanálisis JRA-55 y observaciones de CRU TS 3.21. Para investigar las señales de EP y CP El Niño utilizamos los reanálisis ERA-40 y ERA-Interim. Para analizar la asimetría y la variabilidad de las muestras empleamos un gran ensemble (100 miembros) de simulaciones históricas del modelo MPI-ESM-LR. Los inviernos ENSO se han seleccionado en base a tres regiones, para los dos tipos de El Niño y el único tipo de La Niña. Los inviernos de La Niña se han identificado en la región N34 (5ºN-5ºS, 170ºW-120ºW),

mientras que EP and CP El Niño han sido seleccionados en las regiones N3 (5°N-5°S, 150°W-90°W) y N4 (5ºN-5ºS, 160ºE-150ºW), respectivamente.

Resultados y conclusiones

1. Se ha identificado una vía estratosférica polar para La Niña en el reanálisis, caracterizada por un vórtice polar significativamente frío y asociado a una reducción de la actividad ascendente de las ondas planetarias hacia la estratosfera. Las anomalías significativas en la estratosfera descienden hacia la troposfera y afectan al clima sobre la región NAE. Sin embargo, esta vía estratosférica no se obtiene para inviernos de La Niña débiles, ya que su señal se ve enmascarada por la ocurrencia de CSEs, asociada a fases de la OCB. Por consiguiente, para estudios futuros sugerimos utilizar un umbral relativamente alto para definir La Niña.

2. Además, se han esclarecido las contradictorias señales estratosféricas de EP y CP El Niño, obteniendo resultados robustos independientemente de la definición. Se ha hallado que la ocurrencia de CSEs modula la respuesta estratosférica de CP El Niño: durante inviernos de CP El Niño con CSEs el vórtice está significativamente debilitado, mientras que sin CSEs el vórtice está más fuerte. Del mismo modo, en ausencia de CSEs las señales estratosféricas de EP y CP El Niño son indistinguibles al inicio del invierno. En cambio, sus respuestas son similares durante inviernos con CSEs. Por tanto, para investigar la señal estratosférica de CP El Niño se han de tener en cuenta los CSEs.

3. El análisis de 100 simulaciones históricas ha demostrado la amplia variabilidad en la asimetría de las ATSM. Para EP El Niño y La Niña esta variabilidad gobierna parcialmente la asimetría de las respuestas, pero no para CP El Niño y La Niña. El rango de asimetrías esta modulado por inviernos EP El Niño. La baja asimetría está asociada a EP El Niño débiles y extendidos hacia el oeste, de modo que La Niña domina la asimetría estratosférica, un rasgo no observado hasta la fecha. En cambio, en los miembros de alta asimetría

inviernos fuertes de EP El Niño controlan la asimetría estratosférica. Asimismo, se ha hallado que inviernos EP El Niño y La Niña con ATSM similares dan lugar a anomalías estratosféricas de misma magnitud, pero signo opuesto.

Summary

Introduction

El Niño-Southern Oscillation (ENSO) is the main mode of interannual variability in the tropics and has relevant teleconnections in the North Hemisphere (NH) extratropics (Horel and Wallace 1981). During the warm ENSO phase, El Niño, its tropical tropospheric signal propagates poleward by means of Rossby waves (e.g., García-Herrera et al. 2006), which leads to an increased upward wave activity into the stratosphere (e.g., Manzini et al. 2006). As a consequence, the polar vortex weakens and the mean meridional circulation enhances, with associated polar warm anomalies propagating downwards to the troposphere and impacting the North-Atlantic European (NAE) region climate (Ineson and Scaife 2009; Cagnazzo and Manzini 2009; Bell et al. 2009).

Nonetheless, the stratospheric response to a different El Niño flavor, with the largest anomalies in the Central Pacific (CP) in comparison with the canonical eastern Pacific (EP) El Niño, remains unclear. Contradictory conclusions have been found on the resemblance of CP El Niño with EP El Niño and results seem to depend on the composite size and the definition used (Garfinkel et al. 2013). The stratospheric pathway for the cold ENSO phase, La Niña, is also uncertain, since its stratospheric cooling appears to be weak or non-significant in the observational record (Free and Seidel 2009; Mitchell et al. 2011). Thus, La Niña is believed to be less effective than EP El Niño in its stratospheric response (e.g., Manzini et al. 2006). Indeed, El Niño and La Niña patterns are not symmetric on their sea surface temperature anomalies (SSTA) (An and Jin 2004). However, whether the asymmetry in the tropical Pacific is translated to the stratospheric pathway is an open question. In addition, other sources of variability, such as Stratospheric Sudden Warmings (SSWs) and the

quasi-biennial oscillation (QBO) interact nonlinearly with ENSO on modulating the polar vortex.

Objectives

In this thesis we aim to:

1. Reevaluate the NH La Niña stratospheric pathway in a reanalysis dataset. Analyze the sensitivity of La Niña stratospheric response to different thresholds used to select the events. Explore the influence of SSWs and the QBO on La Niña stratospheric signature.
2. Reexamine EP and CP El Niño NH stratospheric signature and establish whether the responses are distinguishable or not, keeping in mind the possible impact of SSWs and the potential sensitivity of the CP El Niño signal to the index used and composite size.
3. Investigate the existence of sample variability on the asymmetry between El Niño and La Niña in the SSTA, using a large model ensemble. Evaluate if the SSTA forcing asymmetry is a major driver of El Niño and La Niña asymmetry teleconnections on the NH stratospheric pathway.

Data and Methods

To select observed ENSO events, the NCEP/CPC index, based on ERSSTv4, and HadISST data set are used. For La Niña response, we use data from the JRA-55 reanalysis and CRU TS 3.21 observations. To investigate EP and CP El Niño signatures the ERA-40 and ERA-Interim reanalysis are used. To analyze the asymmetry and the sample variability a grand ensemble (100 members) of historical simulations made with the MPI-ESM-LR model are employed. ENSO winters are selected in three regions, for the two El Niño flavors and the unique La Niña type. La Niña winters are identified in the N34 (5ºN-5ºS, 170ºW-120ºW) region, while EP and CP El Niño winters are selected in the N3 (5°N-5°S, 150°W-90°W) and N4 (5ºN-5ºS, 160ºE-150ºW) regions, respectively.

Results and conclusions

1. We identified a polar stratospheric pathway for La Niña in the reanalysis, characterized by a robust cold polar vortex and associated with a reduced upward planetary wave activity into the stratosphere. The significant stratospheric anomalies descend to the troposphere and impact the climate over the NAE region. Nevertheless, this stratospheric pathway is not evident during weak La Niña winters, since their signature is obscured by the occurrence of SSWs, associated with QBO phases. Thereafter, for future studies, we suggest to define La Niña winters with a relatively high threshold.

2. Furthermore, we shed light on EP and CP El Niño stratospheric signatures contradictions, obtaining robust conclusions regardless the definition. We found that SSW occurrence modulates the polar stratospheric response to CP El Niño events: during CP El Niño winters with SSWs a significantly weaker vortex appears, while the vortex is stronger in CP El Niño without SSWs. Accordingly, in the absence of SSWs, CP and EP El Niño stratospheric signatures are distinguishable in early winter. In contrast, EP and CP El Niño responses are similar during winters with SSWs. Therefore, to investigate the stratospheric signatures of CP El Niño winters, the SSW occurrence needs to be considered.

3. Analyzing 100 historical experiments we found large sample variability in the SSTA asymmetry. For EP El Niño and La Niña this variability drives part of the asymmetric responses, but not for CP El Niño and La Niña. The asymmetry range is modulated by EP El Niño winters. Low asymmetry is related to weak, westward extended EP El Niño winters, so the stratospheric asymmetry is dominated by La Niña, a feature not observed to date. In contrast, in members with high asymmetry strong EP El Niño winters control the stratospheric asymmetry. Moreover, we corroborated that EP El Niño and La Niña winters with about equal SSTA intensity lead to comparable in magnitude but opposite signed stratospheric responses.

1 Introduction

El Niño-Southern Oscillation (ENSO), a coupled ocean-atmosphere phenomenon (Bjerknes 1969), is the main mode of interannual climate variability (Trenberth 1997). El Niño, its oceanic component, is characterized by sea surface temperature anomalies (SSTA) in the eastern equatorial Pacific Ocean. The atmospheric counterpart, the Southern Oscillation, is described as a variation of the sea level pressure (SLP) between the western and the eastern Tropical Pacific, between Darwin (12ºS, 131ºE) and Tahiti (17ºS, 149ºW) (Walker 1923, 1924). The ENSO cycle fluctuates between warm (El Niño) and cold (La Niña) phases, with a period ranging from 2 to 7 years. ENSO related anomalies, as SSTA, start to develop between July and October and reach the mature phase during the Northern Hemisphere (NH) winter, between November and February (Rasmusson and Carpenter 1982).

ENSO phenomenon is associated with global climate impacts (Trenberth et al. 1998; Alexander et al. 2002). Early studies showed ENSO related large scale precipitation and surface temperature anomalies in Australia, several regions from North to South America and in the Indian subcontinent (Ropelewski and Halpert 1987, 1989; Aceituno 1988; Kiladis and Diaz 1989; Halpert and Ropelewski 1992). A schematic representation of temperature and

precipitation anomalies associated with warm ENSO episodes during the NH wintertime is shown in Figure 1.1. Impacts were also found over Europe and Africa (Lloyd-Hughes and Saunders 2002; Moron and Plaut 2003).

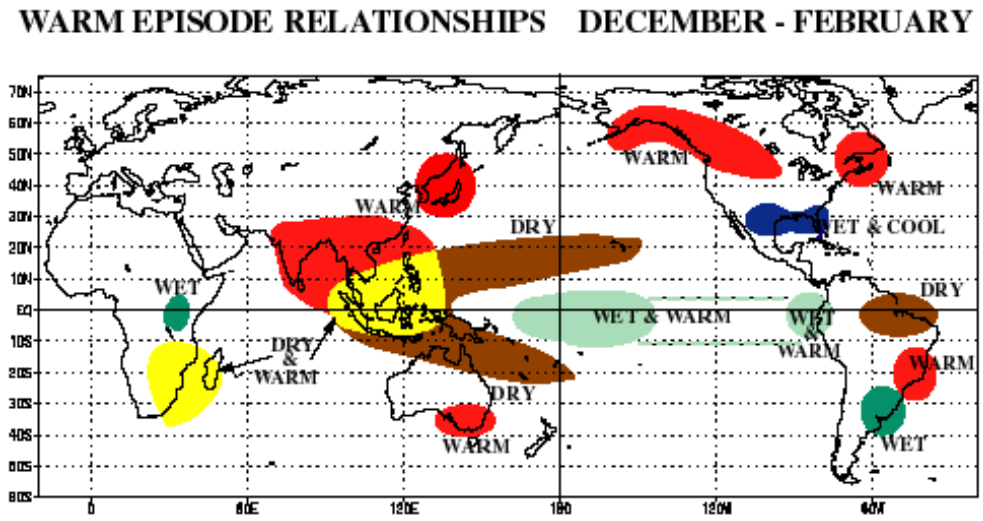

Figure 1.1. Schematic of warm ENSO episodes related temperature and precipitation anomalies during the NH winter season, from December to February. After Trenberth et al. (1998).

1.1 El Niño

1.1.1 El Niño tropospheric teleconnections

During the warm ENSO phase, El Niño, anomalously weaker easterly trade winds in the equatorial Pacific displace warm SSTA from the west to the eastern and central Pacific (Bjerknes 1969). This is illustrated in Figure 1.2, which shows positive sea surface temperatures (SST) during a typical El Niño event in the eastward equatorial Pacific, associated with the anomalous westerly surface wind stress.

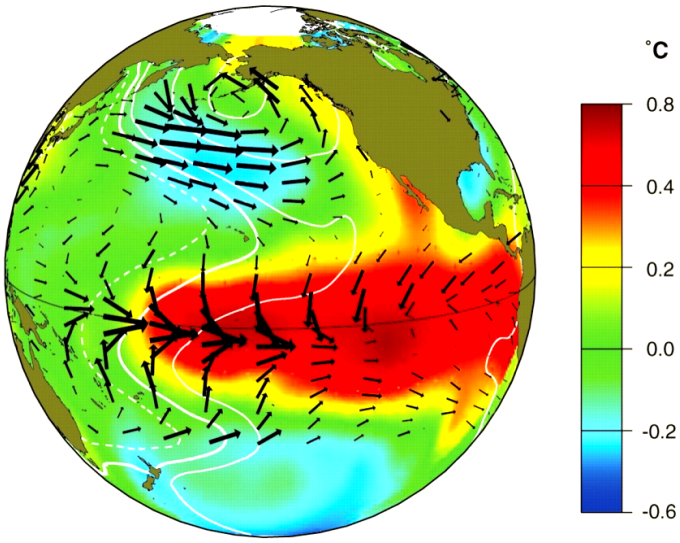

Figure 1.2. El Niño anomalies in SST (colors), surface atmospheric pressure (contours) and surface wind stress (vectors). Contour interval for pressure is 0.5 hPa, with solid (dashed) contours for positive (negative) values. Vectors indicate wind stress direction and intensity (longest equivalent to 1 N m^{-2}). The patterns are derived from a linear regression against SSTA averaged 6°N-6°S, 90°W-180°. From McPhaden et al. (2006).

These changes in the trade winds displace the climatological convective zone, located over the western Pacific, towards the east. Likewise, the thermally driven Walker circulation is also conveyed eastward, from the maritime continent to the eastern Pacific Ocean (Walker and Bliss 1932). The surplus release of latent heat in this region leads to enhanced deep convection and increased precipitation over the central and eastern Pacific, causing atmospheric heating and upper tropospheric divergence. These changes from neutral winters without ENSO, to warm ENSO conditions, are illustrated in Figure 1.3.

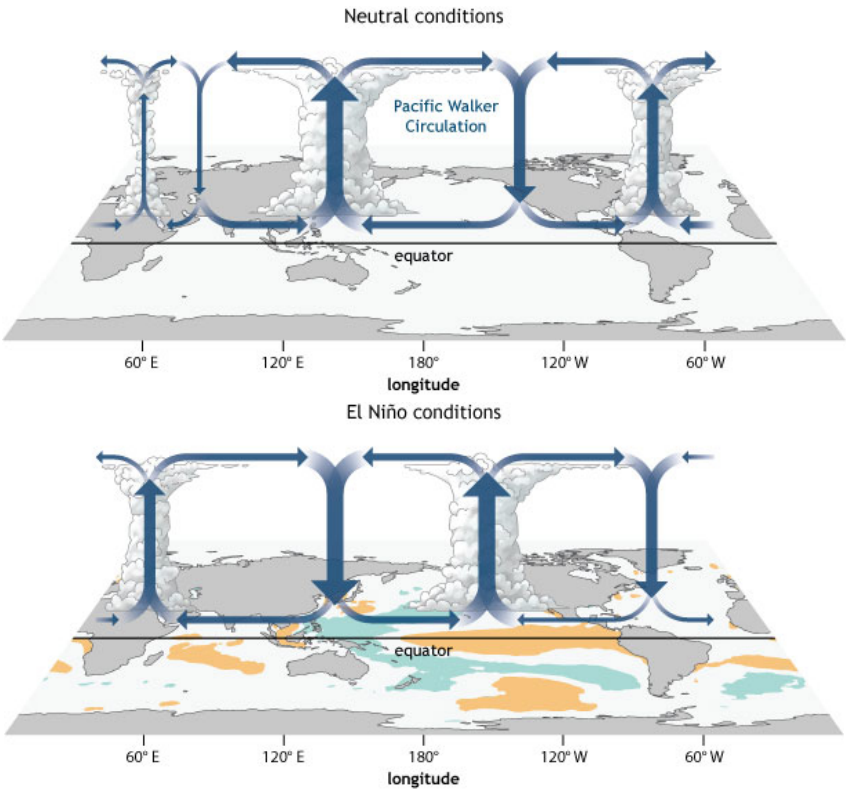

Figure 1.3. Generalized Walker Circulation for December to February mean during (top) ENSO-neutral conditions and (bottom) El Niño conditions. During El Niño winters orange and blue colors denote positive and negative SSTA, respectively. Clouds indicate increased rainfall anomalies over the equatorial Pacific. NOAA Climate.gov drawing by Fiona Martin.

The atmospheric response to tropical heating is described by the Gill-Matsuno response (Matsuno 1966; Gill 1980). It is characterized by two anticyclones at both sides of the equator in the upper troposphere and two cyclones in the lower troposphere. Equatorial Kelvin waves propagate eastward and cause easterlies to the east of the heating source, whereas Rossby waves are propagated westward and are associated with westerlies west of the heating. At the same time, the descending branch of the meridional Hadley cell is enhanced (Reiter 1978), resulting in anomalous tropospheric convergence in the subtropical westerly jets, where the forcing of extratropical Rossby waves is

effective (Sardeshmukh and Hoskins 1988). Indeed, associated with the stronger downwelling branch of the Hadley circulation, divergence in the tropical upper troposphere and convergence in the subtropical region are reinforced, triggering Rossby waves forcing in the subtropics towards higher latitudes (Hoskins and Karoly 1981). These Rossby waves impact the Aleutian low pressure system, in the North Pacific region, inducing a deepening and southward displacement of the Aleutian low (Horel and Wallace 1981; Hoskins and Karoly 1981). The illustration from Shukla and Wallace (1983) in Figure 1.4 represents the teleconnection patterns in response to a equatorial Pacific warming, in terms of the upper tropospheric geopotential height anomalies. In the tropics, the Gill-Matsuno response as upper tropospheric anticyclones is depicted. In the extratropics, linked to the Aleutian low modulation, negative geopotential height anomalies appear over the North Pacific and over the southeastern United States (US) and positive anomalies are located over western Canada. This pattern, enhanced during El Niño winters, is known as the Pacific-North American (PNA) pattern (Wallace and Gutzler 1981).

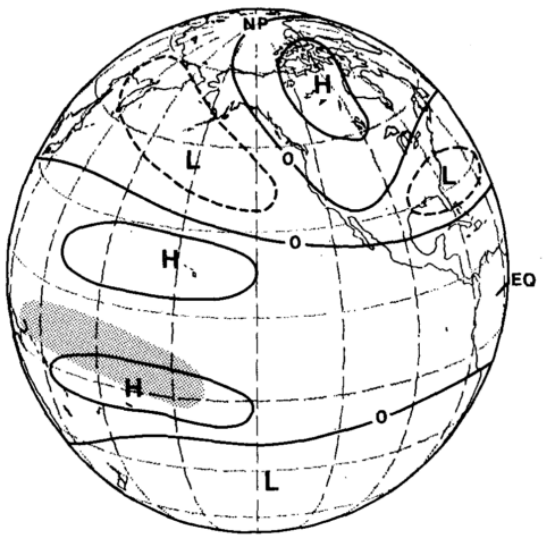

Figure 1.4. Schematic illustration of the upper tropospheric geopotential height anomalies during El Niño winters. Shading denotes the region with enhanced precipitation. From Shukla and Wallace (1983).

1.1.2 Troposphere-stratosphere coupling

In the last decade, several studies have provided observational and modeling evidences for a stratospheric pathway by which El Niño anomalies in the extratropical troposphere can propagate into the stratosphere and back to the surface at high latitudes of the NH (e.g. Manzini 2009). This pathway occurs by means of the troposphere-stratosphere coupling described next.

In the NH winter season, the stratospheric zonal-mean zonal wind are westerly and the vertical propagation of the planetary Rossby waves from the troposphere to the stratosphere is permitted (Charney and Drazin 1961). Thus, the strengthening of the PNA pattern during El Niño events leads to intensified upward propagation of Rossby waves into the stratosphere (e.g. Garcia-Herrera et al. 2006; Manzini et al. 2006), through constructive interference between the anomalous El Niño waves and the climatological stationary waves (Garfinkel and Hartmann 2008; Fletcher and Kushner 2011). Then, the dissipation of these waves in the upper stratosphere is also intensified, decelerating and weakening the polar vortex. Accordingly, the deep branch of the Brewer-Dobson circulation is strengthened into the winter hemisphere and more mass is introduced into the polar cap (Shepherd 2000), generating an anomalous cooling in the tropical stratosphere and a warmer polar stratosphere (e.g. García-Herrera et al. 2006). Therefore, the stratospheric response to El Niño events in the NH polar region is characterized by weaker zonal-mean zonal winds and warmer zonal-mean temperatures, as shown in radiosonde and satellite observations (e.g., van Loon and Labitzke 1987; Free and Seidel 2009; Cagnazzo et al. 2009) and modeling studies (Sassi et al. 2004; Garcia-Herrera et al. 2006; Manzini et al. 2006).

The troposphere-stratosphere coupling in the case of El Niño occurs in both directions. Thus, the polar stratospheric anomalies propagate downwards, from the upper stratosphere in early winter to the troposphere in late winter (as

first shown by Manzini et al. 2006), although the exact mechanism by which this occurs is not clear yet. This downward mass circulation decreases the tropopause height at the pole, increasing the SLP values at polar latitudes in form of a negative Arctic Oscillation (AO) phase. The AO, as defined by Baldwin and Dunkerton (1999), is the leading mode of variability of the wintertime geopotential between 10 and 1000 hPa and is characterized by a center of action over the polar cap. In middle and high latitudes across the Atlantic and Europe the AO is similar to the North Atlantic Oscillation (NAO) pattern (Hurrell et al. 2001), which is defined as the seesaw between the low and high pressure centers over Iceland and Azores. Then, El Niño winters are associated with negative NAO phases (Hurrell 1996; Brönnimann 2007), which displays an anomalous negative gradient over the North Atlantic. In response to these changes, the tropospheric zonal-mean zonal winds weaken at high latitudes and strengthen in mid-latitudes, so the polar jet is shifted southward (Kidston et al. 2015). The related southward displacement of the storms tracks and surface cyclones leads to wet and warmer conditions over southern Europe and the Mediterranean region. In contrast, the reduction of warm air advection to northern and central Europe causes dry and cold situations in these regions.

Therefore, El Niño events can impact tropospheric climate over the NAE region through the stratosphere (Ineson and Scaife 2009; Cagnazzo and Manzini 2009; Bell et al. 2009). However, as these studies have shown, Stratospheric Sudden Warmings (SSWs) play a significant role in the downward propagation of the anomalies and thus in connecting the tropospheric tropical El Niño signal with the NH extratropical teleconnections. The relationship between ENSO and SSWs is discussed in detail in section 1.3. The processes involved in propagating El Niño anomalies from the troposphere into the stratosphere at middle latitudes and then, back down to the troposphere and the surface, comprise what is known as the stratospheric pathway of El Niño teleconnections, which is summarized in Figure 1.5.

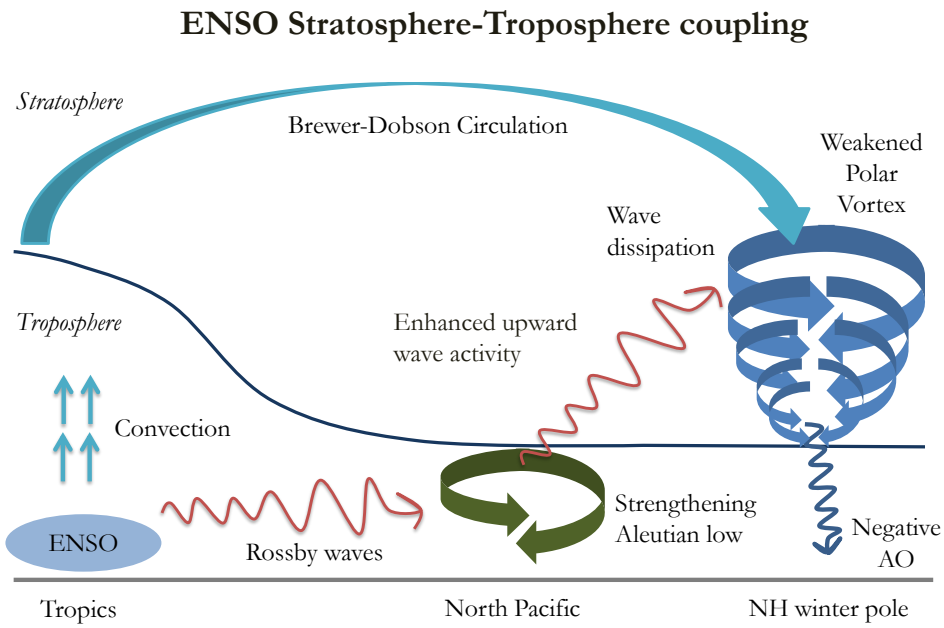

Figure 1.5. Representation of the stratosphere-troposphere coupling during warm ENSO events in the NH winter.

1.1.3 Different El Niño flavors

1.1.3.1 Central Pacific El Niño

As discussed above, traditionally El Niño was characterized by large SSTA in the eastern Pacific. More recently, a different type of El Niño has been diagnosed, distinct from the canonical one (Ashok et al. 2007), characterized by SSTA that peak in the central Pacific. It has received several names, as Dateline El Niño (Larkin and Harrison 2005), El Niño Modoki (EMI, Ashok et al. 2007), Central Pacific El Niño (Kao and Yu 2009) or Warm Pool El Niño (Kug et al. 2009), while the canonical El Niño is now referred as East Pacific (EP) El Niño. Different indices have been used to characterize the new El Niño flavor, such as those based on EOF (empirical orthogonal function) analysis or SSTs averages

over certain regions of the central Pacific (see Capotondi et al. 2015 for a review). Figure 1.6 illustrates the different warm SSTA location for EP and Central Pacific (CP) El Niño.

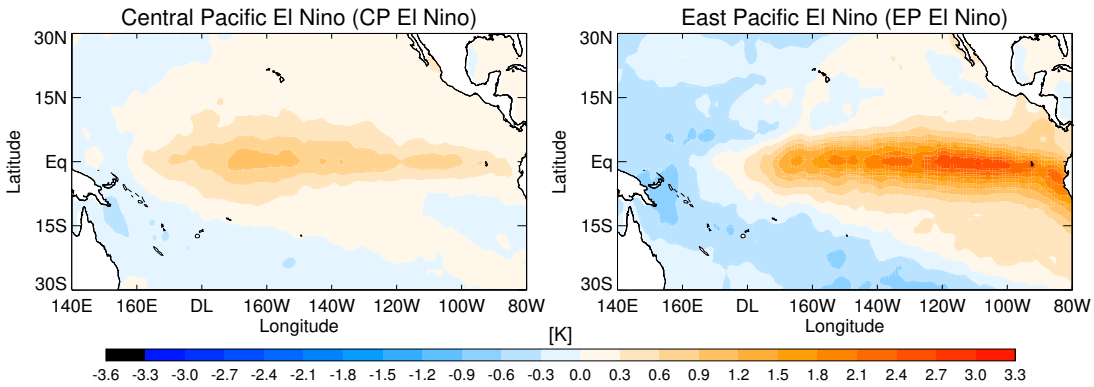

Figure 1.6. Composite of (left) CP El Niño and (right) EP El Niño SSTA from the HADISST dataset. Contour interval is 0.3 K, red (blue) colors indicate positive (negative) anomalies with respect the period 1981- 2010.

Maximum SSTA for CP El Niño events are weaker than for EP El Niño (Ashok et al. 2007; Kug et al. 2009). However, as the Pacific warm pool is already a convective zone (Hoerling et al. 1997), western Pacific SSTA can trigger large precipitation anomalies and are more effective on inducing anomalous convection than the SSTA over the eastern Pacific (Barsugli and Sardeshmukh 2002; Kug et al. 2009). Nonetheless, the different locations for convection between the two El Niño flavors leads to different atmospheric responses (Hoerling and Kumar 2001) and hereafter, EP and CP El Niño are related to different tropospheric teleconnections in the Pacific rim (Weng et al. 2007, 2009; Yu et al. 2012; Yu and Zou 2013; Zou et al. 2014).

As an example, we discuss next the differences for North America. As illustrated in Figure 1.7, anomalous westerlies bring moisture to western North America during EP El Niño winters, in relation to the cyclone over the Aleutian

low region. In contrast, during CP El Niño winters both an anomalous anticyclone and a cyclone appear in the North Pacific, leading to a seesaw of dry and wet conditions in the northwest and the southwest regions.

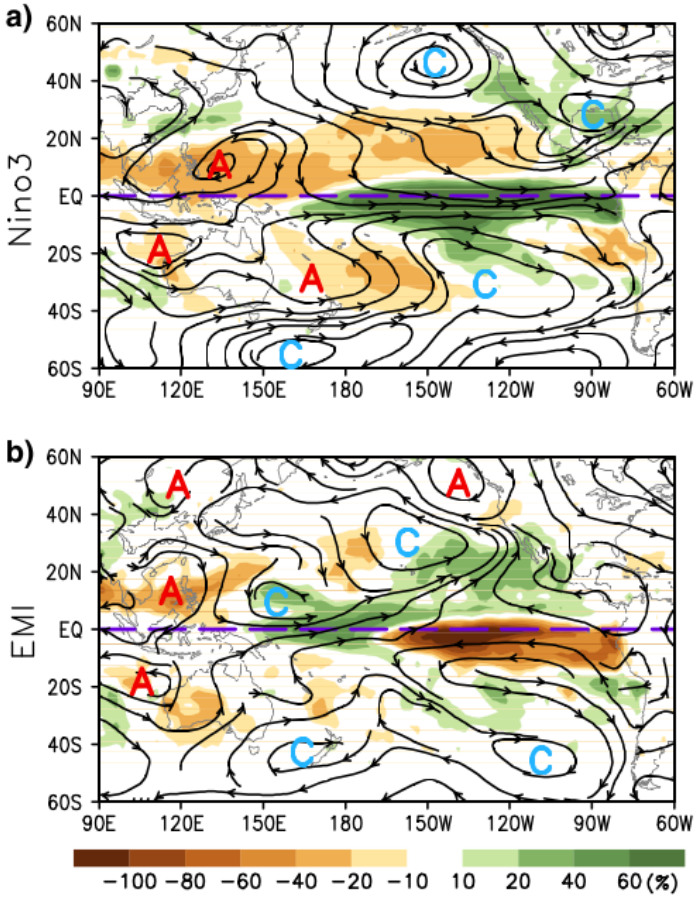

Figure 1.7. Regression patterns of anomalous zonal wind at 850 hPa (stream) and the precipitation anomaly percent of normal (shading) for (a) EP El Niño and (b) CP El Niño (based on EMI index). The cyclones and anticyclones are indicated by C and A capital letters, respectively. From Weng et al. (2009).

Likewise, different impacts are observed on the surface air temperature over the US. While the EP El Niño events mainly affect northeastern and

southwestern US, CP El Niño largest impacts are reported in the northwestern and southeastern US, as shown in reanalysis and observations data in Figure 1.8, from Yu et al. (2012)

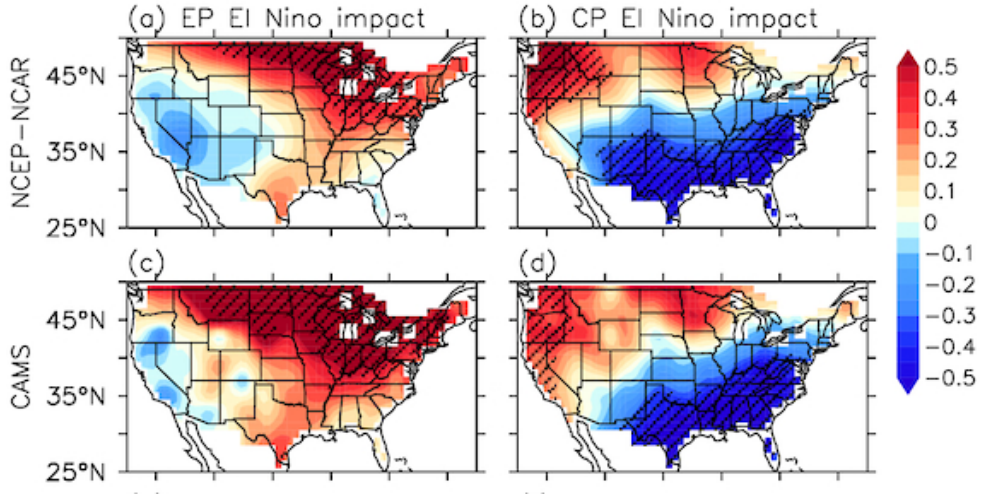

Figure 1.8. Observed US winter (January-February-March) surface air temperature anomalies regressed onto the (left) EP and (right) CP El Niño indices. Observations correspond to (a, b) the NCEP-NCAR reanalysis and (c, d) air temperature data set from the Climate Anomaly Monitoring System (CAMS). Shading indicates significance at the 90% confidence level based on a student t-test. From Yu et al. (2012).

1.1.3.2 Controversy in the stratospheric response to CP El Niño

Since EP and CP El Niño flavors show different teleconnections in the troposphere, and tropospheric teleconnections at mid-latitudes drive the polar stratospheric response to El Niño (see section 1.1.), differences in the stratospheric teleconnections between EP and CP El Niño are also expected. Interestingly, even though the response to the EP El Niño events is robust in the NH polar stratosphere, there is no consensus regarding the response to CP El Niño. Whether EP and CP El Niño stratospheric responses are

distinguishable or not has been under debate in the past years (see e.g. Garfinkel et al. 2013).

Some studies showed that EP and CP El Niño stratospheric signals in the NH are indistinguishable. Thus, Hurwitz et al. (2014) found a similar response between EP and CP El Niño events in the Aleutian low (see Figure 1.9 left). Likewise, they found indistinguishable signatures in the polar vortex seasonal means in both reanalysis data and CMIP5 model experiments. In agreement with Hurwitz et al. (2014), Graf and Zanchettin (2012) showed a weakened stratospheric polar vortex for both EP and CP El Niño in reanalysis data, although the response was weaker and less significant for the latter. Garfinkel et al. (2013) also found similar results between EP and CP events in idealized model experiments. On the contrary, other studies showed an opposite behavior for EP and CP El Niño winters. Fig. 1.9 (right) shows the geopotential height anomalies from Hegyi and Deng (2011), based on the same MERRA reanalysis as Hurwitz et al. (2014), but a different index was applied to define CP El Niño winters, as Hegyi and Deng (2011) considered a larger region to average the SSTs. For EP El Niño (Fig. 1.9 top-right) the deepened Aleutian low appears, but during CP El Niño winters the Aleutian low is anomalously weak and shows positive anomalies (Fig. 1.9 bottom-right). Accordingly, in response to the weaker Aleutian low, Hegyi and Deng (2011) found a stronger and colder polar vortex during CP El Niño winters, opposite to EP El Niño warming. Sung et al. (2014) also showed, in reanalysis data, an opposite response in the polar stratosphere during CP and EP El Niño. In model simulations, Zubiaurre and Calvo (2012) also reported a temperature pattern consistent with a stronger polar vortex for CP El Niño events, identified with El Niño Modoki index, albeit the signal was not significant and inconsistent with the tropospheric PNA pattern. Hence, contradictory results have been reported regarding the NH polar stratospheric response to CP El Niño. However, it should be noted that a direct comparison among studies is difficult, because they use different indices

to categorize the events and so different CP El Niño winters are analyzed in each study.

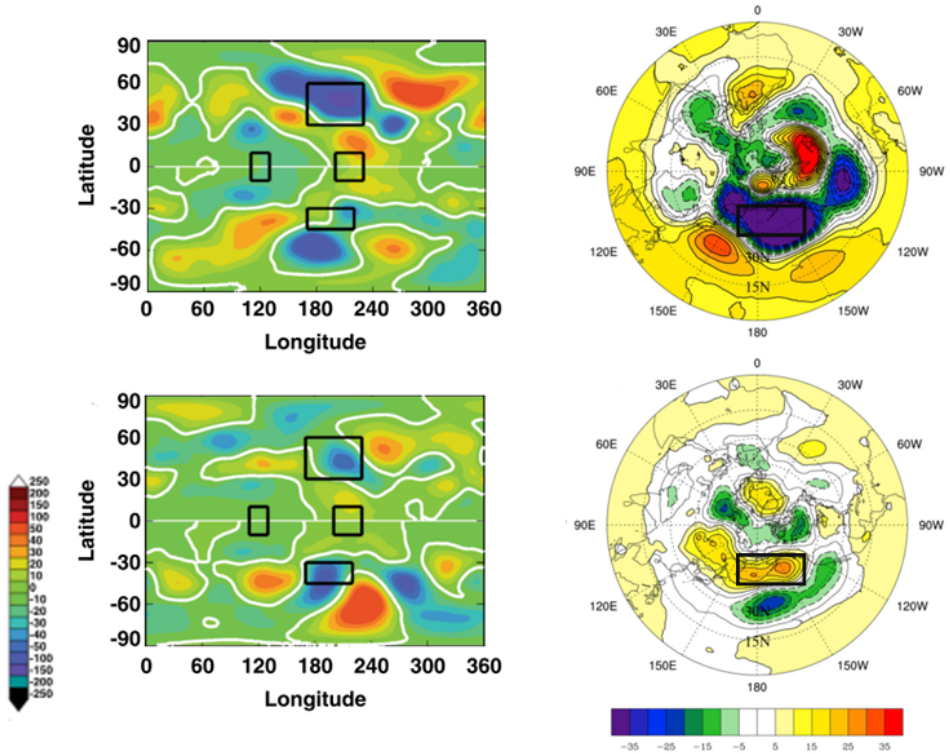

Figure 1.9. Composited anomalies of the NH December-January-February averaged geopotential height anomalies (m) for (top) EP and (bottom) CP El Niño in MERRA reanalysis data at (left) 250 hPa and (right) 500 hPa. Black rectangles (upper in left panels) indicate the Aleutian low region. Modified from (left) Hurwitz et al. (2014) and (right) Hegyi and Deng (2011).

In this regard, Garfinkel et al. (2013) compared the NH polar stratospheric responses to different EP and CP El Niño indices used in the literature and different composite sizes. Figure 1.10, adapted from Garfinkel et al. (2013), shows the temporal evolution of the polar cap geopotential height anomalies for different indices, such that different years are considered for each definition, noted at the left border of each panel. For EP El Niño (panels a, b),

significant positive anomalies, noted with colors, are observed. Interestingly, for CP El Niño (panels c to f), Garfinkel et al. (2013) reported a different response depending on the index used. However, Fig. 1.10 shows that the stratospheric signal over the polar cap was always not significant. The sensitivity of these results to the composite size was also tested. For EP El Niño winters results were robust regardless the number of winters considered, but this was not the case for CP El Niño. Thus, Garfinkel et al. (2013) concluded that CP El Niño polar stratospheric response is not robust and the signal depends on the size of the composite and the index used. Nevertheless, their conclusion also suggests that other sources of variability that affect the polar stratosphere (such as SSWs or quasi-biennial oscillation (QBO), see section 1.3) can be interfering with the CP El Niño signal, so the CP El Niño response might change depending on the winters analyzed.

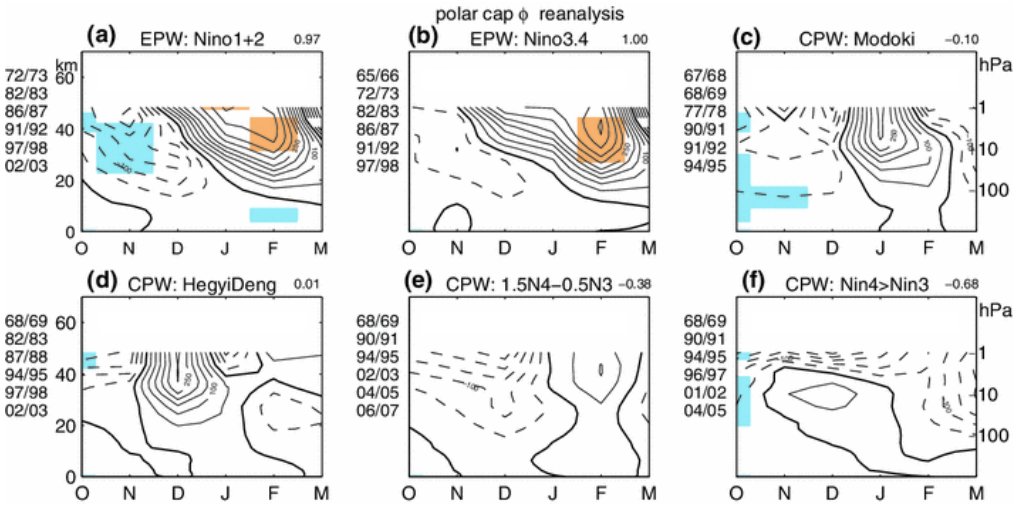

Figure 1.10. Polar cap geopotential height anomalies evolution during EP and CP El Niño winters. (a to b) 2 EP El Niño indices and (c to f) 4 CP El Niño definitions are analyzed. Contour interval is 50 m and significant anomalies at the 90% level are colored. The pattern correlation in December-January-February-March (DJFM) between Niño3.4 composite (panel b) and the height anomalies in the other composites is shown. Modified from Garfinkel et al. (2013).

Therefore, whereas the EP El Niño stratospheric pathway is well known, the potential stratospheric response to CP El Niño winters in the NH still remains an open question. Given that the frequency of CP El Niño events has increased significantly over the last three decades (Lee and McPhaden 2010) and model simulations under climate change scenarios also project an increase in the occurrence of CP El Niño winters (Yeh et al. 2009), understanding the impacts associated with CP El Niño events and their similarities and differences with EP El Niño events becomes highly relevant.

1.2 La Niña

La Niña is the cold phase of the ENSO phenomenon (Philander 1985). Opposite to El Niño, during La Niña winters easterly trade winds are intensified and colder SSTs appear in the eastern Pacific and extend westward, so the heating and the convection in the tropical Pacific decrease, leading to reduced rainfall in this region (Philander 1985). Figure 1.11 illustrates La Niña conditions SSTA and the related Walker cell enhancement, with strengthening of the rising branch over the Maritime continent and the sinking branch over the eastern central Pacific Ocean, where the already small precipitation is further reduced.

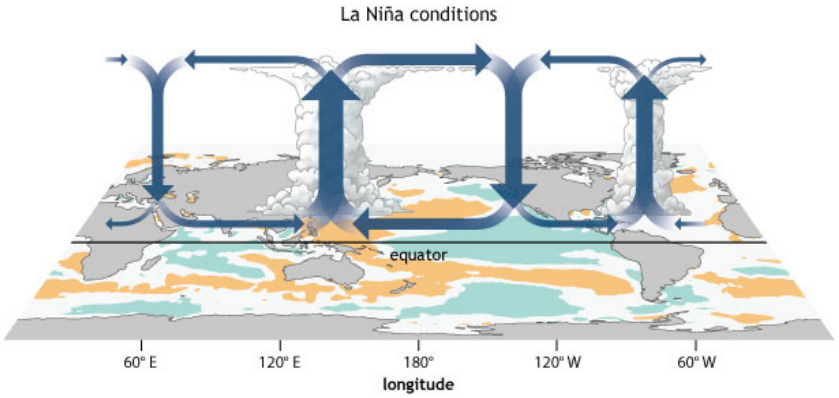

Figure 1.11. As Fig. 1.3 but for cold ENSO, La Niña, events. NOAA Climate.gov drawing by Fiona Martin.

1.2.1 La Niña versus El Niño tropospheric teleconnections

The SSTA pattern associated with La Niña events is displayed in Figure 1.12b. It shows that La Niña negative SSTA tend to be maximum in the central Pacific (Monahan 2001), while the largest positive SSTA during canonical (EP type) El Niño events are located in the eastern Pacific (Fig. 1.12a). Then, in contrast to El Niño, the conventional La Niña events are already located in the central Pacific (Monahan 2001), and different La Niña flavors have not been reported (Kug et al. 2009; Kug and Ham 2011). In addition, strong La Niña SSTA magnitudes are not as high as those during strong El Niño events (An and Jin 2004). In fact, Burgers and Stephenson (1999) reported that the eastern Pacific SSTA are skewed towards higher positive values during strong ENSO events. El Niño and La Niña also differ on their temporal structures (Larkin and Harrison 2002). While El Niño tends to decay faster in summertime, after the mature phase in boreal winter, La Niña can persist in time and can be intensified the consecutive winter (Okumura and Deser 2010). Thereupon, it is clear that El Niño and La Niña are not mirror images. La Niña presents a non-symmetric pattern with respect to that during El Niño in the SSTA signature; such asymmetry is an intrinsic characteristic of ENSO events (An and Jin 2004).

The asymmetry in the SSTA between El Niño and La Niña leads to asymmetric atmospheric responses (Hoerling et al. 2001). As discussed in section 1.1., during the canonical El Niño winters large SSTA prompt convection in the eastern Pacific region. In contrast, La Niña related negative SSTA do not have a substantial impact saturating convection on the prevailing dry conditions over the cold eastern Pacific (Hoerling et al. 1997). The outgoing longwave radiation (OLR) anomalies spatial patterns are shown in Figure 1.12 (bottom). Negative OLR anomalies suggest an enhanced precipitation during El Niño, while the positive anomalies during La Niña imply a decreased precipitation in the central Pacific. In fact, during La Niña winters the

convention center is shifted to the west, compared to El Niño (Kang and Kug 2002). Therefore, as pictured in Figs. 1.3 and 1.11, El Niño and La Niña present different locations in their largest precipitation anomalies in the tropical Pacific Ocean, east of the Date Line during El Niño and westward during La Niña.

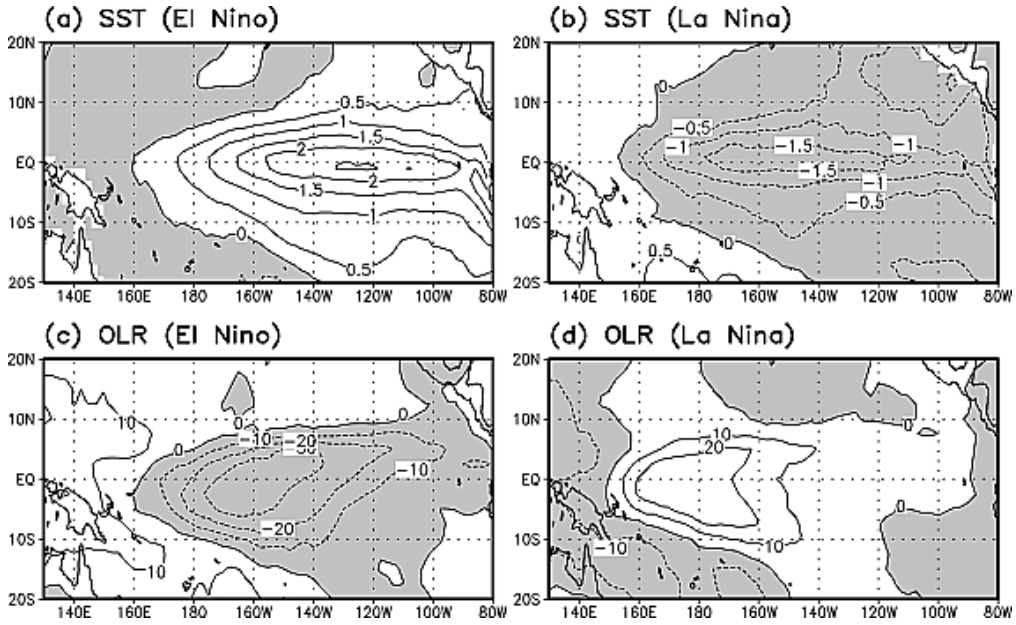

Figure 1.12. Composited SSTA and the outgoing longwave radiation (OLR) anomalies during (EP) El Niño and La Niña mature phases. Contour interval for SSTA is 0.5 ºC and for OLR anomalies 10 W m^{-2}. From Kang and Kug (2002).

These differences between El Niño and La Niña in tropical Pacific convection lead to different Rossby waves forcing, such that El Niño and La Niña reveal opposite but shifted impacts over the Pacific North American region. The typical deepening of the Aleutian low characteristic of canonical El Niño events is shifted eastward with respect the canonical PNA pattern. In contrast, La Niña generates a weakened Aleutian low with its centers of action projected onto the PNA pattern. Thus, canonical El Niño and La Niña anomalies are in quadrature (Hoerling et al. 1997), displaying asymmetrical

atmospheric teleconnections (Hoerling et al. 2001; Wu et al. 2010). However, besides the asymmetry in the SSTA, it has been suggested that the asymmetry in the atmospheric response between El Niño and La Niña could be due to atmospheric internal variability in the mid-latitudes (Hoerling et al. 2001; Zhang et al. 2014). Nonetheless, whether the variability of the atmospheric response asymmetry is due to the internal variability or could also be related to the sample variability in the SSTA forcing asymmetry has not been fully explored.

1.2.2 The stratospheric signature of La Niña

Much less work than for El Niño has been done on La Niña stratospheric response. Initially, most of the studies regarding the ENSO signal in the stratosphere analyzed El Niño-La Niña events composites, assuming opposite signatures for both ENSO phases (e.g. Garcia-Herrera et al. 2006). Nonetheless, following this methodology, Free and Seidel (2009) did not find a significant polar stratospheric response to La Niña in several radiosonde data from 1958 to 2005. However, they acknowledge that among the six La Niña winters considered (see details in Table 2.5), four of them showed a cold Arctic stratosphere, opposite to the response found during El Niño, while during the other two La Niña winters the stratosphere was anomalously warm, resulting in non-robust results. On the other hand, Mitchell et al. (2011), analyzed reanalysis data including two more La Niña events than Free and Seidel (2009). They reported a significant polar stratospheric cooling during La Niña winters, although the response appeared to be weak. Figure 1.13, from Mitchell et al. (2011), displays the temporal evolution of the zonal-mean zonal wind stratospheric anomalies during El Niño and La Niña, showing a larger and robust polar vortex weakening during El Niño than the opposite strengthening found for La Niña. Results agree with the previous study from Camp and Tung (2007), who reported a significantly warmer NH polar stratosphere during El Niño than the cooling during La Niña.

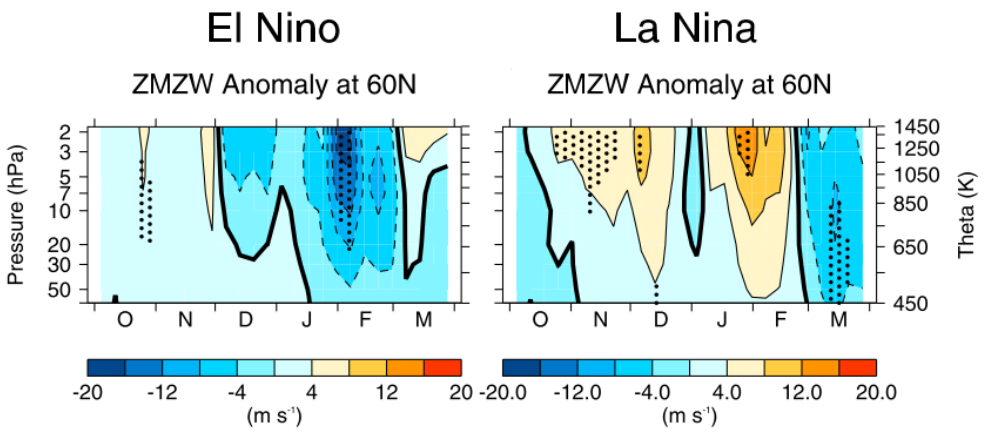

Figure 1.13. Time-pressure cross section of the weekly averaged zonal-mean zonal wind anomalies at 60ºN, averaged for the October-March period from 1958 to 2012, for (left) El Niño and (right) La Niña. Stippling areas indicate the statistical significance at the 95% confidence level according to a Monte Carlo test. Modified from Mitchell et al. (2011).

The absence of agreement in the literature regarding the stratospheric response during La Niña, in observations or reanalysis data, could be related to the short observational record available (and thus small signal-to-noise ratio) or the relatively low threshold (about 0.5ºC in the tropical Pacific SSTA) sometimes used to increase the number of analyzed La Niña events, in particular when ENSO events are classified considering also additional sources of variability, such as SSWs (Butler and Polvani 2011; Barriopedro and Calvo 2014; Domeisen et al. 2015). In fact, Trenberth (1997) and Hoerling et al. (2001) already noted that a low threshold such as 0.5 ºC is not appropriate to characterize La Niña events and that only a threshold of 1ºC or higher leads to appreciable tropospheric teleconnections for La Niña. In addition, the use of different thresholds to select cold ENSO events in studies with either observations or reanalysis datasets, hamper a direct comparison among them.

Longer model simulations do not display a clearer picture for La Niña either. Pioneer works about La Niña stratospheric signal in model simulations show a negligible response, which seems not to be statistically different from

natural variability (Manzini et al. 2006; Sassi et al. 2004). In contrast, recent modeling studies have reported a strong Arctic polar vortex response during La Niña (Calvo et al. 2010; Rao and Ren 2016a), related to suppressed anomalous upward propagation (Li and Lau 2013).

Overall, up to date, the understanding is that the polar stratospheric response to La Niña is small and thus, weaker than during El Niño events or even not distinguishable from internal variability. Different studies show different results in observations, reanalysis data or model simulations (Sassi et al. 2004; Manzini et al. 2006; Garfinkel and Hartmann 2007; Free and Seidel 2009; Mitchell et al. 2011). Identifying a robust stratospheric signal during La Niña winters could imply a possible downward propagation of the anomalies to the troposphere, similar to El Niño case, with perhaps subsequent impacts for climate over the NAE region. Indeed, a linkage between La Niña winters and the NAE region has already been reported. Based on the observational record, analyzed for near a 100 year period, negative SLP anomalies are observed north of 50ºN in late winter during La Niña events (Moron and Gouirand 2003), together with strong precipitation anomalies over the European region (Pozo-Vázquez et al. 2005). This pattern, characterized by enhanced precipitation over Great Britain and Scandinavia and reduced precipitation over the southwestern Mediterranean area, is related to a positive NAO phase, opposite to that found during El Niño winters. However, Pozo-Vázquez et al. (2005) could not provide a physical explanation for the relationship between cold ENSO events and a positive NAO like pattern. A robust polar stratospheric response to La Niña could be the missing link to explain this teleconnection, as it occurs during El Niño. It is therefore clear that the NH stratospheric response to La Niña events still deserves further investigation.

1.3 ENSO and other sources of stratospheric vortex variability

Besides the ENSO influence, the stratosphere-troposphere coupling and the stratospheric polar vortex are also modulated by other sources of variability. Diverse natural forcings, such as the 11 year solar cycle (e.g., Crooks and Gray 2005; Chiodo et al. 2014), volcanic eruptions (e.g., Robock 2000), Stratospheric Sudden Warmings (SSWs) (Scherhag 1952) and the quasi-biennial oscillation (QBO) (e.g., Holton and Tan 1980) can also affect the polar stratosphere and interact nonlinearly with ENSO on impacting the NH winter polar stratosphere. The first studies that investigated the ENSO signal in the stratosphere analyzed its relationship with the QBO and in fact, initial attempts could not separate the ENSO signal from the QBO signal (Hamilton 1993; van Loon and Labitzke 1987). In the past decade the focus extended towards the occurrence of SSWs and their relationship with ENSO events (e.g., Taguchi and Hartmann 2006). Next, we describe briefly these two phenomena and explain their relationship with ENSO.

1.3.1 The quasi-biennial oscillation

The stratospheric tropical variability is dominated by the quasi-biennial oscillation (QBO) (Baldwin et al. 2001). The QBO is manifested as the oscillation of downward propagating easterly and westerly zonal-mean stratospheric winds, with a variable period of about 27 months. During the NH wintertime, through planetary wave breaking in the stratospheric surf zone (McIntyre and Palmer 1983), the QBO can influence the extratropical NH stratosphere (Holton and Tan 1980). Figure 1.14, modified from Baldwin et al. (2001), represents the westerly and easterly zonal-mean wind anomalies. When the QBO is in its easterly phase (EQBO) the zero mean zonal wind line, the critical line between the easterly and westerly zonal-mean flows (black vertical contour), is displaced to the winter hemisphere. This shift on the critical line

causes a narrowing of the planetary waveguide and strengthens the extratropical planetary wave activity (red arrows) at high latitudes, favoring the weakening of the polar vortex. On the other hand, during the westerly phase of the QBO (WQBO) the critical line is displaced far from the polar vortex, and the planetary waves propagate towards the tropics, without disturbing the polar vortex (O'Sullivan and Salby 1990). Thus, the EQBO phase is associated with a weaker and warmer polar vortex, while the WQBO is related to a colder and stronger polar stratosphere (e.g., Holton and Tan 1980). Eventually, it has been shown that the troposphere responds to the QBO modulations on the polar stratosphere, impacting European winter surface climate (Coughlin and Tung 2001; Marshall and Scaife 2009).

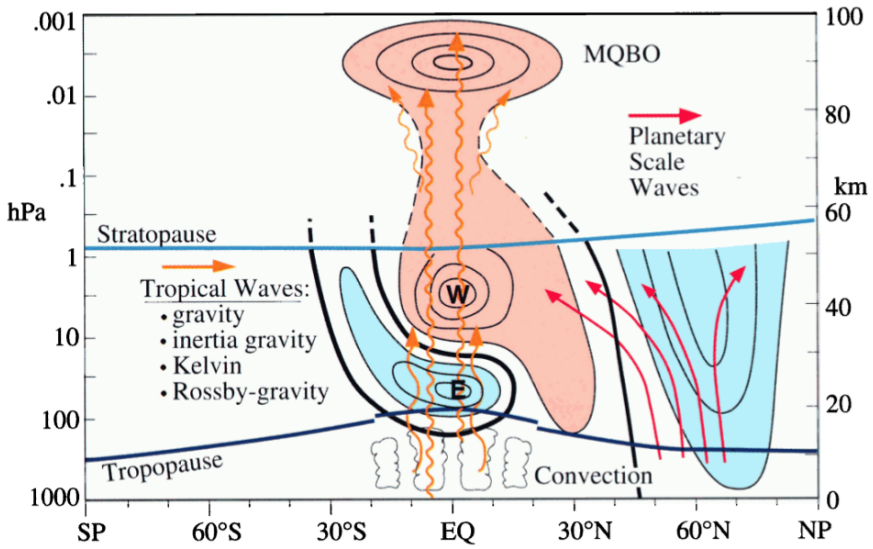

Figure 1.14. Schematic illustration of the QBO during the NH winter. QBO driven tropical waves (orange) and planetary waves (red) upward propagation is depicted. Black contours denote the zonal-mean zonal wind differences between easterly and westerly winds. Easterly (westerly) anomalies are indicated by light blue (orange) colors. From Baldwin et al. (2001).

The polar stratospheric temperature perturbations associated with QBO and ENSO are comparable in magnitude during the NH wintertime (Camp and

Tung 2007), but their combined effects show a nonlinear behavior (Garfinkel and Hartmann 2007, 2008; Calvo et al. 2009). Based on reanalysis data, Garfinkel and Hartmann (2007) found a reduced ENSO influence in the Arctic stratosphere during the EQBO phase. In particular, during La Niña winters with the EQBO phase an anomalous stratospheric warming is observed in early winter, while a non-robust signal is observed during La Niña winters under WQBO conditions. During El Niño, model experiments showed that the EQBO phase advances the stratospheric warm response, while the WQBO delays it (Calvo et al. 2009). At the same time, the polar response to both QBO phases seems to be weak under El Niño conditions, as shown in reanalysis (Garfinkel and Hartmann 2008), model simulations (Calvo et al. 2009), and radiosonde data (Taguchi 2010; Yuan et al. 2014). Regarding the surface response over the NAE region, WQBO and La Niña conditions lead to a positive NAO, whereas during El Niño winters with EQBO a negative NAO is simulated (Hansen et al. 2016). Nevertheless, Richter et al. (2015) suggested that SSWs play a larger role than the QBO on the composited El Niño polar stratospheric response. Indeed, using a set of ensemble members of simulations, they found that the QBO modulations on the ENSO teleconnections occur mainly during winters without SSWs.

1.3.2 Stratospheric Sudden Warmings

Certainly, Stratospheric Sudden Warmings (SSWs) dominate the stratospheric polar vortex variability (see Andrews et al. 1987). Major SSWs are defined by a daily zonal-mean zonal wind reversal, from the wintertime stratospheric westerlies to easterlies (WMO; Mcinturff 1978). The abrupt appearance of easterly winds leads to the polar stratospheric vortex weakening and a sudden warming (Matsuno 1971), for this reason these events were named as Stratospheric Sudden Warmings (Scherhag 1952). These stratospheric events take place in the upper stratosphere (around 10 hPa), with a frequency of

occurrence of about 6 events per decade in the NH (Charlton and Polvani 2007; Palmeiro et al. 2015). However, as shown in Figure 1.15a the originated large stratospheric disruptions, characterized by warm temperature anomalies (contours) and negative zonal-mean zonal winds (colors), can be traced down to the lower stratosphere, penetrating into the troposphere up to two months after the event is detected in the stratosphere (Baldwin and Dunkerton 2001). These changes are well captured by a negative Northern Annular Mode (NAM) index, indicated in Figure 1.15b by reddish colors after the SSWs onset date. The negative NAM pattern projects over the surface as a negative NAO phase, so that SSWs can also impact the surface circulation over the NAE region (Limpasuvan et al. 2004; Charlton and Polvani 2007).

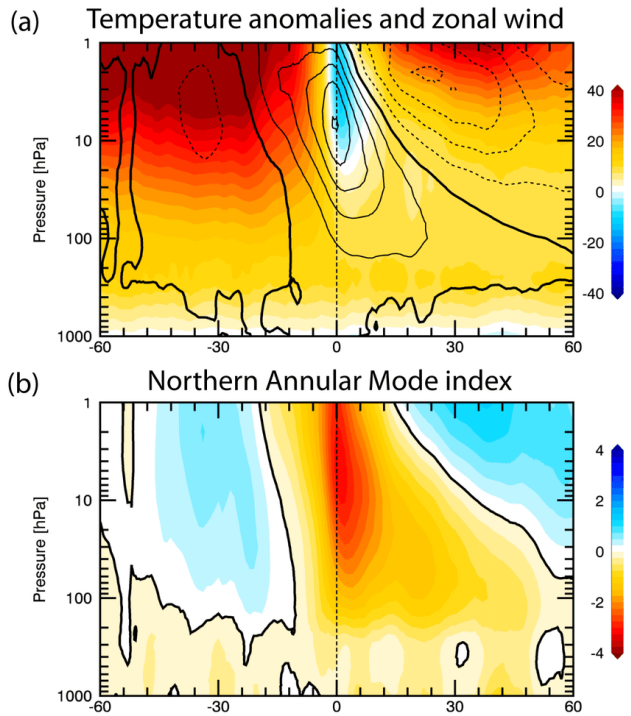

Figure 1.15. Composites of the 60 days before and after SSWs in JRA-55 reanalysis for (a) temperature anomalies averaged from 50–90ºN (contour levels: 2 K and bold line: 0 K) and zonal-mean zonal winds at 60ºN (colors, m s^{-1}), (b) the NAM index (standard deviations). From Butler et al. (2017).

Therefore, SSWs have been suggested as a source of skill of the seasonal predictability over the NAE region (Sigmond et al. 2013). Accordingly, the potential of ENSO on improving seasonal predictability over Europe enhances during winters with SSWs (Domeisen et al. 2015), since SSWs favor the El Niño stratospheric signal downward propagation (e.g., Cagnazzo and Manzini 2009). As Ineson and Scaife (2009) showed, the surface response over the NAE region differs during El Niño winters coincident with a SSW or in SSWs absence (Figure 1.16). During El Niño winters with SSWs (Fig. 1.16a) a negative NAO structure is simulated, with positive SLP anomalies over the Arctic and negative anomalies over the North Atlantic and Eurasia. On the other hand, this pattern is missing during El Niño winters without SSWs (Fig. 1.16b). Hence, it is now recognized that SSWs play a relevant role in connecting El Niño signal with the NAE region through the stratosphere (Cagnazzo and Manzini 2009; Ineson and Scaife 2009; Bell et al. 2009).

However, even though predicting SSW occurrence could improve the seasonal forecast skill (Scaife et al. 2016), SSW predictability is still very limited (Gerber et al. 2009). Polvani and Waugh (2004) established that the primary dynamical source of the SSWs is located in the troposphere and is driven by the upward wave propagation, but their origin is still unknown (Waugh and Polvani 2010). In this regard, due to the enhanced wave activity during El Niño winters, whether El Niño might favor SSW occurrence has been a relevant question. Model simulations reported an increased SSW occurrence during El Niño winters, compared to La Niña and neutral conditions (Taguchi and Hartmann 2006; Li and Lau 2013). But short reanalysis records showed an enhanced SSW occurrence frequency during both El Niño and La Niña winters with respect to neutral winters (Butler and Polvani 2011). Thus, reanalysis and modeling studies disagree on La Niña role on favoring or not SSW occurrence, in line with the unclear stratospheric response to La Niña winters (see section 1.2.2). However, very recently, Polvani et al. (2017) suggested that the cold phase of ENSO does

not affect SSW frequency and only warm ENSO winters show more SSW occurrence than ENSO-neutral winters in the observational record. In any case, the relationship between SSWs and ENSO as well as the mechanisms operating behind still need to be clarified.

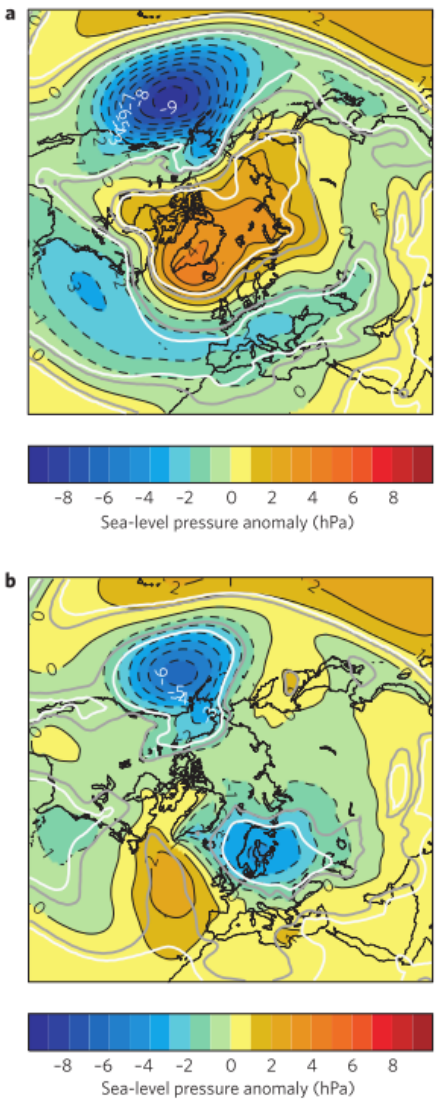

Figure 1.16. Composited SLP anomalies (hPa), averaged for January-February-March (JFM), during El Niño years (a) with and (b) without SSWs. Gray and white contours denote significance at the 95% and 99% confidence levels. From Ineson and Scaife (2009).

1.4 Objectives

The current knowledge on ENSO teleconnections, described in the previous sections, reveals still many open issues concerning the stratospheric ENSO signal. In this thesis, we aim to address three main questions: 1) How robust is the stratospheric pathway of La Niña? 2) How is the polar stratospheric response to CP El Niño events, in comparison to EP El Niño? and finally 3) Which is the impact of El Niño and La Niña asymmetry on the stratospheric pathway? In particular, we will:

1. Reevaluate the NH La Niña stratospheric pathway in a reanalysis dataset. Analyze the sensitivity of La Niña stratospheric response to different thresholds used to select the events. Explore the influence of SSWs and the QBO on La Niña stratospheric signature.
2. Reexamine EP and CP El Niño NH stratospheric signature and establish whether the responses are distinguishable or not, keeping in mind the possible impact of SSWs and the potential sensitivity of the CP El Niño signal to the index used and composite size.
3. Investigate the existence of sample variability on the asymmetry between El Niño and La Niña in the SSTA, using a large model ensemble. Evaluate if the SSTA forcing asymmetry is a major driver of El Niño and La Niña asymmetry teleconnections on the NH stratospheric pathway.

First, La Niña stratospheric signal and its potential effects on tropospheric climate are revisited here using a reanalysis dataset. As previously explained, even though some recent model studies have reported a robust polar stratospheric response to La Niña winters, this signature has not been captured in the observational record. We try to understand this by i) evaluating the sensitivity of La Niña response to the threshold used to select the events and ii)

exploring the role of SSWs and the QBO on modulating La Niña signal, on the grounds that, within a short record and using a low threshold, the interference with the SSWs or QBO signals could lead to an uncertain La Niña response. *Chapter 3* is devoted to this topic.

Second, the question of whether or not the EP and CP El Niño differ in their NH stratospheric responses is investigated in *chapter 4*. This question remains moot, in part, because of the different definitions and years employed in the literature to characterize CP El Niño events. We reexamine this issue by exploring the role of SSWs on the CP and EP polar stratospheric El Niño signals. Since SSWs are major disruptions of the stratospheric polar vortex we hypothesize that their impact might modulate the observed stratospheric response to CP El Niño events. Moreover, we also investigate the sensitivity to different CP El Niño definitions to explain the discrepancies found in the literature in this regard.

Finally, after unveiling the NH polar stratospheric signatures during La Niña and El Niño flavors, *chapter 5* explores the impact of the ENSO asymmetry on the NH stratospheric pathway. To this aim, we make use of a grand model ensemble of 100 members. This large ensemble allows evaluation of the variability range of the asymmetry between El Niño and La Niña in the SSTA forcing and whether this asymmetry is the main driver of the asymmetry found on the stratospheric pathway. Furthermore, we consider the two different El Niño flavors, EP and CP El Niño, so that the ENSO asymmetry in the stratosphere is addressed in a novel fashion.

2 Data and Methods

2.1 Data

To address the goals of this thesis described in the previous section, we make use of a variety of datasets, from observations and reanalysis to a climate model grand ensemble. This section describes the principal characteristics of these datasets. For clarity, the data used in each of the next chapters is summarized at the end of the section in Table 2.2.

2.1.1 Observations

SST data are indispensable for ENSO studies and it is also of large relevance to address climate variability. Several historical SST data reconstructions have been created to provide a globally gridded SST datasets (Huang et al. 2015). In this thesis we made used of two SSTs datasets, HadISST and ERSSTv4. Besides, to avoid reanalysis limitations on surface fields, we used land based observations of precipitation and surface temperature from the CRU TS3.21 dataset. The details of these observational datasets are next described.

a) ERSSTv4

The Extended Reconstructed Sea Surface Temperature (ERSST) dataset version 4 (v4) (Liu et al. 2015; Huang et al. 2015) provides monthly-mean data

from 1854 to the present, in a 2º x 2º grid resolution. The reconstruction from 1975 to 2007 is based on the International Comprehensive Ocean–Atmosphere Data Set (ICOADS) release 2.5. From 2008 to the present, it receives data from the Global Telecommunications System (GTS) from the National Centers for Environmental Prediction (NCEP). Additionally, SSTA from in situ ships and buoys are included, after computing the anomalies for the 1971-2000 period climatology. Comparisons showed that ERSSTv4 SSTs are close to satellite based observations (Huang et al. 2015).

The United States National Oceanic and Atmospheric Administration (NOAA) Climate Prediction Center (CPC) uses the ERSSTv4 for monitoring ENSO. Likewise, based on this database, the NCEP/CPC provides the SST ENSO indices, computed as the averaged SST for the different El Niño regions (more details on ENSO indices are given in Section 2.2.1). The NCEP/CPC data is used in chapters 3 and 4 to identify ENSO events.

b) HadISST

The Hadley Centre Global Sea Ice and Sea Surface Temperature (HadISST1) dataset (Rayner et al. 2003) from the Met Office Hadley Centre for Climate Prediction and Research covers the globe, in a 1º x 1º resolution, from 1871 to the present. The SST observed data are obtained from individual ships from the Met Office Marine Data Bank (MDB). Since 1982 data from the GTS are also included. In addition, to improve the data coverage, monthly median SSTs from Comprehensive Ocean-Atmosphere Data Set (COADS) are used from 1971 to 1995. SST data is reconstructed by an interpolation process of the gridded observations. In chapter 5, where the model results are compared against observations, we focus more on the SSTs pattern than in previous chapters, so we preferred to use monthly-mean SSTs from HadISST, which provides a higher spatial resolution than ERSSTv4.

c) CRU TS3.21

The University of East Anglia Climatic Research Unit (CRU) time series version 3.21 dataset (Harris et al. 2014) offers monthly-mean time series of precipitation and surface temperatures at high resolution, 0.5º x 0.5º grid, and covering the global land surface. Data are obtained from CLIMAT monthly-mean data, based on data exchanged between countries under the World Meteorological Organization (WMO), Monthly Climatic Data for the World (MCDW) produced by the NOAA National Climatic Data Center (NCDC), and World Weather Records decadal data, exchanged between many National Meteorological Services and the NCDC. Overall, about 4000 stations records are obtained from 1901 to 2012. The latest version 4.00 provides data covering the period spanning from 1901 until 2015.

2.1.2 Reanalysis

Reanalysis data sets are an essential tool in atmospheric and climate research studies, as they provide climatological data with a global spatial coverage. Reanalysis are based in a forecast model with an assimilation scheme that for every time step, in a given period, assimilates observational data. The observational networks include several sources, such as radiosondes, ships, buoys, aircrafts, and satellites from 1979 onwards. Thus, a main constrain of the reanalysis is the variable time period and location of the observations, in particular during the pre-satellite era. Figure 2.1 provides a picture of the chronology of the types of observations assimilated by the JRA-55 reanalysis. The forecast model unifies the diverse sources and types of the assimilated observations, so the data are consistent in time with observations and with the physicals laws. Nevertheless, the changing observation system also introduces spurious variability and biases. In addition, different reanalysis present distinct outputs, because of the diversity in assimilation techniques and models used by each center, with different resolutions, lid heights or assimilated observations.

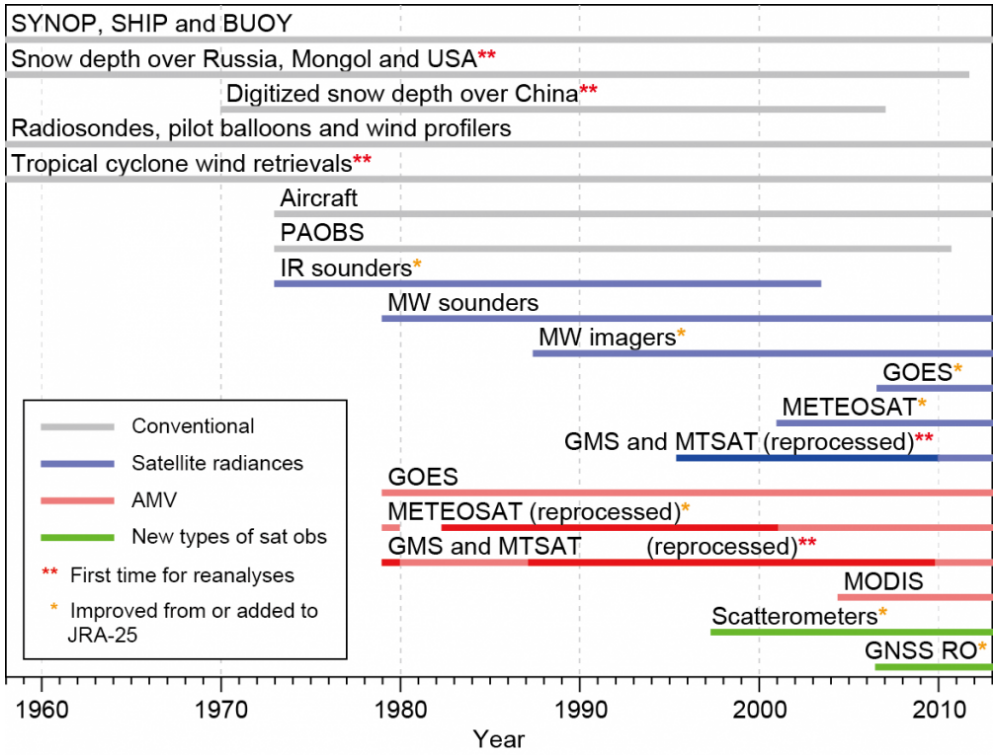

Figure 2.1. List of observational data available for JRA-55 with their corresponding period. Modified from Ebita et al. (2011).

In order to understand these differences and their causes, the SPARC (Stratosphere-troposphere Processes And their Role in Climate) community promoted a Reanalysis Intercomparison Project (S-RIP), connected to the SPARC data assimilation activity and mainly focused on comparing diagnostics in the upper troposphere, the stratosphere and the lower mesosphere across different reanalysis. Table 2.1, modified from Mitchell et al. (2015), summarizes 9 available reanalysis and their principal characteristics. The purpose of S-RIP is also to provide guidance to reanalysis users and to establish a better communication between the SPARC community and the reanalysis centers (Fujiwara et al. 2017). The S-RIP project includes the analysis of newer reanalyzes, with a high resolution and assimilated data from higher latitudes (e.g. ERA-Interim, JRA-55, MERRA), but also previous generation reanalysis, like

ERA-40 or NCEP-NCAR, which are widely used. Regarding the scope of this thesis, the analysis performed by Mitchell et al. (2015) within the S-RIP project, confirmed that the characteristic ENSO and QBO tropospheric and stratospheric signals, for the period from 1979 to 2009, are consistent across reanalysis. Analogously, SSW signatures are not sensitive to the reanalysis analyzed (Palmeiro et al. 2015), despite differences on the SSW frequency or the dates of occurrence across different reanalysis (Butler et al. 2017). To achieve the goals of this thesis, we use ERA-40, ERA-Interim and JRA-55 reanalysis, which are described in more detail next.

Table 2.1. Technical details of the reanalysis datasets. Modified from Mitchell et al. (2015).

Reanalysis	Centre	Period of available data	Horizontal resolution	# of model vertical levels	Lid height of forecast model (hPa)	Reference
MERRA	NASA	1979-Present	2/3◦lat× 1/2◦lon	72	0.01	Rienecker et al. (2011)
ERA-40	ECMWF	Sep 1957-Aug 2002	T159	60	0.1	Uppala et al. (2005)
ERA-Interim	ECMWF	1979-Present	T255	60	0.1	Dee et al. (2011)
JRA-25	JMA	1979-Jan 2014	T106	40	0.4	Onogi et al. (2007)
JRA-55	JMA	1958-Present	TL319	60	0.1	Kobayashi et al. (2015)
NCEP-NCAR (R1)	NOAA/ NCEP-NCAR	1948-Present	T62	28	3.0	Kalnay et al. (1996); Kistler et al. (2001)
NCEP-NCAR (R2)	NOAA/ NCEP-DOE	1979-Present	T62	28	3.0	Kanamitsu et al. (2002)
NCEP-CFSR	NOAA/ NCEP	1979-Present	T382 (T574 from 2010)	64	0.266	Saha et al. (2010)
NOAA-CIRES (20CR)	NOAA/ ESLR-CIRES	1871-2010	T62	28	2.511	Compo et al. (2011)

a) ERA-40 and ERA-Interim

ERA-40 (Uppala et al. 2005) and ERA-Interim (Dee et al. 2011) are the second and third generation reanalysis from the European Centre for Medium-Range Weather Forecasts (ECMWF). ERA-40 covers the period from September 1957 to August 2002 and ERA-Interim is available from January 1979 onwards, with time steps every 6 hours (00, 06, 12, 18 UTC). The horizontal resolution in ERA-40 is T159 (1.125º × 1.125º) and T255 (~0.7° x 0.7°) in ERA-Interim, although we selected data distributed in a horizontal grid of 2.5° × 2.5° for our study. Reanalysis output is provided in 60 model levels, from 1000 hPa to 0.1 hPa, even though we considered the 23 available pressure levels, from 1000 hPa to 1 hPa.

ERA-40 is based in a 6-hourly three dimensional variational (3D-Var) assimilation scheme, also used for the NCEP-NCAR reanalysis (Kalnay et al. 1996). In the pre-satellite period, stratospheric observations are retrieved from radiosonde and rocketsonde data. Since 1979, when ERA-40 started assimilating satellite radiance data, the coverage and quality of the data included have improved substantially. ERA-40 provides an acceptable accuracy for SSW occurrence and the QBO phases, although, it also presents some limitations. In particular, the Brewer-Dobson Circulation is too strong in the stratosphere and in the upper stratosphere temperatures are biased.

More recently, ECMWF developed ERA-Interim. ERA-Interim benefits of a 12-hourly 4D-var assimilation scheme, which results in a more effective use of the observations, presented in Figure 2.2 for the atmospheric component. Compared to ERA40, ERA-Interim provides an improved Brewer-Dobson circulation in the stratosphere (Fueglistaler et al. 2009). To analyze the largest reanalysis record possible, we consider both reanalysis together, ERA-40 is used from 1958 to 1978 and ERA-Interim from 1979 to 2013, similar to previous studies (e.g. Barriopedro and Calvo 2014; Palmeiro et al. 2015). Anomalies are computed after merging ERA-40 and ERA-Interim data products. We tested

different merging methods and we also compared ERA-40 and ERA-Interim anomalies for the common period in both reanalysis, resulting in negligible differences for our study. We make use of this merged reanalysis dataset to understand the differences between EP and CP El Niño events in chapter 4.

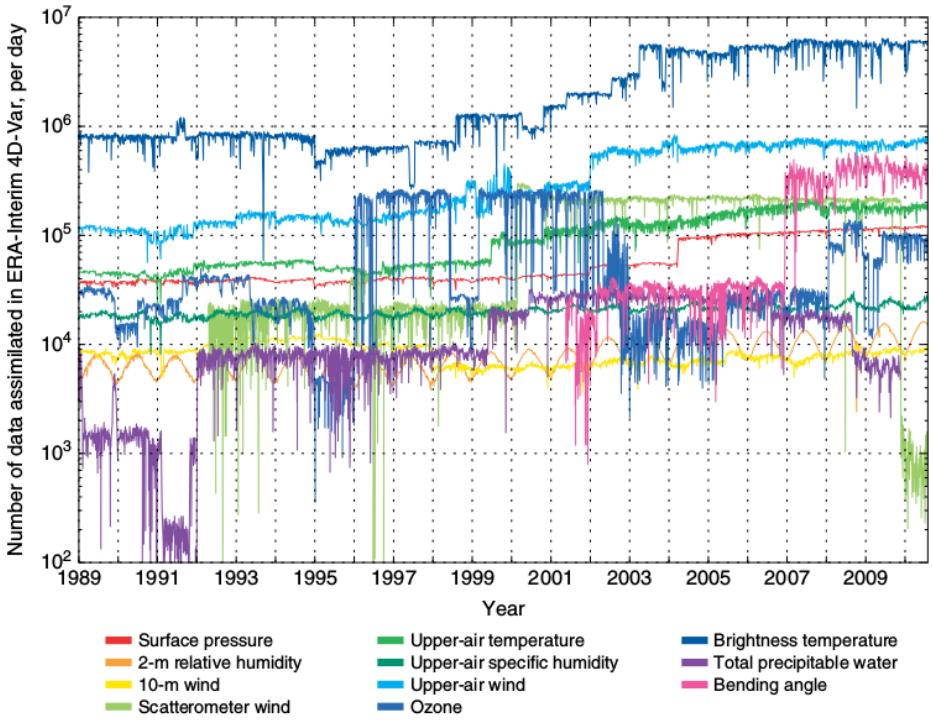

Figure 2.2. Daily counts, on a logarithmic scale, of observations assimilated in the atmospheric analysis component of ERA-Interim. From Dee et al. (2011).

b) JRA-55

The Japanese 55-year Reanalysis (JRA-55) (Ebita et al. 2011; Kobayashi et al. 2015; Harada et al. 2016), from the Japan Meteorological Agency, is the longest third generation reanalysis, as it covers the period from 1958 to the present. The JRA-55 is the updated and improved version of the Japanese 25-year Reanalysis (JRA-25) (Onogi et al. 2007). For the pre-satellite era the

assimilated observational data are the same as for ERA-40, while beyond 1979 it is the same as that included in JRA-25. The JRA-55 forecast model applies the 4D-Var assimilation scheme 6-hourly, with a TL319 (0.5625º x 0.5625º) resolution and 60 levels, up to 0.1 hPa. The JRA-55 reanalysis is used for the results in chapters 3 and 5, with the data distributed in a horizontal grid of 2.5° × 2.5° and 37 vertical pressure levels, ranging from 1000 to 1 hPa.

We have used different reanalysis datasets to achieve different goals of this thesis. Thus, ERA-40 and ERA-Interim were used in chapter 4 to understand the differences between EP and CP events, as there were the longest reanalysis datasets available at the time of the study. Later on, the studies of La Niña and the ENSO asymmetry (described in chapters 3 and 5 respectively) were carried based on the JRA-55 reanalysis. This change was motivated by the improvements of the assimilations schemes from ERA-40 to JRA-55 and because JRA-55 provided the most up to date reanalysis for the longer period (Mitchell et al. 2015). Nonetheless, all the results presented throughout the thesis hold for both reanalysis datasets and also for the NCEP-NCAR (R1) reanalysis (Kalnay et al. 1996; Kistler et al. 2001), which covers the period from 1948 to the present, but its lid is at 10 hPa and thus, it does not include levels in the upper stratosphere.

2.1.3 Model data

Climate model simulations are very useful tools to understand climate variability, as they provide a mathematical representation of the climate system and its interactions with other components of the Earth system. They comprehend long term integrations that can exceed the observational record, and provide data with good horizontal and vertical resolution, in comparison with the limitations of the observational networks, such as the insufficient ocean observations particularly in the SH (Taylor et al. 2012). Many current climate models also offer a well-represented stratosphere, motivated by the advances on

the knowledge of the stratosphere and its interaction with the troposphere in the past two decades (Gerber et al. 2012; Charlton-Perez et al. 2013). In this regard, for the first time, the Coupled Model Intercomparison Project phase 5 (CMIP5) (Taylor et al. 2012) included a large fraction of ocean-atmosphere coupled models with their lid above the stratopause. Long term CMIP5 experiments are performed by Earth system models (ESMs), which include at least an interactive carbon cycle. These core CMIP5 long-term experiments include a *historical* run that covers the industrial period (Taylor et al. 2012). The goal of these historical CMIP5 experiments is to simulate the climate, from 1850 to 2005, under the influence of natural and observed anthropogenic forcings, including: variations of the Earth orbit, solar irradiance, greenhouse gas concentrations, ozone depletions, trospospheric and stratospheric aerosols and changes on the land use. In this thesis we used the historical experiments of one of the models used in the CMIP5, the Max Planck Institute Earth System Model (MPI-ESM) Low Resolution (LR) model (Giorgetta et al. 2013)

a) MPI-ESM-LR

The MPI-ESM is a coupled general circulation model consisting in the ECHAM6 atmospheric component (Stevens et al. 2013), the MPIOM ocean model (Jungclaus et al. 2013), the JSBACH land model (Reick et al. 2013) and the HAMOCC model for marine biogeochemistry (Ilyina et al. 2013). The atmospheric model ECHAM6 (Stevens et al. 2013) is the latest version that followed the previous ECHAM5 atmospheric general circulation model (Roeckner et al. 2006). The LR configuration has a horizontal resolution of T63/1.9º and 47 vertical levels, with the top at 0.01hPa. In this configuration, the model is not able to reproduce a QBO. The ocean component MPIOM (Jungclaus et al. 2013) has a 1.5º horizontal resolution near the equator and 40 vertical levels, including prognostic sea ice. The spatial structure of ENSO and its power spectrum are realistically simulated by the LR model version

(Jungclaus et al. 2013). The precipitation shifts related to ENSO variability are also well reproduced by the atmospheric component (Stevens et al. 2013). Nevertheless, like other coupled models, the MPI-ESM has some caveats regarding the simulation of the SSTs in the upwelling regions west to the continents or the equatorial cold bias in the Pacific (Jungclaus et al. 2013).

In chapter 5 of this thesis, an ensemble of 100-member historical experiments of the MPI-ESM 1.1 version is used to investigate the asymmetry between El Niño and La Niña. This version of the model includes the release of the ECHAM6.3 atmospheric model, where bugs with respect to the CMIP5 version (MPI-ESM 1.0) were fixed. Each member of the historical experiments is integrated from 1850 to 2005, using the CMIP5 forcing, and each members is initialized from different years of a 2000-year preindustrial control simulation, performed with the same model. The different initial conditions support the independence of each realization. The output was saved in monthly means and in our study we only consider years from 1950 to 2005, for consistency with the reanalysis period (from 1958 to 2013).

Table 2.2. Summary of the datasets and periods used in each chapter.

	Chapter 3	*Chapter 4*	*Chapter 5*
Observations	ERSSTv4 (NCEP/CPC) & CRU TS 3.21 (1958 – 2012)	ERSSTv4 (NCEP/CPC) (1958 – 2013)	HadISST (1958 – 2013)
Reanalysis	JRA-55 (1958 – 2012)	ERA-40 & ERA-Interim (1958 – 2013)	JRA-55 (1958 – 2013)
Model data	-	-	MPI-ESM-LR (1950 – 2005)

2.2 Methods

2.2.1 Events detection

a) ENSO in observations

Several indices and methods have been used in the literature to characterize ENSO events. Most of them are either based on SLP differences across the Pacific Ocean (e.g. the Southern Oscillation Index, SOI; Kiladis and van Loon 1988; Larkin and Harrison 2002) or on SSTA averages over certain regions in the tropical Pacific Ocean (Rasmusson and Carpenter 1982; Trenberth 1997). In addition, other indices based on subsurface ocean temperatures (Yu et al. 2011), sea surface salinity (Singh et al. 2011), OLR anomalies (Chiodi and Harrison 2013) or a Multivariate ENSO Index (MEI) (Randel et al. 2009) have been used in the literature.

The canonical El Niño have been traditionally identified based on the SSTA average over the Niño3 region (N3) (5°N-5°S, 150°W-90°W) (Trenberth 1997) indicated in Figure 2.3. More recently, the Niño3.4 region (N34) (5ºN-5ºS, 170ºW-120ºW) (Trenberth and Stepaniak 2001) has also been widely used for El Niño events, particularly because the WMO identified it as the key region to define El Niño events.

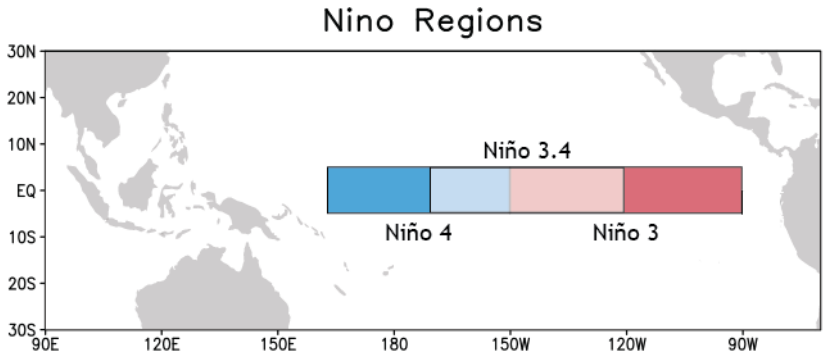

Figure 2.3. Niño regions locations. Modified from NCEP/CPC NOAA.gov

The identification of El Niño flavors leads to a wide range of new definitions, especially to identify the distinct CP El Niño events. Among them, the Trans-Niño index (TNI) (Trenberth and Stepaniak 2001) or El Niño Modoki index (EMI) (Ashok et al. 2007), both based on SSTA. In fact, most used indices are constructed based on anomalies, analyzed by computing their standard deviation (SD) (Kug et al. 2009; Yeh et al. 2009) or performing a principal component analysis (PCA) (Kao and Yu 2009; Yu et al. 2012). These studies employed the Niño4 (N4) (5°N-5°S, 160°E-150°W) region to characterize CP El Niño events, in contrast with the N3 region, which is used to define EP El Niño winters.

In this thesis, to compare the responses to EP and CP El Niño events, we also define EP and CP El Niño events based on the N3 and N4 regions. SST data for N3 and N4 regions are retrieved from NCEP/CPC. After detrending each time series, anomalies are computed and standardized for the November-December-January-February (NDJF) mean and with respect to the period that spans from 1958 to 2013. Then, the selection of the events is based on standardized NDJF ERSSTv4 SSTA from NCEP/CPC. To assure that the same winter is not classified as both EP and CP events, we follow the next methodology: EP El Niño winters are identified whenever N3 exceeds 0.5 SD and N3 is larger than 0.1 times the absolute N4 value. Analogously, CP El Niño winters are defined whenever N4 exceeds 0.5 SD and N4 is larger than 0.1 times the absolute N3 value. Table 2.3 lists the 6 EP and 10 CP El Niño winters identified from 1958 to 2013 using the NCEP/CPC based on ERSSTv4. The corresponding NDJF SSTA spatial pattern is shown in Fig. 1.6.

Table 2.3. Identified EP and CP El Niño winters using the NCEP/CPC index and HadISST observation. For each case the used threshold is indicated. SSWs central dates.

EP El Niño		**CP El Niño**		**SSWs**
NCEP/CPC 0.5 SD	HadISST 1 SD	NCEP/CPC 0.5 SD	HadISST 1 SD	ERA-40 & ERA-Interim
1965/66	1965/66	-	-	16 Dec/23 Feb
-	-	1968/69	1968/69	28 Nov/13 Mar
1972/73	1972/73	-	-	31 Jan
1976/77	-	-	-	9 Jan
-	-	1977/78	-	-
1982/83	1982/83	-	-	-
1986/87	1986/87	-	-	23 Jan
-	-	1987/88	1987/88	7 Dec/14 Mar
-	-	1990/91	-	-
-	1991/92	-	-	-
-	-	1994/95	1994/95	-
1997/98	1997/98	-	-	-
-	-	2001/02	-	30 Dec
-	-	2002/03	2002/03	18 Jan
-	-	2004/05	2004/05	-
-	-	2006/07	-	24 Feb
-	-	2009/10	2009/10	9 Feb

Furthermore, to test our results to different CP El Niño definitions we explore three different indices of CP El Niño used in the literature and analyzed also by Garfinkel et al. (2013) (see Fig. 1.10). El Niño Modoki (EMI) index (Ashok et al. 2007), named as Modoki by Garfinkel et al. (2013), is characterized by a tripolar structure of the SSTA and it is defined based on SSTA averaged over 3 regions: A (165ºE–140ºW, 10ºS– 10ºN), B (110ºW–70ºW, 15ºS–5ºN) and C (125ºE– 145ºE, 10ºS–20ºN), and computed as follows: $EMI = [SSTA]_A - 0.5[SSTA]_B - 0.5[SSTA]_C$ The index noted as Nin4>Nin3 follows the definition applied by Hurwitz et al. (2011) based on the N3 and N4 indices. In particular, CP El Niño events are selected when N4 and N3 region anomalies exceed the 0.5 SD threshold and N4 is larger than N3. The third definition from Garfinkel et al. (2013) is based on the study from Trenberth and Stepaniak (2001). This index introduces a difference between the normalized anomalies using the next equation: $Niño4 = 1.5 \times N4 - 0.5 \times N3$. Then, it is referred as 1.5N4-0.5N3. We have analyzed the largest composite sizes used by Garfinkel et al. (2013) to increase the number of cases when stratifying according to SSWs. The Hegyi-Deng index, used in Garfinkel et al. (2013), has been omitted because two of the winters identified by Garfinkel et al. (2013) as CP El Niño, 1982/83 and 1997/98, are usually considered EP El Niño winters (e.g., Kao and Yu, 2009; Kug et al., 2009; Hegyi and Deng, 2011; Hurwitz et al., 2011). Instead, we have included the definition of CP El Niño winters used by Sung et al. (2014), which is based on the N3 and N4 regions classification from Yeh et al. (2009), using non-detrended SST data. The considered indices and corresponding winters are listed in Table 2.4. For comparison the first column in Table 2.4 shows the same CP El Niño winters indicated in Table 2.3.

Table 2.4. (Left) CP El Niño winters[a] identified in this study using the NCEP/CPC index, (middle) winters defined by Garfinkel et al. (2013) and (right) by Sung et al. (2014)[b].

NCEP/CPC 0.5 SD	From Garfinkel et al. (2013)			Sung et al. (2014)
CP El Niño	**Modoki[c]**	**Nin4>Nin3[d]**	**1.5N4-0.5N3[e]**	**Sung2014**
-	1963/64	-	-	-
-	1965/66[f]	-	-	-
-	1967/68[g]	-	-	-
1968/69[f]	1968/69[f]	1968/69[f]	1968/69[f]	1968/69[f]
1977/78	1977/78	1977/78	-	1977/78
-	-	-	-	1979/80[g]
1987/88[f]	-	-	-	-
1990/91	1990/91	1990/91	1990/91	1990/91
-	1991/92	-	-	-
-	-	-	-	1992/93
1994/95	1994/95	1994/95	1994/95	1994/95
-	-	1996/97	-	-
2001/02[f]	-	2001/02[f]	-	2001/02[f]
2002/03[g]	-	-	2002/03[g]	2002/03[g]
2004/05	2004/05	2004/05	2004/05	2004/05
-	-	2005/06[g]	-	-
2006/07[g]	-	2006/07[g]	2006/07[g]	-
2009/10[g]	-	-	-	-

[a] CP El Niño: N4 > 0.5 SD and N4 > 0.1 x N3.
[b] CP El Niño classification based on Yeh et al. (2009).
[c] EMI index (Ashok et al. 2007; Zubiaurre and Calvo, 2012).
[d] N3 and N4 > 0.5ºC and N4 >N3, similar to Hurwitz et al. (2011).
[e] 1.5 x N4 – 0.5 x N3, similar to Trenberth and Stepaniak (2001).
[f] Winter with early winter SSW occurrence.
[g] Winter with late winter SSW occurrence.

Likewise, to identify La Niña events a diversity of indices has been also used in the literature. Some studies considered the SSTA mean of the different oceanic regions, such as N3 (Hoerling et al. 1997; Manzini et al. 2006) or N4 (Kug and Ham 2011). However, most recent studies used the N34 region and the Niño34 index from NCEP/CPC (e.g., Free and Seidel 2009; Butler and Polvani 2011; Garfinkel et al. 2012; Butler et al. 2014; Barriopedro and Calvo 2014; Domeisen et al. 2015), since this is the region that better captures the centrally located La Niña SST pattern. In addition, these La Niña indices have been computed using SSTA (e.g., Butler and Polvani 2011; Garfinkel et al. 2012) or their standardized values (e.g., Hoerling et al. 1997; Mitchell et al. 2011). Regarding the threshold used to select events, some studies identified La Niña events as those with N34 values below -0.5 ºC (Domeisen et al. 2015) or below -0.7 SD (Pozo-Vázquez et al. 2005), while other studies applied more restrictive thresholds of -1 K (Free and Seidel 2009) or -1 SD (Mitchell et al. 2011). As discussed in the Introduction, the use of unequal thresholds could lead to a diverse range of responses.

To address this issue, we define La Niña winters using the N34 region SST data from NCEP/CPC, based on the ERSSTv4 dataset. After detrending, NDJF averaged SSTA are computed for the 1958 to 2012 climatological period and standardized for that same period. Based on the SSTA N34 index La Niña winters are selected considering two thresholds: -1 SD and -0.5 SD. La Niña events selected below -1 SD will be referred to as *strong La Niña* events (8 events), whereas the events identified below -0.5 SD will be named *extended La Niña* events (20 events). Table 2.5 lists the La Niña winters identified by both thresholds. For comparison, we included the winters identified by Free and Seidel (2009) and Butler and Polvani (2011) who used thresholds of -1 and -0.5 ºC respectively. The comparison shows that for the same period, the use of SST anomalies or their SD does not change the identified La Niña winters (see Table 2.5). Neutral winters are defined as winters with no El Niño or La Niña events.

To make sure neutral years do not include any ENSO signal, we have chosen the threshold of 0.5 SD for El Niño and -0.5 SD for La Niña in the N34 region.

Table 2.5. La Niña winters selected using NCEP/CPC for -1 SD and -0.5 SD thresholds and using HadISST for -1 SD. La Niña winters identified by Free and Seidel (2009) and Butler and Polvani (2011) are also listed. The threshold and analysis periods used in this thesis are indicated and noted by italics. SSWs central dates and QBO phases are also included.

La Niña winters					**SSWs**	**QBO**
NCEP/ CPC *-1 SD* *1958-12*	HadISST *-1 SD* *1958-13*	Free & Seidel -1 K 1958-05	*NCEP/ CPC* *-0.5 SD* *1958-12*	Butler & Polvani -0.5 ºC 1958-10	JRA-55 *1958-12*	
-		-	1962/63	1962/63	30 Jan	-
-		-	1964/65	1964/65	-	W
-		-	1967/68	1967/68	7 Jan	W
1970/71	1970/71	1970/71	1970/71	1970/71	18 Jan / 20 Mar	E
-		-	1971/72	1971/72	-	W
1973/74	1973/74	1973/74	1973/74	1973/75	-	W
-		-	1974/75	1974/75	-	E
1975/76	1975/76	1975/76	1975/76	1975/76	-	W
-		-	1983/84	1983/84	24 Feb	-
-	1984/85	-	1984/85	1984/85	1 Jan	E
1988/89	1988/89	1988/89	1988/89	1988/89	21 Feb	W
-		-	1995/96	1995/96	-	W
1998/99	1998/99	1998/99	1998/99	1998/99	15 Dec / 26 Feb	E
1999/00	1999/00	1999/00	1999/00	1999/00	20 Mar[a]	W
-		-	2000/01	2000/01	11 Feb	-
-		-	2005/06	2005/06	21 Jan	E
2007/08	2007/08	-	2007/08	2007/08	22 Feb	E
-		-	2008/09	2008/09	24 Jan	W
2010/11	2010/11	-	2010/11	-	-	W
-		-	2011/12	-	-	W

[a]Due to the occurrence of a late winter SSW, for our study purposes, this winter is considered as a winter without SSWs.

b) ENSO in the model simulations

Model simulations are used in chapter 5 to investigate the asymmetry between El Niño and Niña. As discussed before, two distinguishable El Niño flavors (EP and CP) appeared in the observational record, characterize by the N3 and N4 regions, but only one type of La Niña, centered in the N34 region. This observed ENSO diversity is not always well captured by general circulation models (Yu and Kim 2010; Kim and Yu 2012), so we first verify that the model used in this thesis is able to reproduce the observations. Then, we investigate the SSTA behavior in the N3, N4 and N34 regions in both warm and cold ENSO phases. To perform this analysis, the model results are compared against HadISST observations as they provide higher spatial resolution than the ERSSTv4.

For both observations and the model, anomalies are computed with respect to the 30-year period from 1971 to 2000. In the model, a preliminary analysis confirmed that differences among the climatology of the 100 members are negligible. Thus, we compute the standardized NDJF averaged SSTA over the referred 3 regions: N3, N4 and N34. To identify El Niño and La Niña winters in each region in the HadISST dataset, we use the 1 SD or -1 SD thresholds, respectively. That is, EP El Niño and EP La Niña winters are selected whenever N3 region SSTA anomalies are above 1 SD and below -1 SD, respectively, and when the absolute N3 value is larger the absolute N4 value. CP El Niño and CP La Niña winters are defined analogously. La Niña events are selected considering winters with N34 values below -1 SD. These events correspond with the strong La Niña events defined in the previous section. In the model the same procedure is followed to select the events for each member. See details in Table 2.6.

Table 2.6. Summary of the dataset and definitions used in each chapter to identify the events. The observed winter's selection is shown in Tables 2.3 and 2.5.

	Chapter 3	*Chapter 4*	*Chapter 5*	
ENSO	NCEP/CPC	NCEP/CPC	HadISST	MPI-ESM-LR
Strong La Niña	N34 < -1 SD	-	N34 < -1 SD	N34 < -1 SD
Extended La Niña	N34 < -0.5 SD	-	-	-
EP El Niño	-	N3 > 0.5 SD & N3 > 0.1 N4	N3 > 1 SD & N3 > N4	N3 > 1 SD & N3 > N4
CP El Niño	-	N4 > 0.5 SD & N4 > 0.1 N3	N4 > 1 SD & N4 > N3	N4 > 1 SD & N4 > N3

Figure 2.4 shows the NDJF averaged SSTA, from 120ºE to 270ºE and averaged 5ºS-5ºN, composited for EP El Niño, CP El Niño, EP La Niña and CP La Niña winters for (Fig. 2.4a) the HadISST dataset and (Fig. 2.4b) each member of our ensemble (with HadISST overlaid in black). HadISST and the ensemble members agree in the anomalies of the two flavors of El Niño (EP and CP), being the SSTAs associated with EP El Niño skewed to larger positive values in the eastern Pacific. We can therefore corroborate the two distinct EP and CP El Niño types in the model. In contrast, EP and CP La Niña composited SSTA behave similarly in agreement with observations. In fact, model and observations highlight a unique central La Niña based on the N34 index, as shown in Fig. 2.4c. We can therefore conclude that the MPI-ESM model reproduces the previously observed properties for the two El Niño flavors and a single La Niña (Kug and Ham 2011). In this fashion, for the HadISST dataset, we identified 6 EP El Niño winters, 6 CP El Niño winters and 9 strong La Niña events. This selection of winters agrees well with those identified using the ERSSTv4 NCEP/CPC (see Tables 2.3 and 2.5). The slight disagreement for strong La Niña (one more winter in HadISST) is due to the different climatology used in HadISST to match the model. For CP El Niño, a higher threshold leads to a reduced number of El CP Niño winters (6 against 10). For EP El Niño, the same number of winters is reported, but with a few disagreements, 1991/92 is selected now, instead, 1976/77 is not. Nonetheless, these differences do not alter our results. For clarity Table 2.6 summarizes the datasets and the definitions used to select the diverse ENSO winters in each chapter.

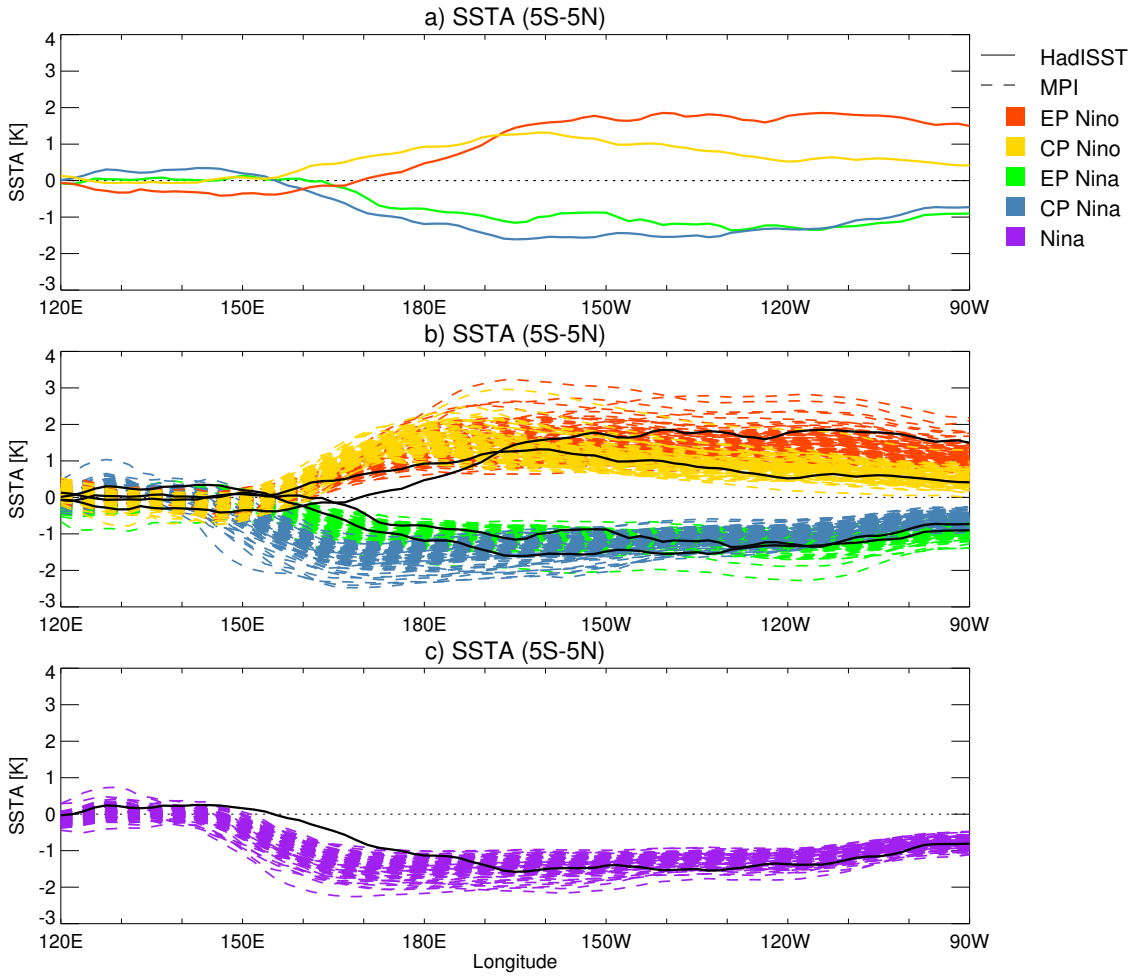

Figure 2.4. Evolution in longitude of the SSTA, averaged between 5ºS-5ºN and NDJF, composited for EP El Niño (red), CP El Niño (yellow), EP La Niña (green) and CP La Niña (blue) winters for (a) HadISST (solid lines) and (b) MPI-ESM individual members (dashes lines), with HadISST values from panel a) superimposed (black solid lines). (c) Evolution of the composited SSTA during strong La Niña for HadISST (solid black line) and MPI-ESM members (purple dashes lines).

c) SSWs

Major SSWs are defined following the criteria of Charlton and Polvani (2007), based on the zonal-mean zonal wind reversal at 10 hPa and 60°N from November to March. For the EP and CP El Niño study, based on ERA-40 and ERA-Interim, the list of SSWs in shown in table 2.3. Note that the frequency of occurrence of SSWs is similar in EP and CP El Niño winters. The central dates of the SSWs that occurred during La Niña winters, based on the JRA-55, are listed in Table 2.5 and agree with those found by Nishii et al. (2011) and Taguchi (2015), using the same Japanese reanalysis. As mentioned previously, differences across reanalysis on the detection of SSW are already documented (Charlton and Polvani 2007; Palmeiro et al. 2015) and do not alter our results in terms of ENSO.

d) QBO

The QBO phases are evaluated in this section to investigate La Niña stratospheric pathway in chapter 3. The QBO phases are defined using the 5ºS–5ºN average zonal-mean zonal wind at 50 hPa, which is close to the most favorable level to find a link with the NH, as reported by Baldwin and Dunkerton (1998). Following the definition used by Butler et al. (2016), westerly QBO phases are classified whenever the zonal-mean zonal wind in November is above 5 m s^{-1}, while easterly QBO phases are identified whenever the zonal-mean zonal wind in November is below -5 m s^{-1}. The phases of the QBO that occur during La Niña events identified in our study are noted in Table 2.5.

2.2.2 Dynamical analysis

a) The Transformed Eulerian-Mean equations

To analyze the different phenomena that occur in the stratosphere, the Eulerian Mean approach is useful (Andrews et al. 1987), as it separates the atmospheric variables into a mean and its disturbances (the eddies) with respect

to that mean. The example below, from Andrews et al. (1987, section 3.3), shows the definition of the zonal mean, denoted by an over bar, and the departure from the zonal mean, the eddy component, denoted by a prime for the zonal wind (u).

$$\bar{u}(\phi,z,t) = (2\pi)^{-1}\int_0^{2\pi} u(\lambda,\phi,z,t)d\lambda \tag{2.1}$$

$$u'(\lambda,\phi,z,t) \equiv u - \bar{u} \tag{2.2}$$

λ and ϕ denote the longitude and latitude horizontal coordinates and z and t are the vertical and temporal coordinates. Likewise, when the departure is computed with respect to a temporal mean, for a given climatological period, the perturbation in this case is referred as anomaly. The zonal average, the eddy component, as well as the temporal mean (or climatology) and the anomalies are widely used in this thesis.

In the stratosphere, the zonal-mean flow and their perturbations or eddies closely interact with each other. That is, the mean flow can modulate the propagation of eddies, while in turn, the eddies can modulate the mean flow. To characterize this wave-mean flow interactions, a modified version of the Eulerian mean equations is used in practice, the Transformed Eulerian Mean (TEM). The TEM formulation approximates the eddy effects as wave induced forces (Holton et al. 1995) and its advantage is that, neglecting small terms in the thermodynamics equation, the wave's forcing only appears in the momentum equation, simplifying substantially the physical interpretation of the interaction between the mean flow and the waves. Substituting the Eulerian zonal-mean circulation $(0,\bar{v},\bar{w})$, where $\bar{v}$ and $\bar{w}$ are the zonal mean of the meridional and vertical components respectively, by the residual mean meridional circulation $\left(0,\bar{v}^*,\bar{w}^*\right)$:

$$\bar{v}^{*} \equiv \bar{v} - \rho_0^{-1}\left(\rho_0 \frac{\overline{v'T'}}{\bar{T}_z} \right)_z \tag{2.3a}$$

$$\bar{w}^{*} \equiv \bar{w} + \left(a\cos\phi\right)^{-1}\left(\cos\phi \frac{\overline{v'T'}}{\bar{T}_z} \right)_\phi \tag{2.3b}$$

The TEM zonally averaged momentum equation in spherical log-pressure coordinates is obtained:

$$\bar{u}_t + \bar{v}^{*}\left[\left(a\cos\phi\right)^{-1}\left(\bar{u}\cos\phi\right)_\phi - f \right] + \bar{w}^{*}\bar{u}_z = \left(\rho_0 a\cos\phi\right)^{-1} \nabla \cdot \mathbf{F} + \bar{X} \tag{2.4}$$

Where ρ_0 is the basic density, *f* the Coriolis parameter, *a* is the radius of the earth and $\bar{X}$ represents the non-conservative forcings, such as friction or gravity-wave drag. Subscripts denote partial derivatives. The vector $\mathbf{F} \equiv (0, F^{(\phi)}, F^{(z)})$ is the Eliassen–Palm (EP) flux (Eliassen and Palm 1961), given by the horizontal and the vertical components in spherical and log-pressure coordinates:

$$F^{(\phi)} \equiv \rho_0 a\cos\phi\left(\bar{u}_z \frac{\overline{v'T'}}{\bar{T}_z} - \overline{v'u'}\right) \tag{2.5a}$$

$$F^{(z)} \equiv \rho_0 a\cos\phi\left\{ \left[f - \left(a\cos\phi\right)^{-1}\left(\bar{u}\cos\phi\right)_\phi \right] \frac{\overline{v'T'}}{\bar{T}_z} - \overline{w'u'} \right\} \tag{2.5b}$$

Eliassen and Palm (1961) considered steady linear waves on a basic zonal flow, where non-conservative forcings are neglected, so the EP flux divergence, defined in Eq. (2.6), gathers the eddy terms of the zonal momentum equation of the TEM formulation .

$$\nabla \cdot \mathbf{F} \equiv \left(a\cos\phi\right)^{-1} \frac{\partial}{\partial\phi}\left(F^{(\phi)}\cos\phi \right) + \frac{\partial F^{(z)}}{\partial z} \tag{2.6}$$

The EP flux and its divergence are measures of the planetary waves propagation and dissipation in the stratosphere (Andrews et al. 1987). The horizontal

component of the EP Flux, Eq. (2.5a), is dominated by the meridional eddy momentum flux ($\overline{v'u'}$) and the main contributor to the vertical component, in Eq. (2.5b), is the zonal-mean eddy meridional heat flux ($\overline{v'T'}$), which provides information related to the wave activity penetrating into the stratosphere (Newman et al. 2001). Indeed, Newman et al. (2001) found a high correlation between the mid-late winter eddy heat flux at 100hPa and the polar stratospheric temperature in late winter. In this thesis, to investigate the ENSO impact on the stratosphere, we will analyze the anomalies, with respect to the climatology, of the zonal-mean meridional eddy heat flux during ENSO events. The calculation of these anomalies is explained in detail next.

b) Anomalous zonal-mean meridional eddy heat flux

Based on the framework from Nishii et al. (2009), the anomalous zonal-mean meridional eddy heat flux can be decomposed as follows into two terms, one that represents the interference between the climatological and anomalous planetary waves and another that represents the contribution of the anomalous wave propagation (Eq. 2.12). This decomposition is used in chapter 3 to investigate the upward wave activity during La Niña winters.

To reach this decomposition, first, the total eddy heat flux anomaly can be written as:

$$\overline{v'T'}_a = v'T' - \overline{v'T'}_c \tag{2.7}$$

where v and T denote the meridional wind and temperature, respectively. The subscripts 'c' and 'a' stand for the climatology and the daily anomaly. Note that Nishii et al. (2009) notation uses asterisks to indicate the eddy components (perturbations with respect to the zonal mean) and vertical bars for the zonal mean. Anomalies for the meridional wind and the temperature are defined as follows:

$$v'_a = v' - v'_c \tag{2.8}$$

$$T'_a = T' - T'_c \tag{2.9}$$

Thus, considering the decompositions in Eq. (2.8) and (2.9), the anomalous eddy heat flux in Eq. (2.7) can be written as:

$$\begin{aligned}\overline{v'T'}_a &= \left(v'_a + v'_c\right)\left(T'_a + T'_c\right) - \overline{\left(v'_a + v'_c\right)\left(T'_a + T'_c\right)}_c \\ &= v'_a T'_a + v'_a T'_c + v'_c T'_a + v'_c T'_c \\ &\quad - \overline{\left(v'_a T'_a\right)}_c - \overline{\left(v'_a T'_c\right)}_c - \overline{\left(v'_c T'_a\right)}_c - \overline{\left(v'_c T'_c\right)}_c\end{aligned} \tag{2.10}$$

Since

$$\overline{\left(v'_a T'_c\right)}_c = 0 \text{ and } \overline{\left(v'_c T'_a\right)}_c = 0\,, \tag{2.10a}$$

while

$$v'_c T'_c = \overline{\left(v'_c T'_c\right)}_c \tag{2.10b}$$

$$\overline{\left(v'_a T'_a\right)}_a = v'_a T'_a - \overline{\left(v'_a T'_a\right)}_c \tag{2.10c}$$

Then it follows:

$$\begin{aligned}\overline{v'T'}_a &= v'_a T'_c + v'_c T'_a + v'_c T'_c + \overline{\left(v'_a T'_a\right)}_a - v'_c T'_c \\ &= v'_a T'_c + v'_c T'_a + \overline{\left(v'_a T'_a\right)}_a\end{aligned} \tag{2.11}$$

Each term of the Eq. (2.11) is computed for each day of every year. To focus on understanding the upward wave activity during ENSO winters, composites for the selected ENSO winters are performed next:

$$\left\langle \overline{v'T'}_a \right\rangle = \left\langle v'_a T'_c + v'_c T'_a \right\rangle + \left\langle \overline{\left(v'_a T'_a\right)}_a \right\rangle \tag{2.12}$$

where the <> denote the composite mean.

Equation (2.12) means that the sum of $\langle v'_a T'_c + v'_c T'_a \rangle$ and $\langle \overline{(v'_a T'_a)}_a \rangle$ is exactly equal to the composited $\langle \overline{v'T'}_a \rangle$ total eddy heat flux anomaly. Following Nishii et al. (2011), the term $\langle v'_a T'_c + v'_c T'_a \rangle$ is referred as the interference term, as it accounts for the interference between the climatological stationary waves and the anomalous waves. The second term $\langle \overline{(v'_a T'_a)}_a \rangle$ is the anomalous wave packet term and it reflects the activity of the anomalous wave itself. Thus, the advantage of Eq. (2.12) is that the composited anomalous total heat flux can be decomposed into the interaction between the anomalies and the planetary waves and the sole contribution of these waves anomalies.

2.2.3 Statistical analysis

a) Composites

In the following chapters results are mainly presented as winter monthly-mean composites, although the signals have also been investigated month to month. Before compositing, reanalysis time series for each field are detrended by applying a linear regression. In the reanalysis dataset the polar stratospheric response is investigated in the December–January–February (DJF) average, whereas the November- December (ND) or the November–December–January (NDJ) averages are used to analyze the preceding mechanisms. The surface impact is analyzed in January–February (JF), when the largest signals are observed. In the model, we found that the largest anomalies are lagged around one month with respect to the reanalysis, so for the corresponding analysis and comparison with the reanalysis, January-February-March (JFM), DJF and February-March (FM) averages are considered for the composites.

b) Asymmetry evaluation

To evaluate the symmetry and the asymmetry between El Niño and La Niña in chapter 5, we follow Hoerling et al. (1997), so that the asymmetric component of the ENSO signal is defined as the sum of El Niño and La Niña composited anomalies, while the symmetric component is defined as the difference of El Niño minus La Niña composited anomalies. Given our approach, two asymmetries and symmetries are defined for each field and each realization: EP El Niño+La Niña and CP El Niño+La Niña, EP El Niño-La Niña and CP El Niño-La Niña. To quantify what we refer as the degree of asymmetry, and following Zhang et al. (2014), we compute in a monthly-mean basis the root-mean-square (RMS) of the asymmetry (over area- and pressure-weighted regions) for different relevant fields. This is a widely used statistic to measure absolute differences (Taylor 2001). To evaluate the asymmetry in the stratospheric ENSO pathway the following RMS diagnostics are employed: 1) NDJF mean of the SSTA over the Pacific equatorial area covering the three ENSO regions (160ºE-270ºE, 10ºS-10ºN); 2) December-January-February (DJF) mean of the eddy geopotential height anomalies (Z'a) at 500 hPa over the Pacific North American region (120ºE-60ºW, 30ºN-75ºN); 3) January-February-March (JFM) mean of the zonal-mean zonal wind anomalies (Ua) between 10-30hPa and 50ºN-80ºN and; 4) February-March (FM) mean of the sea level pressure anomalies (SLPa) over the NAE region (25ºW-30ºE, 20ºN-90ºN).

c) Correlation analysis

In chapters 3 and 5, to measure the association between two variables, the Pearson coefficient of linear correlation (r) is calculated (Gorgas García et al. 2011). Given variables x and y, the Pearson correlation is defined in Eq. (2.13) as the ratio of the sample covariance of the two variables to the product of the two standard deviations.

$$r_{xy} = \frac{Cov(x,y)}{s_x s_y} = \frac{n\sum x_i y_i - \sum x_i \sum y_i}{\sqrt{\left(n\sum x_i^2 - \left(\sum x_i\right)^2\right)\left(n\sum y_i^2 - \left(\sum y_i\right)^2\right)}} \quad (2.13)$$

d) Statistical significance

The statistical significance (when indicated) is assessed with a Monte Carlo test of 1000 random subsamples. For the reanalysis, random groups, with the same number of winters as those included in the composites we want to test, are selected from the entire period and composited afterwards to create the Monte Carlo distribution. We found that 1000 random subsamples were enough to create a robust distribution. For the model, a similar procedure is followed and random winters are chosen within the model members used to make the composite. In both cases, the signal is statically significant at the 90% (95%) confidence level whenever the value from the reanalysis or member's composited value is below the 5th (2.5th) or above the 95th (97.5th) percentile of the corresponding Monte Carlo distribution.

A Student's *t*-test is also applied, when necessary. The t-test is a parametric test based on the null hypothesis that a sample mean $\bar{x}$, with a standard deviation s, has been drawn from a population with a mean μ and a standard deviation σ (Gorgas García et al. 2011). The statistics t-test is given by Eq. (2.14), with (n-1) degrees of freedom:

$$t_{n-1} = \frac{\bar{x} - \bar{\mu}}{s/\sqrt{n}} \quad (2.14)$$

To compare the means of two samples that follow a normal distribution, the t-test is a parametric test based on the null hypothesis that two random samples have equal means (Gorgas García et al. 2011). The statistics test for the case of unequal variances is given by Eq. (2.15):

$$t = \frac{\overline{x_1} - \overline{x_2}}{\sqrt{\frac{s_1^2}{n_1} + \frac{s_2^2}{n_2}}} \tag{2.15}$$

n_1, n_2 and s_1, s_2 are the sizes and the variances of the samples. The null hypothesis is rejected when t is outside an interval defined by f degrees of freedom, computed as in Eq. (2.16) and for the 90% confidence level.

$$f = \frac{\left(\frac{s_1^2}{n_1} + \frac{s_2^2}{n_2}\right)^2}{\frac{\left(s_1^2/n_1\right)^2}{n_1+1} + \frac{\left(s_2^2/n_2\right)^2}{n_2+1}} - 2 \tag{2.16}$$

The statistical significance of the correlation between two samples is assessed using a Student's t-test. The null hypothesis is that the two samples are independent and it is accepted when the statistic t, in Eq. (2.17), is outside an interval defined by n-2 degrees of freedom.

$$t = \frac{|r|\sqrt{n-2}}{1-r^2} \tag{2.17}$$

In this thesis the statistical significance of the correlations is calculated at the 95% the confidence level.

3 The Stratospheric Pathway of La Niña

As presented in the Introduction, the polar stratospheric response to La Niña winters appears to be weak or not significant in reanalysis datasets, although a robust response on the NAE region has been observed during La Niña winters. This chapter revisits the NH polar stratospheric pathway for La Niña events, based on the JRA-55 reanalysis data for the 1958-2012 period. We focus on the dynamical mechanisms in the troposphere-stratosphere coupling and the link between La Niña SSTA and a robust surface impact over Europe. Moreover, the previously reported lack of a robust polar stratospheric signature during La Niña winters is investigated, by studying the sensitivity of the signal to the threshold used to select the events and by analyzing SSW occurrence and the QBO phase's impact. The results of this chapter can be found in Iza et al. (2016).

3.1 La Niña stratospheric pathway

First, the response to strong La Niña events (those identified using the -1 SD threshold as explained in section 2.2.1) is analyzed (see Table 2.5 1st column). Figure 3.1 shows the latitude-pressure DJF average of the zonal-mean temperature (Fig. 3.1a) and zonal-mean zonal wind (Fig. 3.1b) composited for the strong La Niña events detected. In the tropics, La Niña signal is characterized by an anomalous significant cooling (about -0.7 K) in the troposphere and anomalous significant warming in the lower stratosphere. These anomalies in temperature are accompanied by a significant weakening of the subtropical jets. In the high latitudes, a significant cooling (peaking at about -3 K) appears in the stratosphere (from about 300 hPa to 10 hPa) together with a robust strengthening of the zonal-mean zonal winds that extends into the troposphere and reaches the surface. The observed significant temperature pattern was also reproduced in model simulations with the Whole Atmosphere Community Climate Model (WACCM) by Calvo et al. (2010). This robust pattern also holds for the NCEP-NCAR and ERA (ERA-40 for 1958-1978 and ERA-Interim for 1979-2012) reanalysis for the same period.

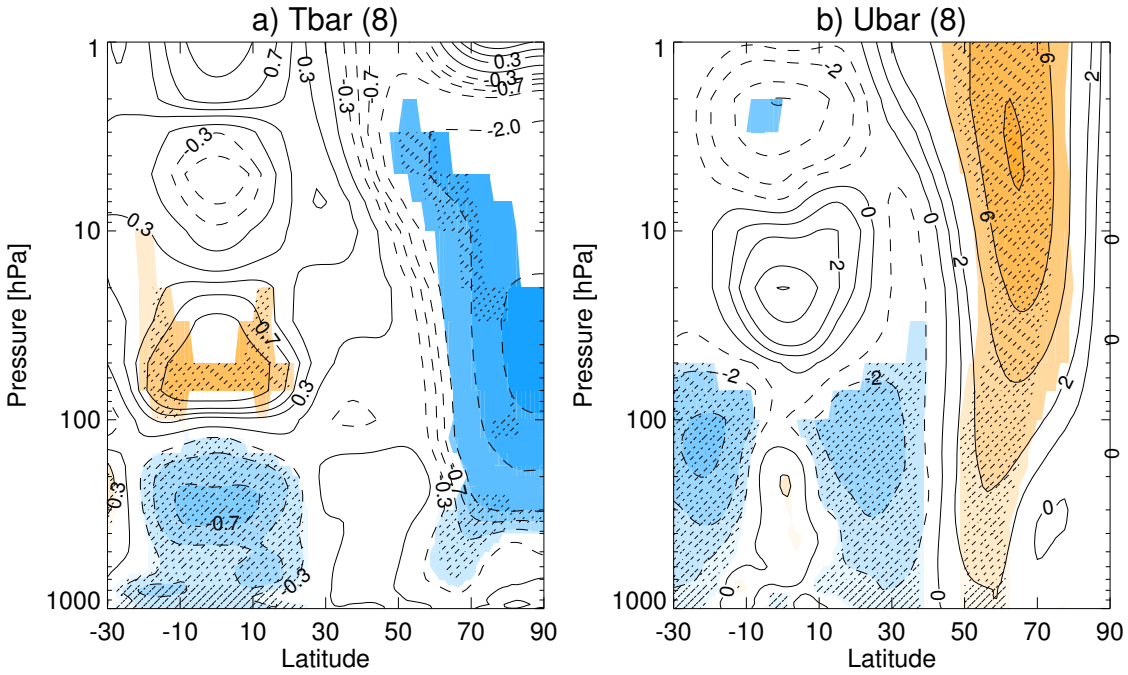

Figure 3.1. Latitude-pressure cross sections of the strong La Niña events (-1 SD threshold) composite of DJF average of monthly zonal-mean (a) temperature and (b) zonal wind anomalies. Contour intervals for temperature are ± 0.3, 0.5 and 0.7 K up to ± 1 K and every 1 K thereafter. Contours for zonal wind are ± 1 m s^{-1} up to ± 2 m s^{-1} and every 2 m s^{-1} thereafter. Solid (dashed) contours denote positive (negative) anomalies. Numbers in brackets indicate the number of winters in each composite. Colors indicate significant area at 90% confidence level and stippling indicates significance at the 95% level.

The identified significant stratospheric zonal-mean temperature and wind anomalies shown in Fig. 3.1 during strong La Niña events are indicative of a strong and cold polar vortex. The evolution of zonal-mean temperature and zonal wind throughout the winter is depicted in Figure 3.2, averaged from 70ºN to 90ºN for the former and 50ºN to 70ºN for the latter. Detailed inspection of these panels reveals a downward propagation of the anomalies from the upper stratosphere in early winter to the lowermost stratosphere and the troposphere in late winter (January-February). The large-scale character of the anomalies is demonstrated by the zonal-mean zonal wind significant anomalies (Fig. 3.2b), which reach the surface in January and February, in thermal wind balance with the temperature patterns. Fig. 3.2 also shows the evolution of the NAM index, which is a compact measure of the vortex strength (Baldwin and Dunkerton 2001) and stratosphere-troposphere coupling. The NAM index is computed by projecting daily geopotential height anomalies onto the first EOF of the 60-day low-pass geopotential height anomaly (20º-90ºN). The NAM index (Fig. 3.2c) shows significant positive values (red colors) reflecting a strong vortex, which is amplified in the lower stratosphere and shows a temporal development in line with the temperature and wind anomalies (Figs. 3.2a, b).

In summary, a robust polar stratospheric response, in the form of a stronger and colder polar vortex that reaches the surface is observed during strong La Niña winters. It is interesting to note that our results are based on a data record that includes two more events (the latest two events of 2007/08 and 2010/11 winters) than previous studies (Free and Seidel 2009; Mitchell et al. 2011), who did not find a robust signal in the polar lower stratosphere and the troposphere even though they used the same threshold (-1 SD). Therefore, with the caution of a still short dataset and the sampling uncertainty, we suggest that the use of a longer dataset helps to capture a significant stratospheric signal during strong La Niña winters.

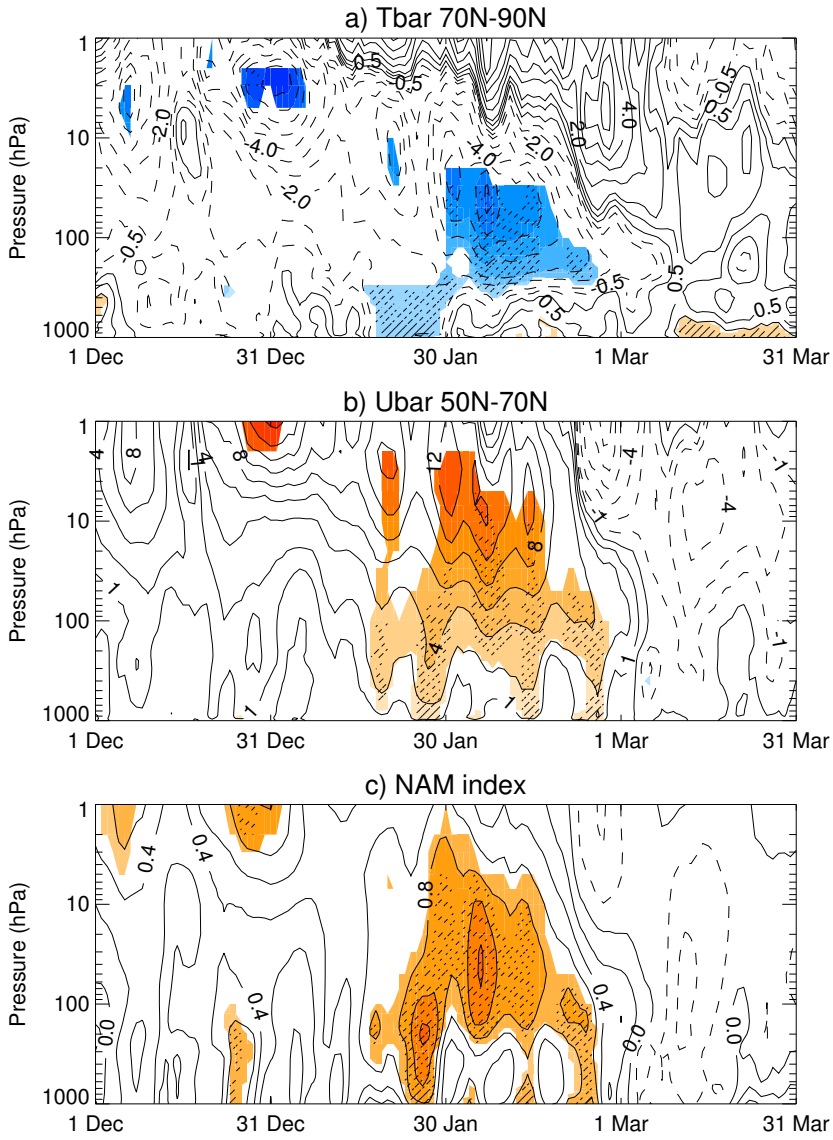

Figure 3.2. Composites of time–pressure December to March evolution daily zonal-mean of (a) temperature anomalies at 70ºN-90°N, (b) zonal wind anomalies at 50ºN-70ºN and (c) NAM index (contour interval: 0.2) for strong La Niña winters (-1 SD threshold). Contour intervals for temperature are ± 0.5 K up to ± 1 K and every 1 K thereafter. Contours for zonal wind are ± 1 m s^{-1} up to ± 2 m s^{-1} and every 2 m s^{-1} thereafter. Solid (dashed) contours denote positive (negative) anomalies. Colors indicate significant area at 90% confidence level and stippling indicates significance at the 95% level.

Fig. 3.2. revealed downward propagation of the stratospheric La Niña anomalies into the troposphere and the surface over the polar cap. Next, we analyze the surface impact of the identified stratospheric response over the Arctic and the NAE region, for the January-February average, when the largest signal at the surface was observed (Fig. 3.2). The Arctic region displays negative SLP anomalies during strong La Niña winters, while positive SLP anomalies appear over the Atlantic and southern Europe (Figure 3.3a). Anomalies are about -8 hPa over the Icelandic low and 4 hPa over the Azores high, resembling a positive NAO phase. Notably, these anomalies are of the same order (but opposite in sign) to those found in response to El Niño events by Cagnazzo and Manzini (2009) in reanalysis data. Consistent with the SLP anomalies, a significant anomalous warming is observed at the surface over Northern and Central Europe (Fig. 3.3b). Its largest value (3 K) is reached over Scandinavia. The positive NAO-like pattern is also related to a decrease in precipitation over the Mediterranean region and increased precipitation over Scandinavia (Fig. 3.3c). The pattern in precipitation is similar to that found by Pozo-Vázquez et al. (2005), who already related it to La Niña events and a positive NAO phase, but without providing a dynamical mechanism to explain it. The novelty of our study is that we reveal the role of the stratosphere in the NH La Niña winter response over the NAE region. Hence, our results indicate that strong La Niña events could be as useful as El Niño events to improve wintertime seasonal predictability over Europe.

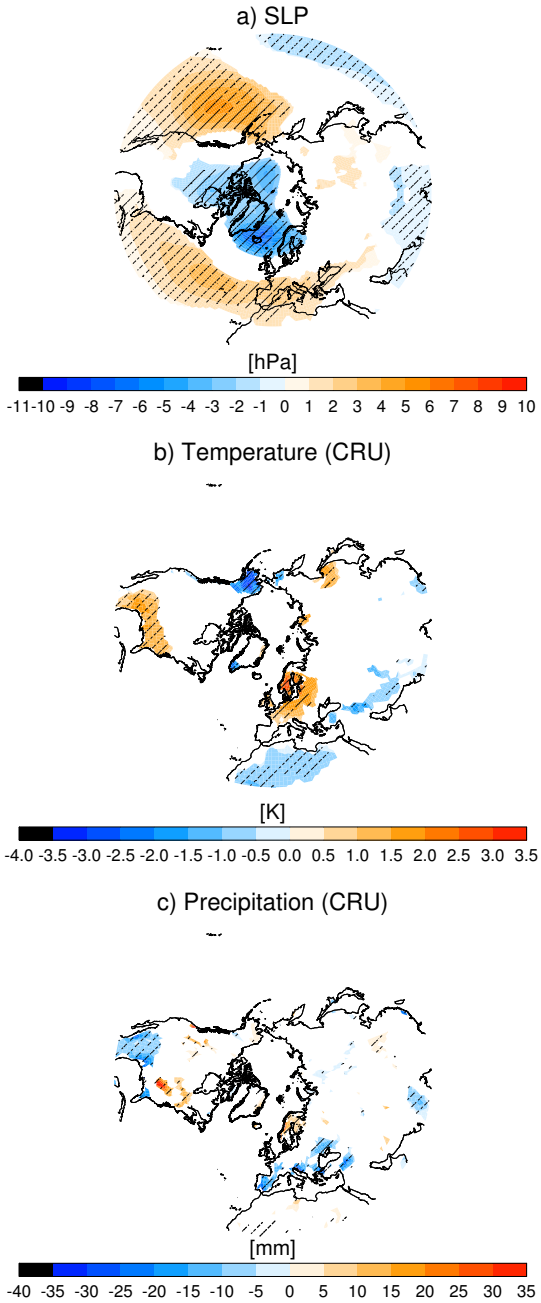

Figure 3.3. Longitude-latitude polar projection composite of the January-February average (a) SLP, (b) surface temperature and (c) precipitation during strong La Niña winters. Colors indicate significant area at 90% confidence level and stippling indicates significance at the 95% level.

3.2 Dynamical Mechanisms

Once we have shown the robust La Niña response in the polar stratosphere and in the NAE region, next we address the dynamical mechanisms that lead to these signals. As noted in chapter 2, temperature in the lower stratosphere is mainly driven by planetary wave dissipation. The Eliassen-Palm cross section (Edmon et al. 1980) in Figure 3.4a shows the NDJ climatology (1958-2012) of the EP flux (arrows) and EP flux divergence (colors). During winter, planetary waves propagate upwards and are refracted towards the equator in the upper stratosphere. The negative values of the EP flux divergence indicate the regions where the atmospheric planetary waves deposit zonal momentum. During strong La Niña events (Fig. 3.4b), the anomalies of EP flux point downwards in the troposphere between 40ºN and 60ºN and throughout the entire stratosphere between 60°N and 90°N. The anomalies in the EP flux divergence are positive in the stratosphere, and exceed 0.5 m s^{-1} day^{-1} in the upper region. These results indicate that during strong La Niña winters, the climatological upward wave propagation and dissipation is reduced in the polar stratosphere, which leads to a stronger and colder polar vortex as shown in Figs. 3.1 and 3.2. This behavior in the wave-mean flow interaction during La Niña was already shown in a model experiment (Li and Lau 2013), but this is the first time it is found in reanalysis data.

To provide further insight into the mechanism behind the reduced wave activity penetrating into the stratosphere, we focus on the zonal-mean eddy meridional heat flux, which is the main contributor to the vertical component of the EP Flux (Newman et al. 2001). Following the framework of Nishii et al. (2009) and as shown in chapter 2, we decomposed the anomalous zona-mean meridional eddy heat flux in Eq. (2.12), in an interference term, that accounts for the interference between the climatological stationary waves and the

anomalous waves associated with La Niña, and an anomalous wave packet term, that reflects the activity of the anomalous La Niña waves.

For convenience, Eq. (2.12) is rewritten below as Eq. (3.1):

$$\left\langle \overline{v'T'}_a \right\rangle = \left\langle v'_a T'_c + v'_c T'_a \right\rangle + \left\langle \overline{\left(v'_a T'_a\right)}_a \right\rangle \qquad (3.1)$$

The total eddy meridional heat flux, the interference term and the anomalous wave packet term during the selected winters composites are noted in Table 3.1.

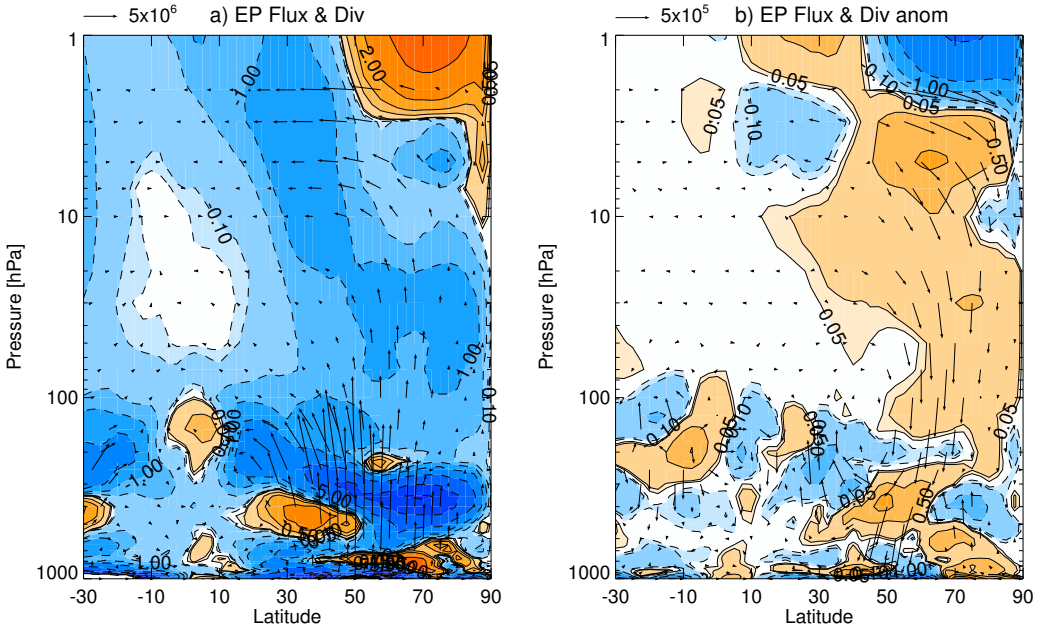

Figure 3.4. Latitude-pressure cross sections of the NDJ average of the EP flux (arrows) and EP flux divergence (contours) (a) climatology and (b) anomalies during strong La Niña winters. Contours are drawn at ± 0.05, 0.1, 0.5, 1, 2, 5, 10, 15, 20 m s^{-1} day^{-1}. Arrows scale is shown up left for (a) 5 x 10^6 kg s^{-2} and (b) 5 x 10^5 kg s^{-2}.

Table 3.1. Total anomalous meridional eddy heat flux terms and the decomposition into interference and anomalous wave packet terms in [m K s^{-1}] units for neutral winters, strong La Niña winters (-1 SD threshold), strong La Niña winters with SSWs, strong La Niña winters without SSWs, extended La Niña winters (-0.5 SD threshold), extended La Niña winters with SSWs and extended La Niña winters without SSWs.

Winters	Total	Interference term	Anomalous wave packet term
Neutral	-0.16	0.06	-0.22
Strong La Niña	-0.96	-0.88	-0.08
Strong La Niña SSW	-1.16	-0.72	-0.44
Strong La Niña noSSW	-0.75	-1.03	0.28
Extended La Niña	-0.18	-0.29	0.11
Extended La Niña SSW	0.55	0.09	0.46
Extended La Niña noSSW	-1.07	-0.75	-0.32

Figure 3.5 shows the total anomalous meridional eddy heat flux at 100hPa for the NDJ mean, averaged between 45ºN and 75ºN and composited for strong La Niña (gray) and neutral (yellow) winters (Fig. 3.5a). Its decomposition into the interference and anomalous wave packet terms appears in Figs. 3.5b and 3.5c respectively. The corresponding values are summarized in Table 3.1. During both strong La Niña and neutral winters, the anomalous meridional heat flux is negative (Fig. 3.5a), indicating that in both cases the upward wave activity is reduced compared to the climatology, as was already shown in Fig. 3.4. However, the magnitude of the total anomalous heat flux is much larger during La Niña winters than in neutral winters (-0.96 against -0.16m K s-1) indicating a much larger reduction of upward propagating wave activity in this case. Interestingly, the decomposition into different terms reveals the contribution of different factors during neutral and strong La Niña winters. During strong La Niña winters, the interference term (-0.88 m K s^{-1}) accounts for 92% of the anomalous eddy heat flux. This interference term is statistically different from that in neutral winters at the 90% confidence level according to a

t-test. Unlike La Niña winters, the total anomalous meridional eddy heat flux term during neutral winters is dominated by the anomalous wave packet term, contributing 73% to the total. Thus, strong La Niña winters are characterized by a large reduction in the upward wave activity through destructive interference between the anomalous planetary waves and the climatological eddies.

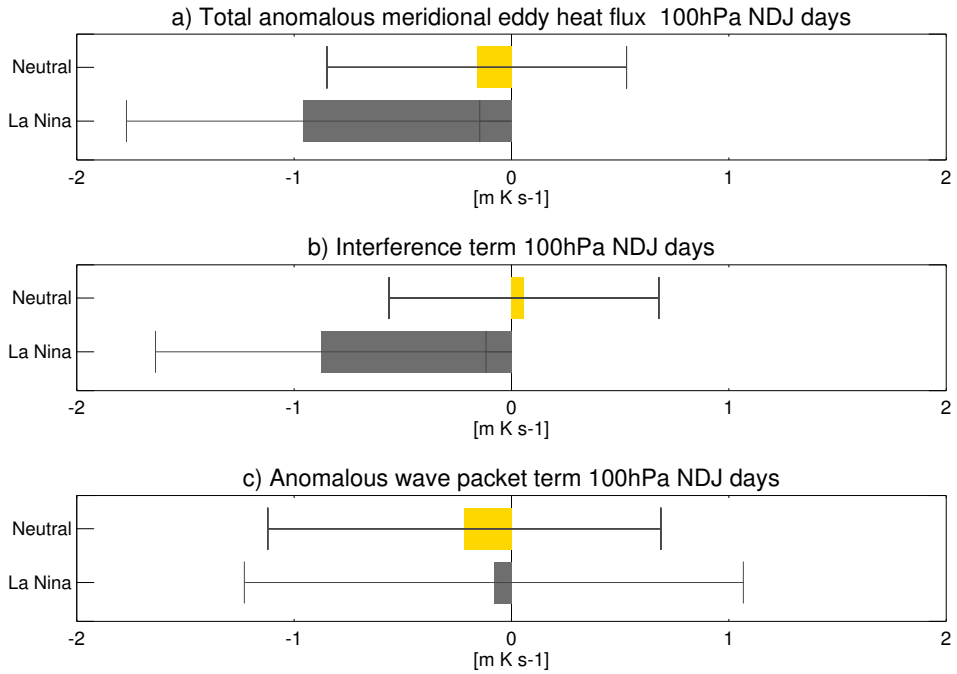

Figure 3.5. 100 hPa total anomalous meridional eddy heat flux response (a) and the contribution of interference (b) and anomalous wave packet (c) terms for neutral (yellow) and strong La Niña (gray) winters, for NDJ days mean, averaged between 45ºN-75ºN. Error bars indicate the lower and upper confidence limit for the mean at the 95% confidence interval.

The evaluation of both terms of the interference reveals that $v'_a T'_c$ in Eq. (3.1) is the main contributor to the interference term (not shown). Next, to understand the dynamical mechanism behind this term, Figure 3.6a shows the patterns of T'_c and v'_a at 100hPa during strong La Niña events. During

strong La Niña winters, prior to a polar stratospheric cooling, the anomalous eddy meridional wind at 100 hPa is equatorward (negative values) over Alaska and the Bering Sea region, where the eddy temperature is climatologically warm. Such anomalous interference is associated with the tropospheric wave pattern in eddy geopotential height anomalies, whose average for NDJ is shown in Fig. 3.6b. A dipole of anomalies is observed over the Northeast Pacific and North America, in quadrature to that during El Niño winters (Hoerling et al. 1997). The dipole, with the node over the ocean, is characterized by significant negative anomalies over North America and large significant positive anomalies over the North Pacific Ocean. These positive anomalies extend towards the Northwest Pacific leading to a weakened Aleutian low.

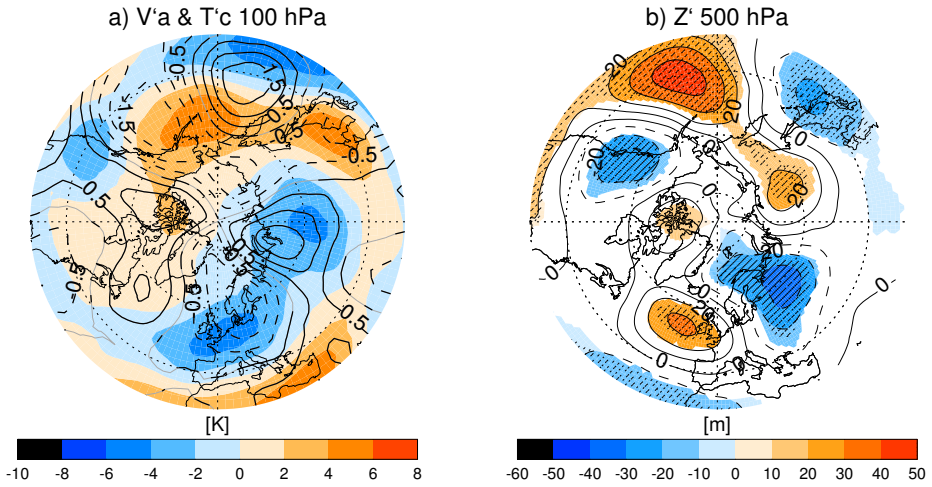

Figure 3.6. Longitude-latitude polar projection composite of strong La Niña winters, NDJ average. (a) Eddy meridional wind anomalies (contour intervals: 0.5 m s^{-1}) and climatological eddy temperature (colors) at 100 hPa. For wind field's solid (dashed) contours denote positive (negative) values. Black lines over (gray lines) indicate significant (non-significant) eddy meridional wind anomalies at 90% confidence level. (b) Eddy geopotential height anomalies at 500 hPa. Solid (dashed) contours denote positive (negative) anomalies. Colors indicate significant area at 90% confidence level and stippling indicates significance at the 95% level. Longitude grids are depicted every 90º (from 0º E) and latitude grids every 20º (from 40º N).

In summary, the analysis carried out here explains the origin of the stratospheric pathway presented in the previous section by consistent dynamical mechanisms. During strong La Niña winters an anomalous weak Aleutian low leads to suppressed anomalous upward wave activity into the stratosphere, via destructive interference between the anomalous and climatological stationary waves, which in turn strengthens the stratospheric polar vortex.

3.3 Sensitivity to La Niña threshold

The results presented here raise the question of why previous studies did not find similar robust responses to La Niña events in the NH stratosphere. We already mentioned in the Introduction that the use of a lower threshold is a common methodology that has been followed in other studies to allow for a larger composite size. Next, we investigate the relevance of the threshold in obtaining a robust response to La Niña events. To do so, we define extended La Niña events whenever the standardized SST anomalies (SSTA) over the N34 region are below -0.5 SD (the events are listed in Table 2.5). To understand the impact of La Niña events with different SSTA intensities, in Figure 3.7 we show the scatterplots of the standardized NDJF SSTA Niña3.4 index vs. the DJF zonal-mean zonal wind anomalies at 10 hPa for the 50ºN and 70ºN average (Fig. 3.7a) and the DJF polar cap temperature anomalies between 70ºN and 90ºN at 50hPa (Fig. 3.7b). A clear relationship between La Niña SST anomalies and the polar stratospheric response is observed. The significant correlation coefficient between the extended La Niña index and the DJF zonal-mean zonal wind anomalies is r = -0.56, suggesting that the stronger the La Niña events, the stronger the polar vortex. Correspondingly, the correlation coefficient between the extended La Niña index and polar temperature is r=0.53. This means that the stronger the La Niña events, the colder the stratospheric anomalies. A similar correlation coefficient is obtained when only strong La Niña events are considered and it is comparable to the coefficients obtained by Free and Seidel

(2009) for both ENSO phases. It is important to note that in Fig. 3.7 the linear fits (red lines) cross over zero in zonal-mean zonal wind and zonal temperature very close to the -1 SD threshold for the N34 index, which suggests that the use of thresholds below -1 SD might not be adequate to define strong La Niña winters. Also note that La Niña events with N34 indices between -0.5 SD and -1 SD show a larger spread in their stratospheric response than the strong La Niña events.

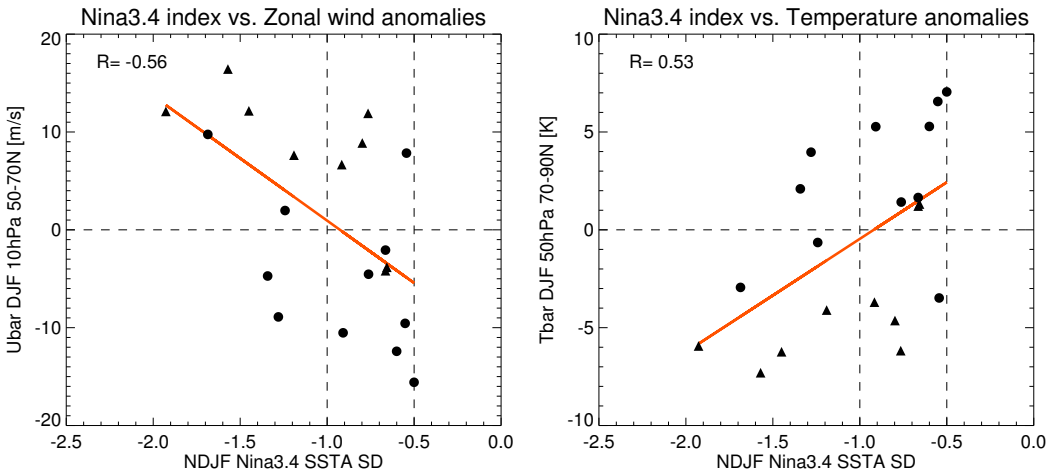

Figure 3.7. Scatterplots of the standardized NDJF SSTA Niña3.4 index vs. (a) the 50°N-70°N DJF zonal-mean zonal wind anomalies at 10 hPa and (b) the 70°N-90°N DJF zonal-mean temperature anomalies at 50 hPa. In each scatterplot, the red line indicates the linear fit for the La Niña events below -0.5 SD and the vertical dashed lines denote the -1 SD and -0.5 SD thresholds used to identify La Niña events. The correlation coefficient is noted in the upper left corner of each scatterplot. Winters with at least one SSW are plotted with dots and winters without SSWs are plotted with triangles.

To compare the stratospheric response to strong and extended La Niña events in more detail, left panels in Figure 3.8 show the latitude-pressure composite of extended La Niña winters for the DJF zonal-mean temperature (Fig. 3.8a) and zonal-mean zonal wind (Fig. 3.8d), similar to Fig. 3.1. Not

surprisingly, the magnitude of the tropospheric cooling in the tropics is slightly weaker in the composite of extended La Niña winters than in strong La Niña events (-0.5 K versus -0.7 K). Differences are also observed in the lowermost tropical stratosphere, where the warming is substantially smaller and not significant in the extended La Niña winters. Likewise, in the polar stratosphere the zonal mean responses in temperature and zonal wind are much weaker than for strong La Niña events and not significant, in agreement with previous studies that used the same criteria.

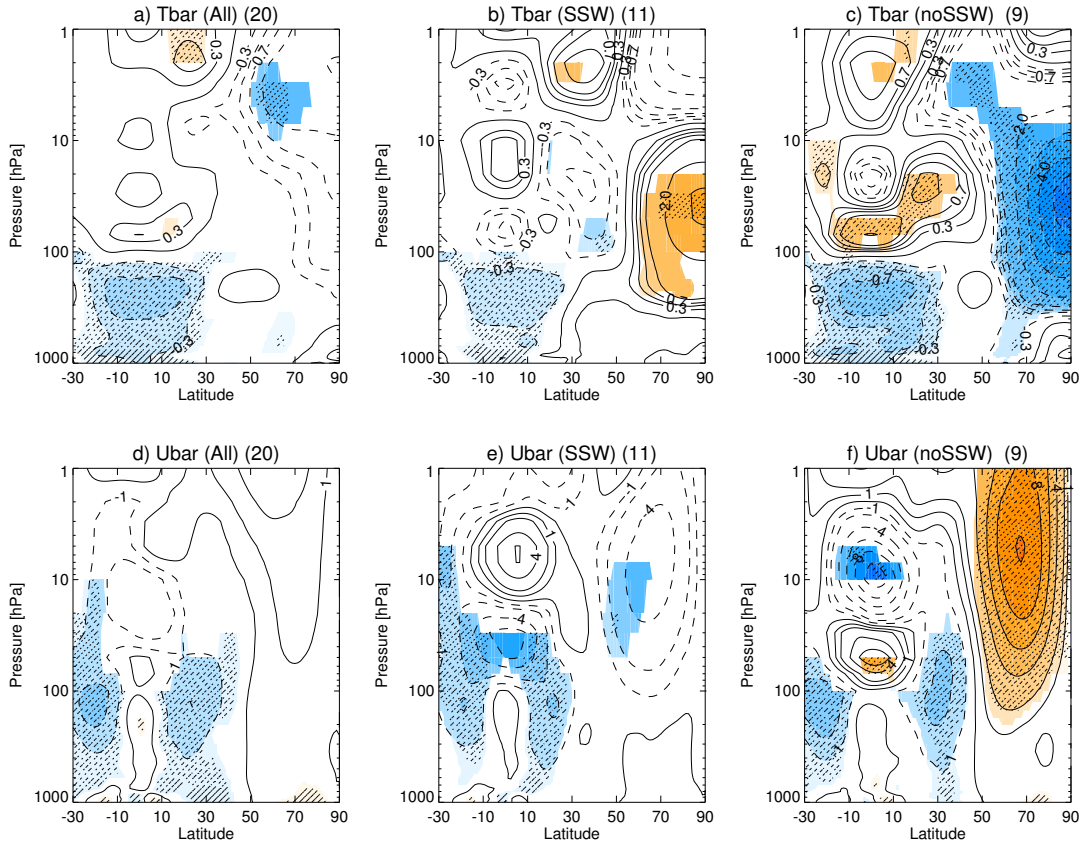

Figure 3.8. Same as Fig. 3.1, but for (a, d) extended La Niña winters (-0.5 SD threshold), (b, e) extended La Niña winters with SSWs and (c, f) extended La Niña winters without SSWs (see Table 2.5 for details). Numbers in brackets indicate the number of winters in each composite.

Therefore, our sensitivity study indicates that the -0.5 SD threshold is not adequate to extract the La Niña response in the stratospheric circulation. This might be because the extended La Niña events are simply not strong enough to generate a polar stratospheric response or because even though they are able to modulate the polar stratosphere, their weaker signals are masked by other sources of variability. We next investigate the latter possibility.

3.3.1 SSWs role

To investigate the role of SSWs on the polar stratospheric response to La Niña, we first mark the extended La Niña winters with and without SSWs in Fig. 3.7. It is remarkable that La Niña winters with SSWs (dots) are mostly related to negative wind anomalies (weaker polar vortex) and warmer polar anomalies, whereas La Niña winters without SSWs (triangles) are linked to stronger wind and cold temperature anomalies. The frequencies of winters with at least one SSW (between November and February) are similar for strong and extended La Niña winters. They are 0.50 and 0.55 respectively. The composited zonal-mean temperature and zonal-mean zonal wind anomalies for the extended La Niña winters with and without SSWs are shown in Fig. 3.8. Similar results are obtained when the anomalies are computed with respect to a climatology based exclusively on winters without SSW occurrence. During extended La Niña winters with SSWs (Figs. 3.8b, e), a significant warming is observed in the lower polar stratosphere accompanied by negative zonal-mean zonal winds. This behavior is opposite to that shown during strong La Niña events (Fig. 3.1) and reflects the occurrence of the SSWs. In contrast, when extended La Niña winters without SSWs are composited (Figs. 3.8c, f) a robust cooling and significant positive zonal wind anomalies appear in the polar stratosphere, similar to the pattern obtained for strong La Niña events (Fig. 3.1). Note that the magnitude of the anomalies is even larger than that in Fig. 3.1 (-5 K versus -3 K and 10 m s^{-1} versus 8 m s^{-1}). However, unlike strong La Niña events,

significant zonal-mean zonal wind anomalies do not penetrate into the troposphere. For comparison, we also stratified strong La Niña winters into winters with and without SSWs, in Figure 3.9. Interestingly, the stratospheric response during strong La Niña winters with SSWs is not significant (Figs. 3.9b,e), probably related to the counteracting effects of the SSWs-related warming and strong La Niña cooling on the small sized composite (only 4 winters are composited in this case). As expected (Fig. 3.9c) a strong significant cooling (about -8 K) appears during strong La Niña winters without SSWs. Indeed, these strong events dominate also the signature of the extended La Niña events without SSWs (Figs. 3.8c, f).

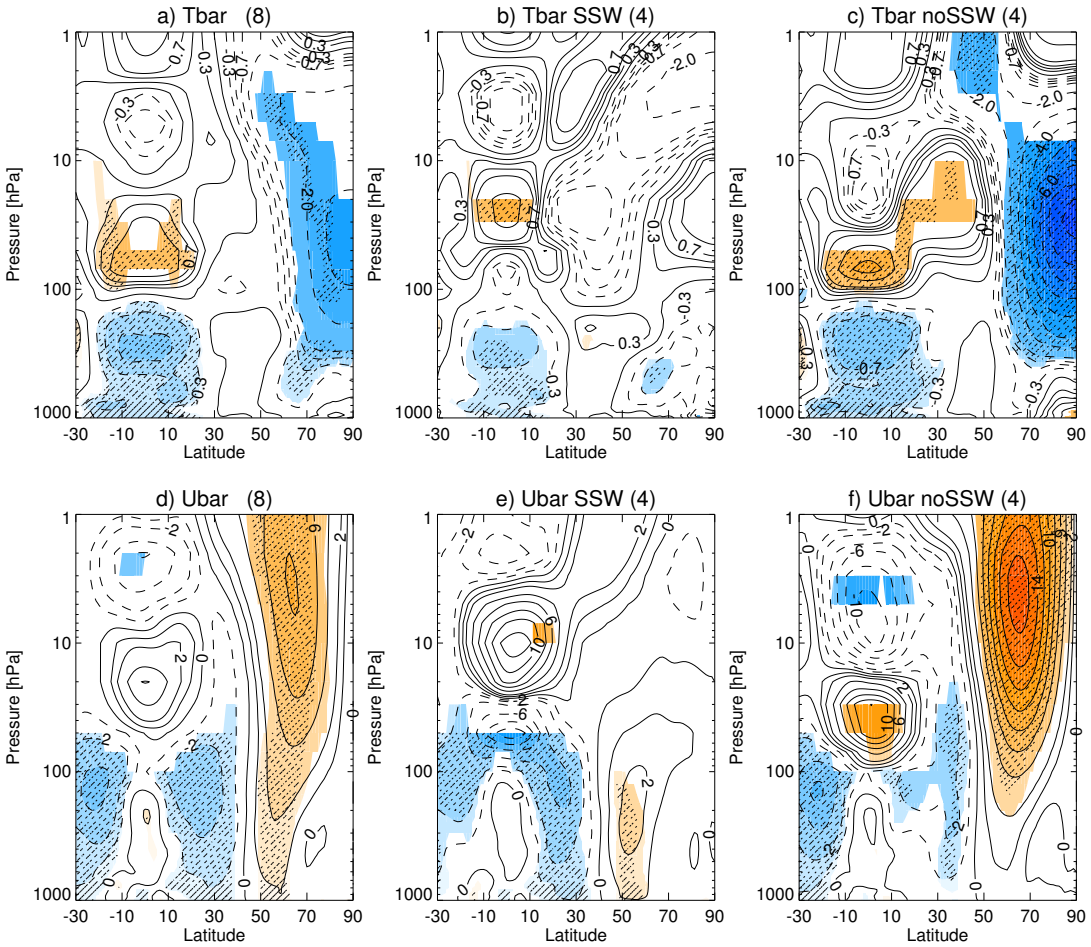

Figure 3.9. As Fig. 3.8 but for strong La Niña events (-1 SD threshold).

In the tropical troposphere, the cold signature observed for strong La Niña events is also present for the extended La Niña winters with and without SSWs (Figs. 3.8b, c), although during winters with SSWs this signal is weaker and the anomalous cooling does not reach -0.5 K (Fig. 3.8b). In fact, the composite of the standardized SST anomalies in the N34 region during extended La Niña events with SSWs is -1 SD, which is lower and statistically different from the -1.46 SD value, obtained for extended La Niña winters without SSWs. Thus, the tropical Pacific SSTA are on average weaker for the extended La Niña events with SSWs than for those without SSWs. Still, in both cases the tropical response in the troposphere is an anomalous cooling, which cannot explain by itself the opposite signs found in the polar stratosphere during extended La Niña events with or without SSWs. Hence, it is clear that SSWs play a relevant role in modulating the observed polar stratospheric signal for extended La Niña winters, which, we claim, is characterized by a robust cooling.

To better understand the role of the SSWs during La Niña winters in terms of dynamics, Figure 3.10 extends Fig. 3.5b, by including the interference term of the eddy heat flux during extended La Niña events and strong and extended La Niña winters with and without SSWs. As explained before, the interference term represents the interference between the climatological waves and the anomalous waves. The extended La Niña events (green) show a negative but small interference contribution (Table 3.1), not statistically different from neutral winters (yellow). This is in line with Sassi et al. (2004) results using a model simulation. The division of extended La Niña winters into winters with and without SSWs provides additional information. During extended La Niña winters without SSWs the interference term is negative (blue), indicative of reduced upward wave activity, and similar to that during strong La Niña winters (- 0.75 m K s^{-1} vs. - 0.88 m K s^{-1}, no statistical differences are found). Instead, during extended La Niña winters with SSWs (orange), the interference

contribution to the anomalous heat flux is positive, reflecting anomalous upward wave activity in this case. On the contrary, La Niña winters selected with a threshold of -1 SD display a negative interference term in winters with and without SSWs (purple and brown). This indicates destructive interference regardless of the SSW occurrence, albeit the reduced composite size introduces widespread error bars. Interestingly, the contribution of the interference and anomalous wave packet terms to the total anomalous heat flux is very different during the extended La Niña winters with and without SSWs. While the interference term (destructive interference) dominates during extended La Niña winters without SSWs (see Table 3.1), similar to the behavior found during strong La Niña winters, the contribution of the anomalous wave packet term is larger in the case of extended La Niña winters with SSWs (Table 3.1). This is consistent with the analysis of NH anomalous heat flux composites of Smith and Kushner (2012) who found that the interference term was more important in composites with lower heat flux values, in our case, this would correspond with strong La Niña and extended La Niña events without SSWs.

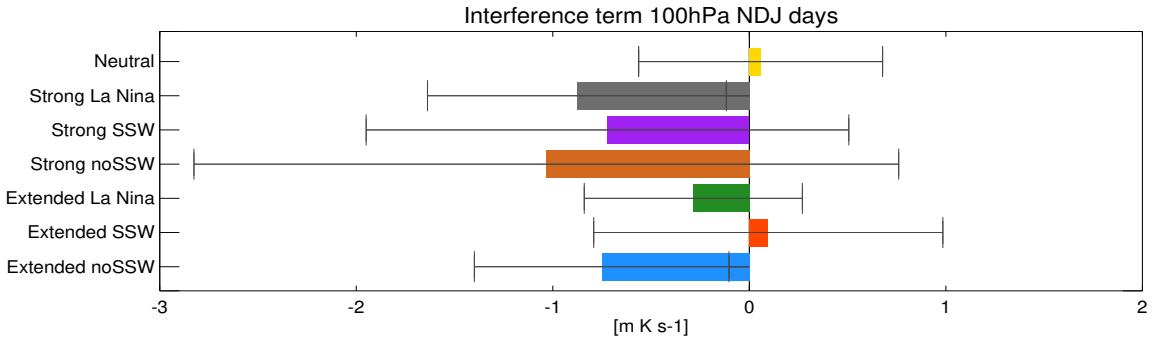

Figure 3.10. As Fig. 3.5b, but for (yellow) neutral winters, (gray) strong La Niña winters (-1 SD threshold), (purple) strong La Niña winters with SSWs, (brown) strong La Niña winters without SSWs, (green) extended La Niña winters (-0.5 SD threshold), (orange) extended La Niña winters with SSWs and (blue) extended La Niña winters without SSWs.

To sum up, La Niña signal is related to destructive interference between the climatological and anomalous planetary waves in both strong La Niña events and extended La Niña winters without SSWs. However, constructive interference takes place when SSWs occur, supporting our hypothesis that the polar stratospheric signal observed during extended La Niña events with SSWs reflects the behavior of the SSWs.

To add consistency to our conclusions we plot components T'_c and v'_a of the interference term and geopotential height anomalies (analogous to Fig. 3.6) for extended La Niña winters with and without SSWs (Figure 3.11). During extended La Niña winters with SSWs (Fig. 3.11a) the anomalous meridional eddy wind over Alaska and the Bering Sea region is poleward (positive values), while it is equatorward during extended La Niña winters without SSWs (Fig. 3.11b), leading to constructive and destructive interference respectively. Differences are also found in the eddy geopotential height anomalies in the troposphere. During extended La Niña winters without SSWs (Fig. 3.11d) an anomalous dipole, similar to that found during strong La Niña winters (Fig. 3.6), is observed, although the positive anomalies extend more to the northwest and are weaker. During extended La Niña winters with SSWs (Fig. 3.11c), the dipole is shifted eastward, positive anomalies are confined to lower latitudes and do not reach the Bering Sea and Alaska region. Garfinkel et al. (2012) identified this region (near 62°N and 180°E) as a precursor of SSWs, as they detected negative geopotential height anomalies therein prior to the occurrence of SSWs, leading to a weaker vortex. The interference of negative geopotential height anomalies before the SSWs together with positive anomalies associated with La Niña winters (Fig. 3.11c) results in non-significant anomalies in this region. Therefore, the lack of a polar stratospheric response during extended La Niña winters could be related to a sampling problem, as the signal to noise ratio in this case is largely reduced due to the occurrence of SSWs.

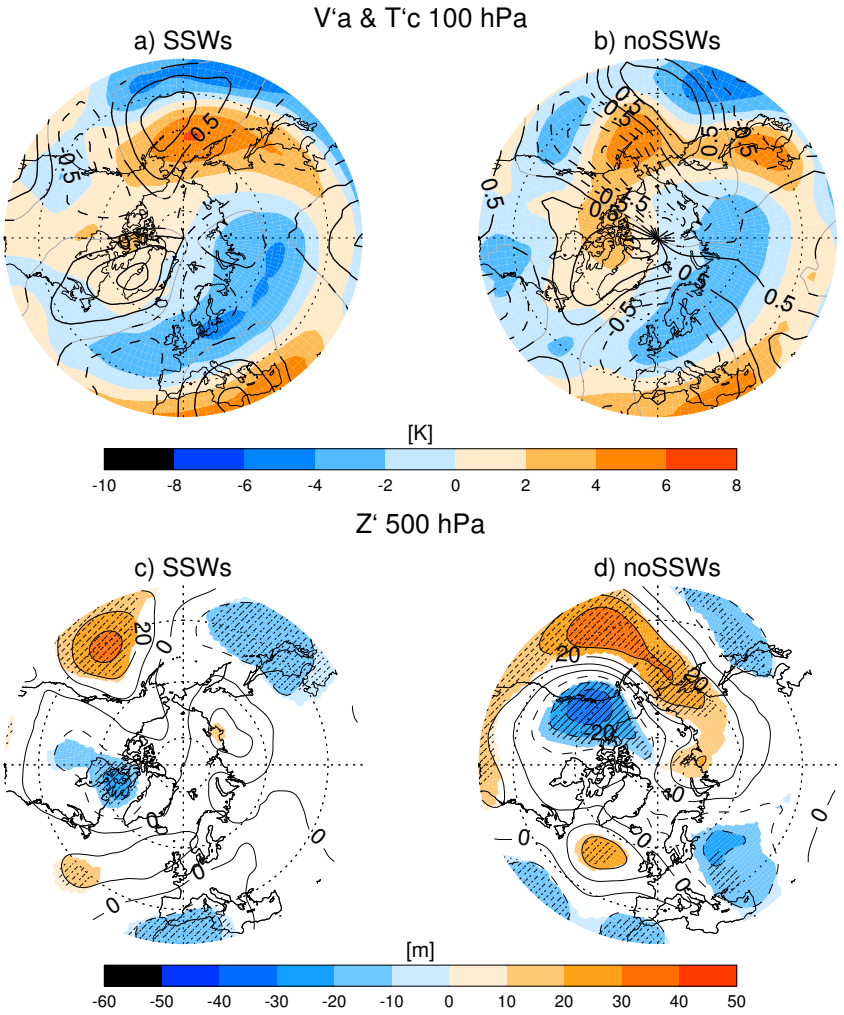

Figure 3.11. Similar to Fig. 3.6, but for (a, c) extended La Niña winters with SSWs and (b, d) extended La Niña winters without SSWs.

3.3.2 QBO phases impact

In addition to the influence of SSWs, inspection of the zonal-mean zonal wind anomalies in the tropics in Fig. 3.8 suggests the QBO could be also playing a role on modulating the stratospheric signal during extended La Niña winters. Fig. 3.8e shows easterly wind anomalies at the equator between 20 hPa

and 60 hPa during extended La Niña winters with SSWs, while westerlies are observed during La Niña winters without SSWs (Fig. 3.8f). Table 2.5 shows the QBO phase for each extended La Niña Winter. We identify 6 EQBO La Niña winters (5 of them with SSWs) and 11 WQBO La Niña winters (3 of them with SSWs). This means that SSWs occur in 83% of the EQBO winters and they are absent in 73% of the WQBO winters. The percentage above indicates that there seems to be a relationship between extended La Niña winters with SSWs and the EQBO phase and extended La Niña winters without SSWs and WQBO. Dunkerton et al. (1988) already noted that SSWs are not prone to occur during the WQBO phase, when more waves propagate into the subtropics, or could be delayed to mid- and late winter under WQBO conditions (Lu et al. 2008). However, the percentages we obtained during extended La Niña winters are reduced when we consider the entire 55 winters without classifying with respect to La Niña winters: SSWs occur in 61% of the EQBO phase winters and SSWs do not occur in the 61% of the WQBO phase winters. Similar to the sub-setting performed in Fig. 3.8, the classification of extended La Niña winters into EQBO and WQBO phases also depicts significant and opposite polar stratospheric anomalies (not shown), but such E/WQBO division is closely related to the SSW occurrence/absence. Nonetheless, we can determine that the SSWs/QBO induced modulations of the polar vortex are strong enough to hide La Niña signal when a low threshold is selected (-0.5 SD).

On the other hand, the polar stratospheric response to strong La Niña events (-1 SD) is robust, even though the signal in the tropical stratosphere is weakly positive suggesting a weak WQBO predominance (Fig. 3.1b). Figure 3.12 shows the classification of strong La Niña winters into EQBO and WQBO phases. Strong La Niña during EQBO (Figs. 3.12b,e) results in non-significant temperature and wind responses. If we assumed that strong La Niña events had no stratospheric impact, strong La Niña events during EQBO should lead to a significant signal in response to the EQBO. We show in Fig. 3.12 that this is not

the case, because, as we reported above, the strong La Niña events do have a stratospheric signature. Therefore, the strong La Niña signal and the EQBO phase impacts may cancel each other, resulting in non-significant responses. In contrast, strong La Niña events during WQBO (Figs. 3.12c,f) show an anomalously strong polar vortex, stronger than when all strong La Niña are composited together. The stronger signal in La Niña during WQBO could be related to both signals reinforcing, but cannot be due exclusively to the WQBO phase.

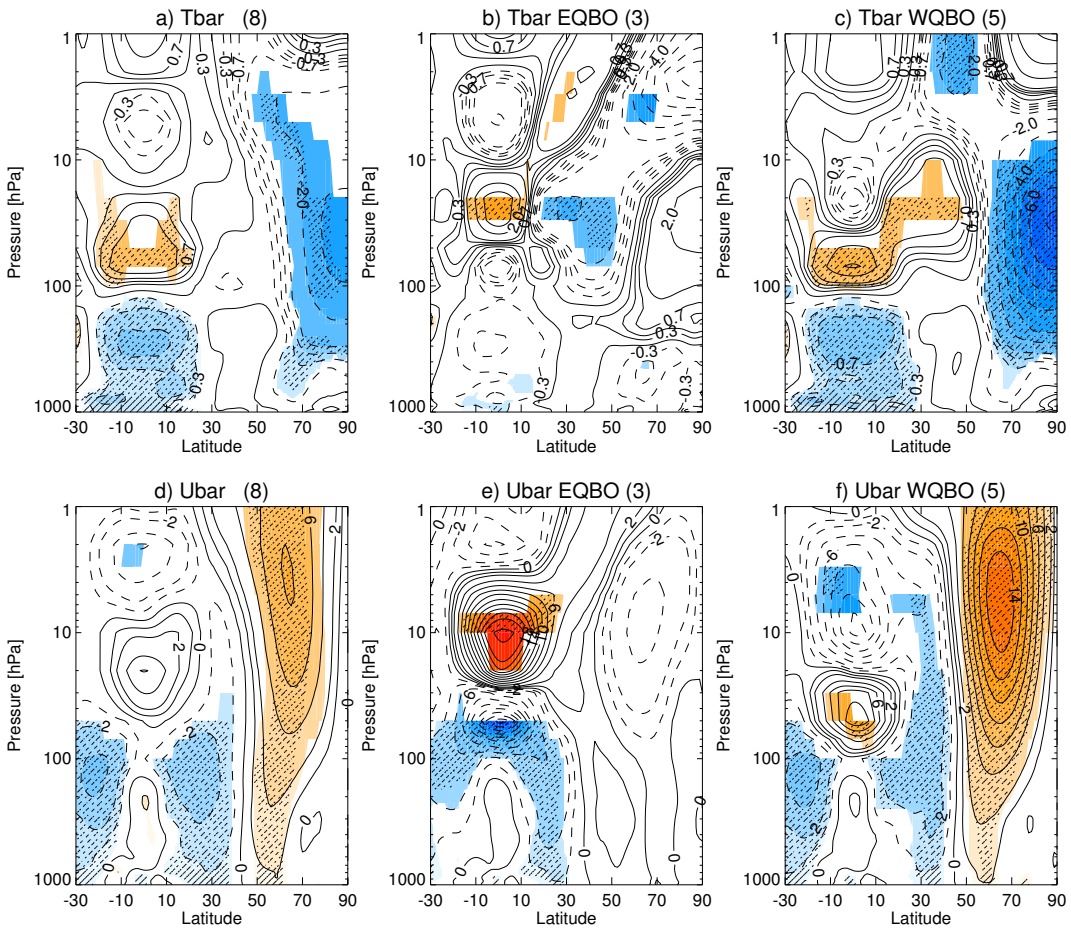

Figure 3.12. As Fig. 3.8 but for strong La Niña events (-1 SD threshold) (b, e) strong La Niña winters and EQBO phase and (c, f) strong La Niña winters and WQBO phase.

Thus, the classification of strong La Niña events into E and WQBO phase winters suggests, despite the limited sample, no predominance of the QBO signal over the strong La Niña stratospheric signature. Unfortunately, the limited reanalysis record hampers a deeper analysis on the relationship between SSWs and QBO phases during La Niña winters.

3.4 Summary and Discussion

This study reveals for the first time a stratospheric pathway for La Niña and its teleconnections in the NAE region, using the JRA-55 reanalysis and the CRU dataset. With 55 years of reanalysis data we have found a significant strong and cold polar stratospheric vortex during strong La Niña events. These events are defined as those with a NDJF N34 index lower than -1 SD. Zonal mean stratospheric anomalies are later on propagated downwards, from the upper stratosphere in late December to the troposphere in January-February, when they reach the surface. The consequent surface impact presents a robust pattern of negative SLP anomalies over the Arctic and positive anomalies over the NAE region. These anomalies increase the advection of warm air from the North Atlantic Ocean to Europe and so, an anomalous warming is detected in Northern and Central Europe, while reduced precipitation is observed in the Mediterranean area and enhanced precipitation over Scandinavia.

Our analysis also reveals the mechanism behind this pathway. A significant anomalously weak Aleutian low is observed during strong La Niña events and prompts destructive interference between the climatological and the anomalous La Niña stationary waves. This in turn, leads to reduced upward propagating wave activity into the stratosphere and weaker wave forcing, strengthening the polar vortex. In short, we have established a stratospheric link between the tropospheric anomalies in the tropics and anomalies in the NAE region during strong La Niña winters. Consequently, distinct but analogous to El Niño, our results also show that strong La Niña events (defined by the -1 SD

threshold) could be also relevant to improve seasonal predictability over Europe.

Furthermore, we explain the lack of a robust La Niña response in the stratosphere reported in previous observational and reanalysis studies: the competing influences of SSW occurrence and the QBO during extended La Niña events (defined by the -0.5 SD threshold) lead to a non-significant response in the polar stratosphere. Therefore, we conclude that a threshold of -0.5 SD in the N34 index is not appropriate to obtain the atmospheric teleconnections of La Niña. For this reason, we recommend defining La Niña events with a relatively high threshold of -1 SD for the N34 index. At the same time, we also noted that our longer dataset includes the two latest La Niña events, which were not considered before and are characterized by a mid-winter strong polar stratospheric cooling.

On the relationship between La Niña events and the occurrence of SSWs, the frequencies of SSW occurrence per winter, defined from November to March, are 0.88 and 0.70 for strong and extended La Niña events (note that more than one SSW occur during some La Niña winters). Such frequencies are similar to El Niño winters SSW frequency (0.76) and higher than for the neutral winters (0.44). Then, we report enhanced occurrence of SSWs during La Niña winters, similar to El Niño, in agreement with the study of Butler and Polvani (2011). However, it is remarkable that strong La Niña events selected in this study are mainly related to late winter SSW occurrence. During strong La Niña winters, five out of the seven SSWs registered occurred late in winter (beyond the 20th of February). Instead, during the extended La Niña winters only one additional SSW is found late in winter (See Table 2.5). These results suggest that the reduced upward wave activity related to strong La Niña events might not inhibit, but delay to late winter the occurrence of SSWs. Nonetheless, owing to the short reanalysis record this hypothesis needs to be investigated in the future in long model simulations.

Compared to previous studies based on reanalysis, it is important to notice that our results suggest a stratospheric pathway that does not reconcile with the one defined by Butler et al. (2014). While Butler et al. (2014) consider the stratospheric pathway active only when one or more SSW occur, we searched for a stratospheric pathway for La Niña, irrespective of SSW occurrence, and we found that La Niña is associated with a strong vortex, which can as well have an impact at the surface (Baldwin and Dunkerton 2001). In addition, we found discrepancies in the detection of strong La Niña events compared to those in Mitchell et al. (2011) who also used reanalysis data. Applying the -1 SD threshold, similar as we do for strong La Niña events, they impose the SSTA to exceed -1 SD for at least 3 months including December. In this fashion, they identified 8 La Niña winters based on HadISST over the 1958-2002 period. However, according to our selection, based on ERSSTv4 NCEP/CPC N34 index and using a longer period to compute the climatology, two of those winters (1983/84 and 1984/85) cannot be identified as strong La Niña winters (their NDJF anomalies do not reach the -1 SD threshold), although using the HadISST dataset, the 1984/85 winter does appear to be a strong La Niña (see Table 2.5). In any case, this means that Mitchell et al. (2011) included some extended La Niña winters in their composites, and this probably confined their significant signal to the upper stratosphere (see Fig. 1.13). In contrast, in the recent reanalysis study of Rao and Ren (2016b), contemporary to ours, they also report an effective stratospheric response during strong La Niña, not found in moderate La Niña events.

As mentioned in the Introduction, modeling studies on La Niña response in the polar stratosphere show contradictory results. The pioneer modeling works of Sassi et al. (2004) and Manzini et al. (2006) found a negligible response to La Niña events in the polar stratosphere, which was not statistically different from neutral winters. In contrast, more recent modeling studies reported a significant stratospheric cooling during La Niña (Calvo et al. 2010;

Rao and Ren 2016a) and a robust strong vortex related to suppressed anomalous upward propagation (Li and Lau 2013). Since none of these modeling studies investigated the possibility of a stratospheric effect over the NAE region and given that model simulations allow for much larger composites sizes than the reanalysis record, it would be of interest to analyze the role of the stratosphere in NH tropospheric La Niña teleconnections in long model simulations. This issue will be partially addressed in chapter 5.

4 Contrasting EP and CP El Niño signatures

Role of Stratospheric Sudden Warmings

This chapter addresses the controversy on the EP and CP El Niño polar stratospheric signatures. Whether the response to CP El Niño is distinguishable from EP El Niño is still an unresolved feature, since contradictory results have been reported depending on the definition and the composite size considered. In the previous chapter, we revealed the impact that SSWs might have in the polar stratospheric response to La Niña. Accordingly, this chapter presents the analysis of the role of SSWs on the CP El Niño stratospheric signature. The period of study spans from 1958 to 2013 and ERA-40 and ERA-Interim reanalysis datasets are used as explained in section 2. The main results of this chapter are presented in Iza and Calvo (2015).

4.1 EP versus CP El Niño stratospheric responses

First, we analyze EP and CP El Niño polar stratospheric responses, based on the events defined in chapter 2 using the ERSSTv4 NCEP/CPC data (see Table 2.3). Figure 4.1 shows the time-pressure evolution of EP and CP El Niño anomalies for zonal-mean temperature at 80ºN (left panels). Similar results are found at several high-latitude averages. A significant polar warming appears in the upper stratosphere in November and December during EP El Niño winters.

The warming descends to the middle stratosphere and becomes significant again in February. This is in agreement with previous studies (e.g., Manzini et al. 2006; Cagnazzo and Manzini, 2009), who showed warm anomalies propagating downward during canonical El Niño winters. Next, the influence of SSWs in the EP El Niño response is investigated by distinguishing winters with and without SSWs (Figs. 4.1b and 4.1c). The significant warming in early winter (November and December) appears in the upper stratosphere in both composites and it is consistent with anomalous wave dissipation in the stratosphere following the warm ENSO event (e.g., García-Herrera et al. 2006). However, the downward propagation of the warm temperature anomalies towards the lower stratosphere is only observed during winters with SSWs, while it is missing in the composite without SSWs. These differences are significant in the lowermost stratosphere (Fig. 4.1d). We are aware of the small composite size of the EP El Niño without SSWs in the observational record. Nonetheless, the role of SSWs in propagating the canonical El Niño signal to the lower stratosphere found here is in line with results reported from model simulations with larger composite sizes (Ineson and Scaife, 2009; Cagnazzo and Manzini, 2009; Bell et al. 2009).

The composite of all CP El Niño winters (Fig. 4.1e) reveals a much weaker and non-significant response compared to EP El Niño, consistent with results by Zubiaurre and Calvo (2012) and Garfinkel et al. (2013). However, when the zonal-mean temperature responses are analyzed for winters with and without the occurrence of SSWs separately, significant and opposite anomalies are obtained from November to January in the middle and lower stratosphere. During CP El Niño winters with SSWs (Fig. 4.1f), a significant anomalous warming appears in the middle stratosphere, while in the absence of SSWs (Fig. 4.1g), a significant cooling is observed in the middle and lower stratosphere. These differences are significant at the 95% level (Fig. 4.1h). Additionally, our results reveal that, in SSWs absence, the response of the polar stratosphere to CP El Niño in early winter is different to that of EP El Niño.

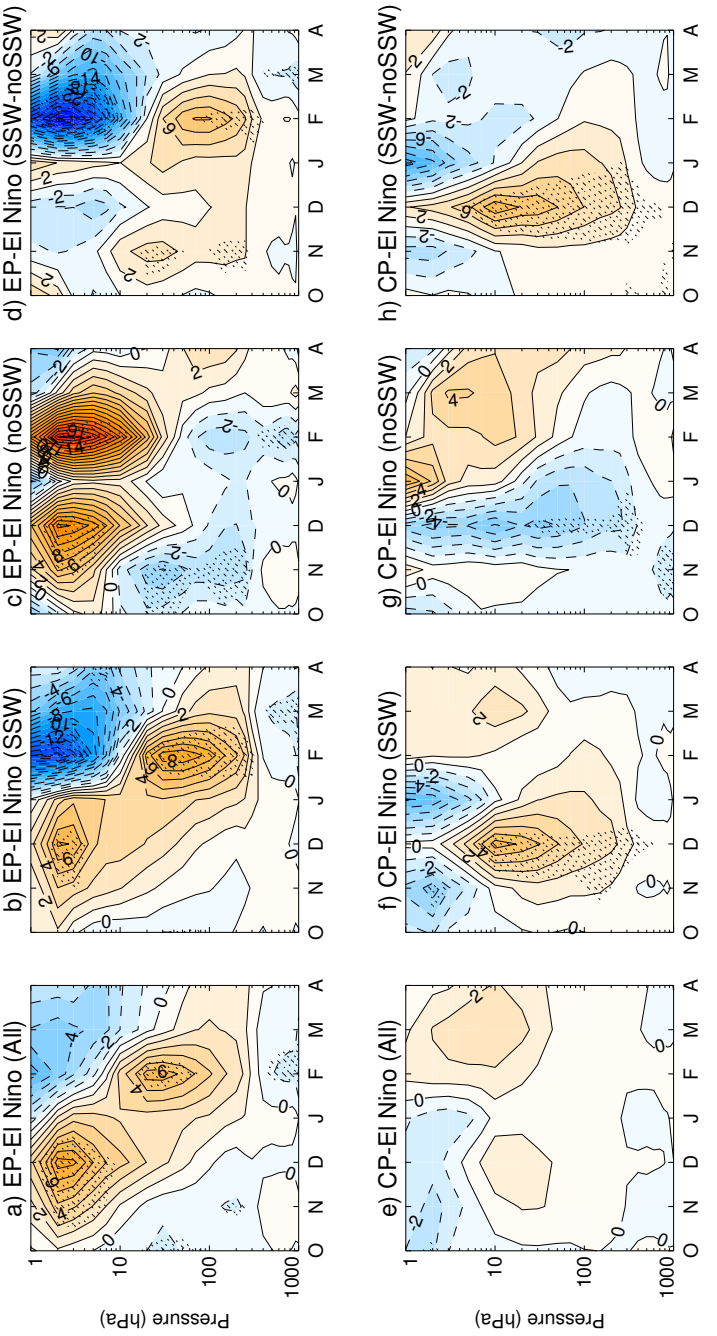

Figure 4.1. October to April composite of the monthly mean zonal-mean temperature anomaly at 80°N for (a–d) EP El Niño and (e–h) CP El Niño. Niño composites for all winters (Figs. 4.1a and 4.1e), winters with SSWs (Figs. 4.1b and 4.1f), winters without SSWs (Figs. 4.1c and 4.1g), and the difference between winters with and without SSWs (Figs. 4.1d and 4.1h). Contour interval is 1 K, and 2 K for differences. Solid (dashed) contours denote positive (negative) anomalies. Stippling indicates significance at the 95% level.

At this point, it should be stressed that the observed warming during CP El Niño winters with SSWs is likely due to the occurrence of the SSW itself, and cannot be attributed to a downward propagating CP El Niño warm signal, since the significant warm anomalies observed in early winter in the upper stratosphere during EP El Niño are absent for CP El Niño and the warming does not appear in the absence of SSWs.

4.2 Sensitivity to CP El Niño definition

As pointed before, the lack of a robust CP El Niño signal reported in previous studies was attributed to the different definitions and composite sizes (Garfinkel et al. 2013). To test the robustness of our results to the different indices and composite sizes, we analyze three different definitions of CP El Niño used in the literature and also analyzed by Garfinkel et al. (2013). In addition, we explore the CP El Niño winters used in the study by Sung et al. (2014). Details on the considered indices are explained in chapter 2 and corresponding winters are listed in Table 2.4.

Figure 4.2. shows the composite of the winters defined by Garfinkel et al. (2013) and the CP El Niño events investigated by Sung et al (2014). When all CP El Niño events are considered together without stratifying according to the SSW occurrence (Figs. 4.2a, e, i, m), the response is weak, not significant and depends on the index chosen, reproducing the results of Garfinkel et al. (2013). For CP El Niño winters with SSW occurrence (Figs. 4.2b, f, j, n) all composites show a warming in the middle stratosphere from November to January. In contrast, during CP El Niño winters without SSWs an anomalous cooling appears in early winter, robust across the different indices (Figs. 4.2c, g, k, o). Similar to Fig. 4.1 differences between CP El Niño winters with and without SSWs are statistically significant (Figs. 4.2d, h, l, p). Note that results are robust to different composite sizes. In short, the results presented here reveal that the CP El Niño polar stratospheric response is modulated by the SSWs signal.

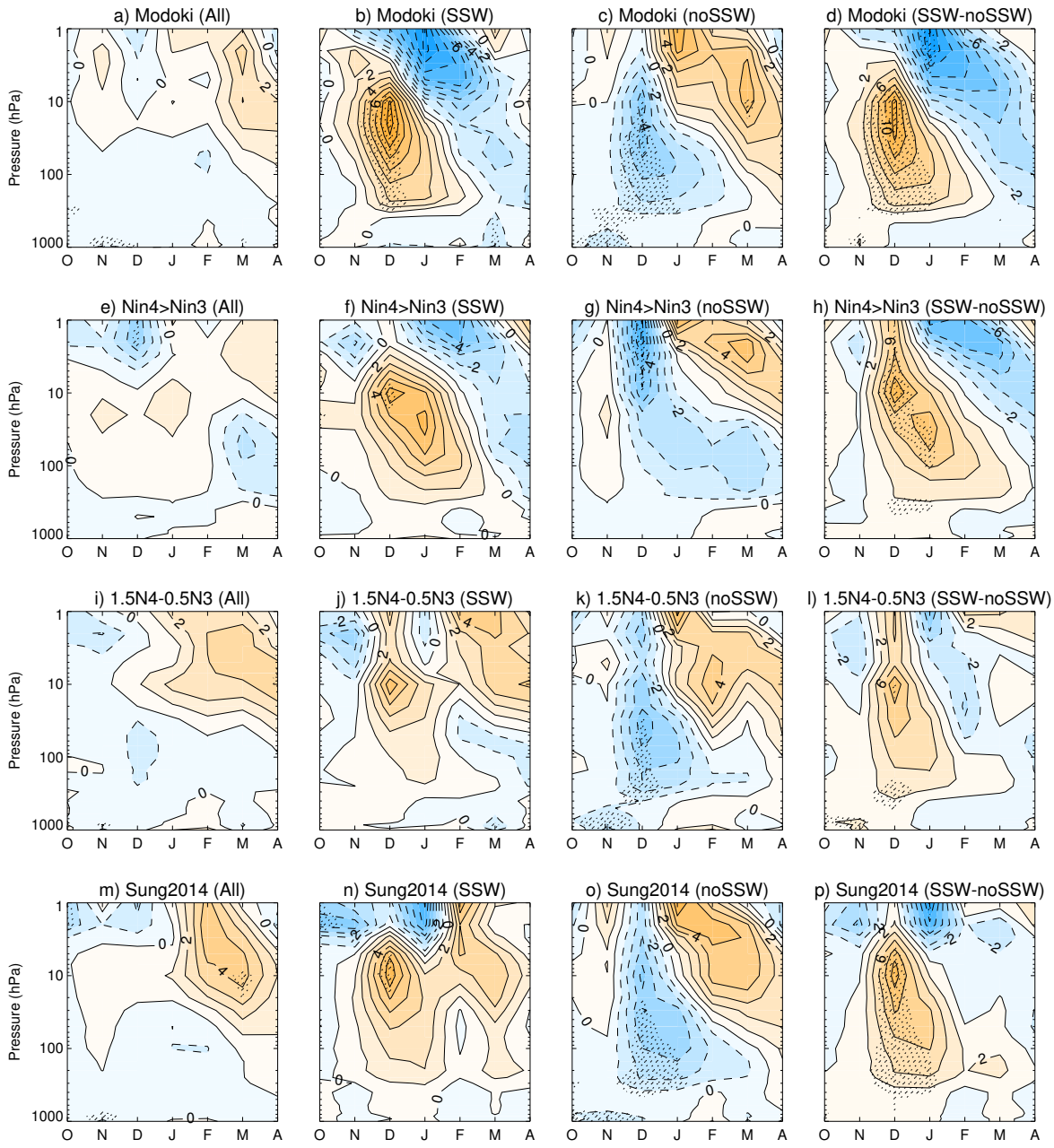

Figure 4.2. Same as Fig. 4.1, for the indices used by Garfinkel et al. (2013) and winters identified by Sung et al. (2014). (a–d) Modoki index, (e–h) Nin4>Nin3 index, (i–l) 1.5N4–0.5N3 index, and (m–p) Sung et al. (2014) events (see Table 2.4 for details).

4.3 The impact of SSWs timing

To evaluate whether the timing of SSWs affects the impact of the SSWs on the stratospheric response to CP El Niño we performed an additional analysis. SSWs occurring during CP El Niño are classified into early winter SSWs (November-December) and late winter SSWs (January-February). The classification is included in Table 2.4, where 3 winters with early SSWs and 3 winters with late SSWs are marked with f and g subscripts correspondingly. Note that the frequency of early and late SSWs is the same on the CP El Niño winters identified in our study. Figure 4.3 shows the time-pressure evolution of the zonal-mean temperature at 80ºN for CP El Niño winters. For an easier comparison, the first row (Fig 4.3a to c) is analogous to Fig. 4.1 (panels e, f and g). When we classify the CP El Niño events with SSWs into two groups, for early and late SSWs (Fig. 4.3e and 4.3g), the composite during CP El Niño and early winter SSWs (Fig. 4.3e) shows a stronger warming over a larger significant region, compared to the composite where all SSWs are averaged together (Fig. 4.3b). In contrast, when only late winter SSWs are considered (Fig. 4.3g), the anomalous warming is observed in late winter, reflecting the impact of the SSWs in late winter, although the effect on zonal-mean temperature is not significant. In this case, a small and not significant cooling appears in early winter.

Overall, the behavior of CP El Niño winters with late winter SSWs resembles that of CP El Niño signal without any SSWs (Fig. 4.3c). Thus, although the impact on the stratosphere is different for early and late winters SSWs, and the average of all SSWs can smooth their effects (compare Fig. 4.3b with 4.3e and 4.3g), the signals do not cancel each other. This is because the impact of early winter SSWs during CP El Niño winters is stronger than the effect of late winter SSWs (compare Fig.4.3e and 4.3g). This is also evident in Figs. 4.3d and 4.3f, which show, for early and late winter SSWs respectively, the sum of CP El Niño winters with and without SSWs. When early winter SSWs

are considered together with CP El Niño winters without SSWs (Fig. 4.3d), their signal dominates over the significant cooling observed during winters without SSWs. In contrast, the sum of CP El Niño winters with late winter SSWs and CP El Niño winters without SSWs (Fig. 4.3f) shows a significant cooling in early winter and a more similar behavior to the CP El Niño signal without SSWs.

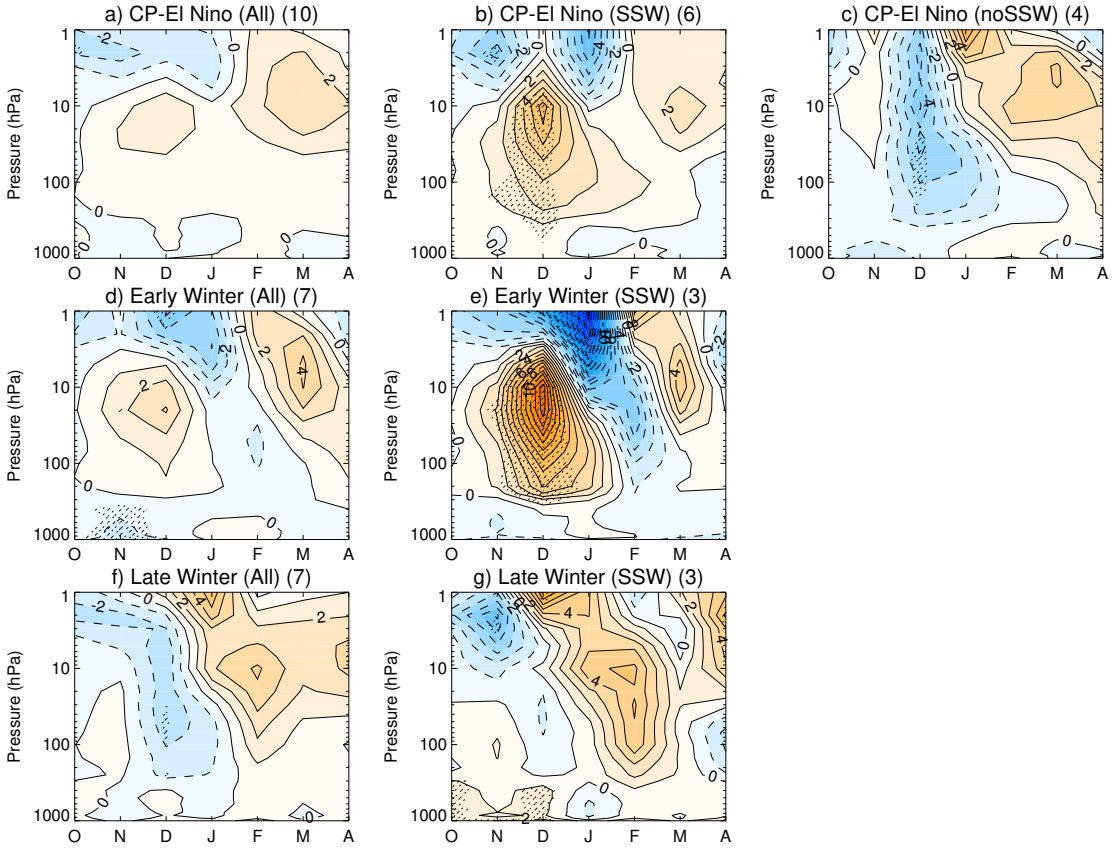

Figure 4.3. October to April composites of the monthly mean zonal-mean temperature anomaly at 80ºN for (a, d, f) CP El Niño all winters, (b, e, g) CP El Niño winters with SSWs and (c) CP El Niño winters without SSWs. Second row (d-e) includes only early winter SSWs and third row (f-g) includes only late winter SSWs (see details in Table 4.2). The number in brackets indicates the number of winters in the composite. Contour interval is 1K. Solid (dashed) contours denote positive (negative) anomalies. Stippling indicates significance at the 95% level.

We have reproduced this analysis in the other definitions used for CP El Niño in Fig. 4.2 and results are robust across indices, supporting the fact that the timing of SSWs can affect the observed CP El Niño signal. At the same time, the early/late winter SSWs distinction reinforces our conclusion about the role of SSWs on the CP El Niño response, as we have shown that the signal is modulated by the timing of SSWs. In particular, the analysis performed here reveals that early winter SSWs, those occurring in November and December, are more effective in masking the signal of CP El Niño events than those occurring later on, in January and February.

4.4 Preceding mechanisms

Section 4.1 showed that the CP El Niño response is robust in the absence of SSWs, and opposite to that of EP El Niño from November to January. Next, we investigate the mechanism behind these differences. As discussed in the Introduction, the Aleutian low, through the PNA pattern, is known to be the main pathway whereby ENSO modulates the polar vortex. Figure 4.4 shows the November-December (ND) mean eddy geopotential height anomalies at 500hPa in winters with and without SSWs. ND mean is chosen as these months show the largest signals in the polar stratosphere (Fig. 4.1). Results are very similar for the NDJ average. EP El Niño events (with and without SSWs) (Figs. 4.4a, c) and CP El Niño events with SSWs (Fig. 4.4b) feature a strengthening of the PNA pattern: significant positive height anomalies over North America and a deepened Aleutian low. The deepening of the Aleutian low is weaker and shifted south in EP El Niño events that occur during winters with SSWs (Fig. 4.4a). This is likely related to weaker EP El Niño events, indeed the composite of the standardized SSTA in the N3 region during EP El Niño winters with SSWs is 1.24 SD, much weaker than the 2.92 SD value obtained during EP El Niño events without SSWs. Likewise, the weaker signal could be due to the delayed SSW occurrence: while during CP El Niño winters

with SSWs (Fig. 4.4 b) half of the SSWs occurred in November or December, during EP El Niño winters SSWs mainly occur in January, consistent with a deeper Aleutian low from January to February. Contrary to the behavior during EP and CP El Niño winters with SSWs, it is evident that CP El Niño winters without SSWs are characterized by a significant "reverse PNA" pattern, with large negative height anomalies over North America and an anomalously weak Aleutian low, as reported by Hegyi and Deng (2011) and Sung et al. (2014) for early winter. Thus, PNA-like patterns of opposite sign are found for CP El Niño winters with and without SSWs (Figs. 4.4b vs. d), and also between all EP El Niño winters and CP El Niño winters without SSWs (Figs. 4.4a,c vs. d).

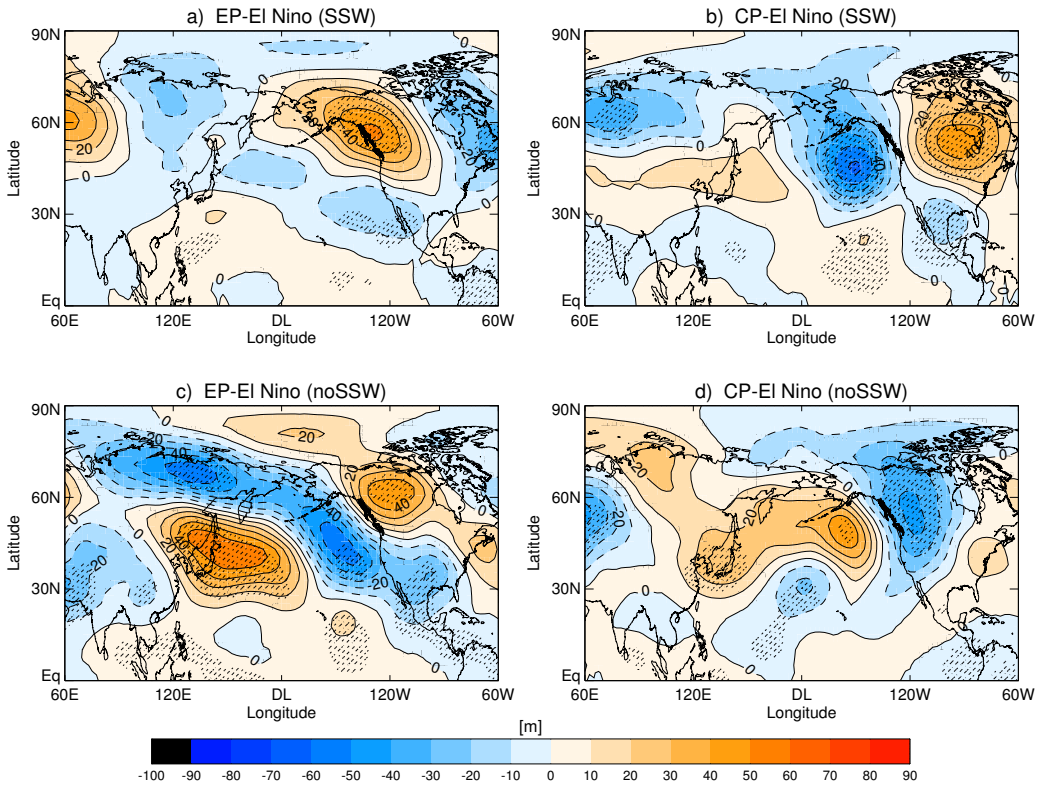

Figure 4.4. Longitude-latitude composite of the ND average eddy geopotential height anomalies at 500hPa for (a,c) EP El Niño and (b,d) CP El Niño winters (a,b) with and (c,d) without SSWs. Solid (dashed) contours denote positive (negative) anomalies. Stippling indicates significance at the 95% level.

The observed different PNA patterns during EP and CP El Niño in the absence of SSWs seem to be related to differences in tropical convection due to the distinct location of SSTA in the tropical Pacific. As explained in the Introduction, the largest SSTA are located westward in the Tropical Pacific Ocean during CP El Niño compared to EP El Niño. This leads to differences in tropical convection and the associated tropospheric teleconnections for each El Niño type (Weng et al. 2007, 2009; Kao and Yu 2009; Zubiaurre and Calvo 2012; Sung et al. 2014). In this respect, Weng et al. (2009) already showed different PNA patterns for EP and CP El Niño (see Fig. 1.7). These patterns are very similar to ours in the absence of SSWs. Sung et al. (2014) also reported different behaviors for the Aleutian low between CP and EP El Niño events. As they show, the more westward the maximum in tropical SSTA during an El Niño event, the weaker the Aleutian low. Similarly, the more eastward the maximum in tropical SSTA, as in EP El Niño events, the deeper the Aleutian low. However, this does not explain the differences in the CP El Niño pattern between CP El Niño winters with and without SSWs.

Still, we need to understand the differences between CP El Niño winters with and without SSWs. Recently, Hurwitz et al. (2012) found, in an idealized modelling study, a weaker Aleutian low and a colder polar stratosphere in response to positive SSTA over the North Pacific. To understand if anomalous SSTs in this region can explain the weaker Aleutian low in the case of CP El Niño events without SSWs, Figure 4.5 shows the SSTA for ND mean during CP El Niño winters. Similar results are obtained for NDJF mean. We focus the attention over two regions. First, the inspection of the SSTA on the North Pacific region (40ºN-50ºN, 160ºE-200ºE), as defined by Hurwitz et al. (2012), does show significant differences for CP El Niño winters with and without SSWs (Fig. 4.5c). For CP El Niño winters without SSWs, warmer SSTA appear in that region (Fig. 4.5b) coinciding with a weakening of the Aleutian low, and in

agreement with results from Hurwitz et al. (2012). In contrast, during CP El Niño winters with SSWs the region presents colder SSTA (Fig. 4.5a).

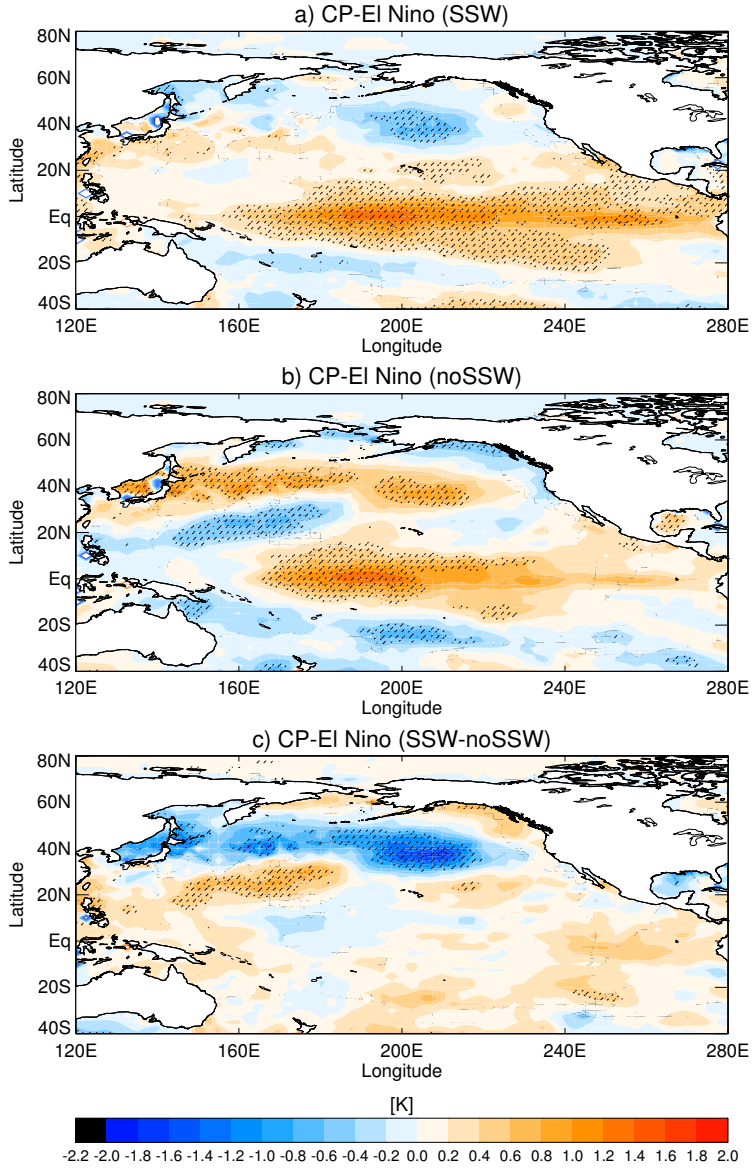

Figure 4.5. Composite of the ND average SSTA for CP El Niño winters (a) with and (b) without SSWs. (c) Differences between winters with and without SSWs. Solid (dashed) contours denote positive (negative) anomalies. Stippling indicates significance at the 95% level with a Monte Carlo test.

Interestingly, the evaluation of the tropical SSTA do not show significant differences between CP El Niño winters with and without SSWs (Fig. 4.5c). Therefore, the detected different PNA patterns in CP El Niño winters with and without SSWs cannot be directly attributed to differences on tropical SSTA. Whether or not the different SSTs in this North Pacific region are due to the individual CP El Niño cases included or might be due to the signal of SSWs precursors is unknown and could be the aim of a future study.

The weakened PNA pattern for CP El Niño winters without SSWs reported in Fig.4.4 is in agreement with the subsequent observed stratospheric polar cooling, as it likely inhibits upward wave propagation. This is confirmed by the analysis of upward propagation of planetary waves that might induce winter polar vortex perturbation. Figure 4.6 shows the longitude-pressure cross-sections of wave number 1 and wave number 2 components of geopotential height anomalies, averaged from 45ºN to 75ºN and ND. To perform the wave number decomposition, a Fourier analysis is applied to the geopotential height field. Only EP and CP El Niño winters without SSWs are shown, as these can be understood in terms of linear dynamics, when interference theory applies.

EP El Niño events display wave number 1 geopotential height anomalies (colors) in phase with the climatology (contours) (Fig. 4.6a), so the stationary wave number 1 is enhanced (Manzini et al. 2006; Garfinkel and Hartmann, 2008). Also, the anomalies exhibit a westward tilt with height, indicating upward propagation of Rossby waves. Wave number 2 anomalies (Fig. 4.6c) are almost in quadrature with respect to the climatology, showing a mild weakening of wave number 2. These results are consistent with the extratropical wave modulation known for the canonical El Niño (e.g., Garfinkel and Hartmann, 2008). In contrast, CP El Niño wave number 1 anomalies (Fig. 4.6b) are out of phase with the climatology such that the climatological stationary wave number 1 is weakened. This leads to suppressed anomalous upward propagation and a stronger polar vortex. Wave number 2 anomalies

(Fig. 4.6d) are weak in amplitude and tend to weaken the climatological pattern in the troposphere, while in the stratosphere they are almost negligible.

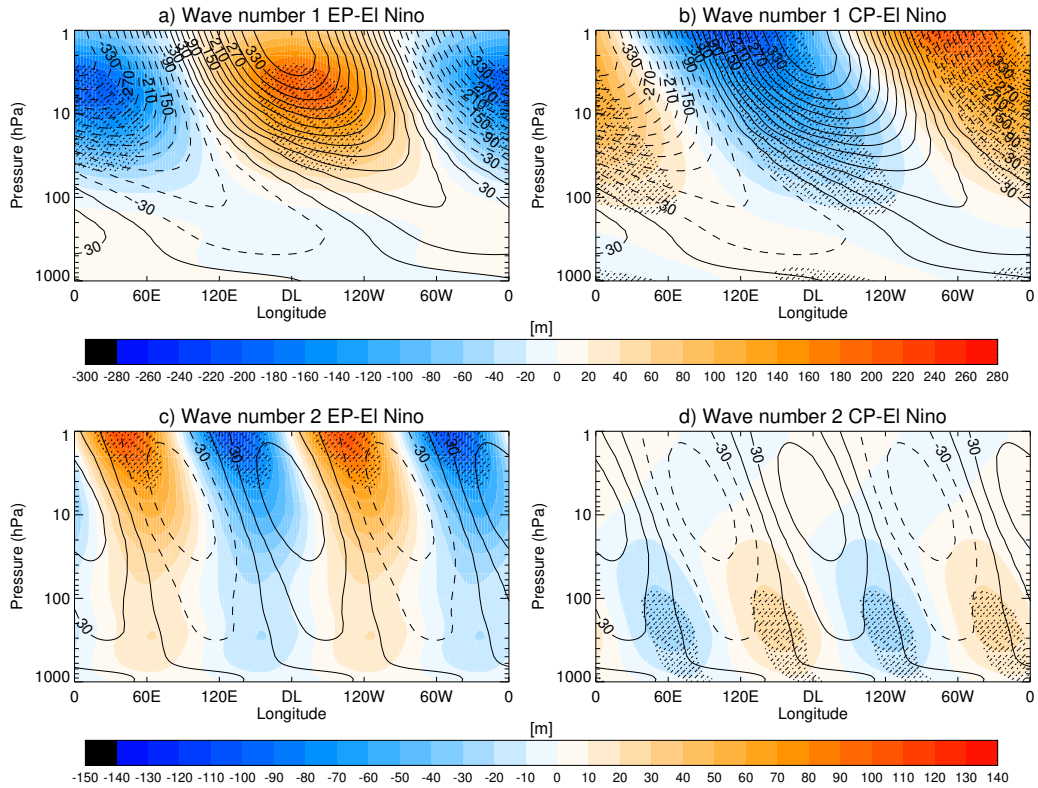

Figure 4.6. Longitude-pressure cross sections of the composite of (a, b) wave number 1 and (c, d) wave number 2 components of 45ºN-75ºN ND averaged geopotential height anomalies (color contours), for (a, c) EP El Niño and (b, d) CP El Niño winters without SSWs. Solid (dashed) line contours denote positive (negative) values of the climatology averaged for November and December (interval of 30 m). Stippling indicates significance at the 95% level.

We conclude that, in the absence of SSWs perturbations, a robust negative PNA pattern is observed during CP El Niño winters, which weakens the climatological wave number 1 pattern and its upward propagation into the stratosphere, in accordance with the previously shown stratospheric cooling for CP El Niño winters without SSWs.

4.5 Summary and Discussion

This chapter uses ERA-40 and ERA-Interim reanalyzes to identify EP and CP El Niño signals in the NH polar stratosphere, characterized by N3 and N4 indices. We have found that the SSW occurrence, particularly SSWs of November and December, modulates the CP El Niño signal in the polar stratosphere. CP El Niño winters without SSWs exhibit a significant cooling in the middle polar stratosphere, while in winters with SSWs a significant warming appears. Examination of the PNA pattern and the wave anomalies in the stratosphere support the reported stratospheric signals. In the absence of SSWs, EP El Niño winters are characterized by a strengthened PNA pattern and enhanced propagation of planetary wave number 1 into the stratosphere, while the opposite occurs during CP El Niño winters. Insofar as wave dissipation in winters without SSW might be expected to depend linearly on wave amplitude, this is consistent with a weaker polar vortex during EP El Niño winters and a stronger vortex during CP El Niño winters (Manzini et al. 2006; Garfinkel and Hartmann, 2008; Hegyi and Deng, 2011).

Contrary to previous studies that investigated the CP El Niño signal in the NH polar stratosphere, our results are robust regardless of the CP El Niño definition and the size of the composite used. Thus, this work demonstrates that the influence of SSWs needs to be taken into account to obtain a statistically significant polar stratospheric response during CP El Niño winters. Then, better predictions of the boreal winter polar stratosphere during El Niño events would require better understanding of SSW precursors.

Our study also explains why different results have been reported regarding the CP El Niño NH stratospheric response (e.g., Garfinkel et al. 2013), since, when compositing all CP El Niño cases together, the occurrence of SSWs can mask the CP El Niño signal, leading to non-robust results. Moreover, our results shed light on the comparison of EP vs. CP El Niño signals. For

winters with SSWs the observed middle stratospheric signal for EP and CP El Niño is similar, due to the predominant impact of SSWs. In the absence of SSWs, the stratospheric responses to EP and CP El Niño events are distinct from November to January.

We are aware that the observational record is short, especially when distinguishing EP and CP El Niño winters with respect to the occurrence of SSWs. Nonetheless, the polar stratospheric response to CP El Niño has been analyzed using four different indices and different thresholds to allow changes in the composite sizes, following the methodology of Garfinkel et a. (2013). The results were found to be consistent in all cases. That is, we invariably find that the polar stratospheric response to CP El Niño is ruled by the occurrence of SSWs: anomalously warm during winters with SSWs and anomalously cold during winters without SSWs. It would be of interest to see whether this result can be found in numerical models with a well resolved stratosphere.

In this regard, the very recent modelling study by Calvo et al. (2017) confirms our reanalysis results. Indeed, high-top CMIP5 models simulate a robust weaker polar vortex during EP El Niño winters, while the signal of CP El Niño is not significant, as it depends on SSW occurrence. Considering the CMIP5 models used by Calvo et al. 2017, we reproduce the time-pressure evolution of the zonal-mean temperature as in Fig 4.1. Resulting Figure 4.7 is analogous to Figure 7 in Calvo et al. (2017), where the zonal-mean zonal wind is shown. CMIP5 model results in Fig. 4.7 are in remarkable agreement with Fig. 4.1.

During EP El Niño winters, a significant warming is simulated in the upper stratosphere in December regardless of the occurrence of SSWs (Figs. 4.7a to c). However, this response propagates downwards only during EP El Niño winters with SSWs (Fig. 4.7b), reaching the troposphere from February to April. In contrast, in the absence of SSWs in the EP El Niño composite (Fig. 4.7c), the upper stratospheric warm anomaly in December does not propagate into the troposphere. Again, these differences in the EP El Niño signal highlight the role of SSWs in propagating the signal towards the troposphere, in agreement with previous single-model studies (e.g., Cagnazzo and Manzini 2009).

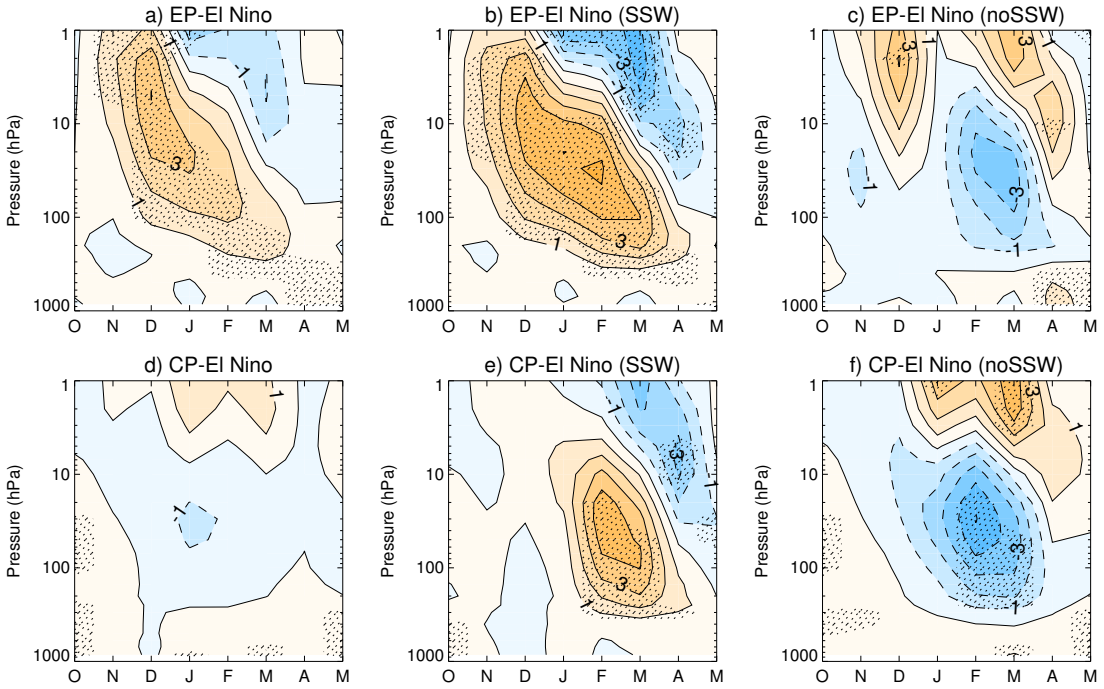

Figure 4.7. Time-pressure cross section of the zonal mean temperature anomalies at 80ºN composited for (a) EP El Niño and (d) CP El Niño. (b) and (e) for EP and CP El Niño winters with SSWs. (c) and (f) for EP and CP El Niño winters without SSWs. Contour intervals is 1 K. Solid (dashed) contours denote positive (negative) anomalies. Stippling indicates significance at the 95% confidence level for a Monte Carlo test. The CMIP5 models used here are listed in Calvo et al. (2017).

During CP El Niño winters (Fig. 4.7d), the lack of a robust signal appears, as in reanalysis data. During CP El Niño winters with SSWs (Fig 4.7e), significant warm anomalies are simulated in the middle stratosphere and in the troposphere (from February to April). Note that contrary to EP El Niño winters, the response in the upper stratosphere in early winter (December) is positive, but very weak and non-significant. During CP El Niño winters without SSWs (Fig. 4.7f), a significantly stronger stratospheric polar vortex is simulated in February and March, in agreement with reanalysis results. Therefore, our conclusions, based on reanalysis, have been corroborated by a set of high-top CMIP5 models (Calvo et al. 2017).

Moreover, our investigation allowed better understanding the recent 2015/16 El Niño winter, one of the strongest events on record (L'Heureux et al. 2016) and of a unprecedented nature (Palmeiro et al. 2017). As noted by Palmeiro et al. (2017), who used our same definitions to select EP and CP El Niño events (see chapter 2), the 2015/16 El Niño was classified as an EP El Niño type, but, at the same time, record breaking SSTA were reported on the CP El Niño region. These high values of SSTA together with the absence of SSWs during the 2015/16 winter, lead to a stronger and colder polar vortex in early winter with very low values of polar stratospheric ozone. Note that the polar vortex response to El Niño 2015/2016 is in agreement with our result for CP El Niño winters without SSWs (Figs. 4.1 and 4.2). Analogously, Palmeiro et al. (2017) observed an anomalously weak Aleutian low and a reduced upward wave activity in November and December, similar to the tropospheric teleconnections we found for CP El Niño winters without SSWs (Figs. 4.4d and 4.6b). Thus, our results have been of relevance in order to explain the complex behavior of the 2015/16 El Niño winter.

5 El Niño and La Niña Asymmetry

Its impact on the Stratospheric Pathway in a Model Grand Ensemble

As mentioned in the Introduction the asymmetry in the stratospheric response between El Niño and La Niña has not been widely explored, mainly because previous reanalysis and observational studies did not report a strong or significant stratospheric signal during La Niña winters. However, in chapter 3, we have identified a robust NH stratospheric pathway for La Niña in reanalysis data, characterized by a robust colder and stronger polar vortex in the stratosphere and a positive NAO phase at the surface, opposite to the well-known stratospheric pathway for EP El Niño. At the same time, the two types of El Niño have not been considered separately in previous studies of atmospheric ENSO asymmetry. Nevertheless, in chapter 4 we showed that EP and CP El Niño events present different stratospheric signatures. While EP El Niño winters are associated with a robust weaker and warmer polar vortex, the stratospheric signal of CP El Niño events is modulated by SSW occurrence.

In light of these results, we aim to introduce a distinct perspective on the study of the asymmetry between El Niño and La Niña, by: 1) analyzing the different El Niño flavors against a unique La Niña type and 2) extending the assessment of the asymmetry from the SSTA to the stratospheric pathway and its influence over the NAE region. Furthermore, we also address El Niño and La Niña asymmetry in a novel way, because we make use of a much larger ensemble than previous studies. Zhang et al. (2014), using 16 ensemble members, that were resampled to generate 256 asymmetry estimates, did not report any sampling variability in the SSTA forcing asymmetry. In contrast, we have a total of 100 members, each one representing a feasible realization of the historical period. Therefore, we are able to investigate the sample variability of the El Niño and La Niña asymmetry in the SSTA forcing and whether, if exists, this is a major driver of the variability in the atmospheric asymmetry response. The results of this chapter have been submitted for publication (Iza et al. 2017, submitted to *J. Climate*).

5.1 Model performance

In this chapter, we use the large MPI-ESM-LR ensemble model (hereafter "MPI model"). The stratosphere of the ECHAM6 atmospheric component is modeled following the previously documented version of the MPI atmospheric component, namely, the ECHAM5 model. Thus, the MPI model simulates the stratospheric pathway of EP El Niño, characterized by a weakening of the polar vortex and higher surface pressure over the Arctic, in the same manner as the ECHAM5 model (see Manzini et al. 2006; Cagnazzo and Manzini 2009). Moreover, given the large number of events from the grand ensemble, not available at the time of ECHAM5, we have additionally found that the MPI model captures (1) the differences in the stratospheric pathway between CP and EP El Niño, as previously documented in the multi-model assessment by Calvo et al. (2017) (see Fig. 4.7) and (2) La Niña stratospheric

pathway that we reported in reanalysis data (see chapter 3). The MPI model has also been previously used by Domeisen et al. (2015) to analyze the stratospheric pathway of ENSO in relation to seasonal predictability.

5.2 Asymmetry sample variability

First, we explore the existence of sample variability in the asymmetry of the forcing, i.e., the asymmetry in SSTA. Figure 5.1 shows the distribution of the RMS SSTA asymmetry (see chapter 2 for details) for EP El Niño+La Niña (Fig. 5.1a) and CP El Niño+La Niña (Fig. 5.1b), exposing a substantial spread among the members. In particular for EP El Niño and La Niña the range spans about an order of magnitude. This pioneer result reveals sample variability in the SSTA asymmetry across the MPI 100 members. Note that this feature was missing in the previous study of Zhang et al. (2014), raising the question of whether their method of re-sampling 16 individual members to obtain 256 asymmetry samples might diminish the forcing variability.

EP El Niño+La Niña and CP El Niño+La Niña RMS SSTA distributions present similar mean values, 0.4 K and 0.35 K, respectively (noted by vertical dashed lines). However, EP El Niño+La Niña RMS values are distributed within a larger range (1.05 K, three times the median, 0.35 K), than CP El Niño+La Niña, whose range (0.55 K) is about 50% lower. Likewise, whereas CP El Niño+La Niña distribution is closer to a normal distribution, the large kurtosis for EP El Niño+La Niña (4.49 K against 0.72 K for CP El Niño+La Niña) indicates a higher number of members with high asymmetry.

Fig. 5.1 also includes the RMS SSTA asymmetry in HadISST observations (black squares). For EP El Niño+La Niña, the observed RMS asymmetry is located between the 50th and 75th percentiles of the all-members' distribution (see Table 5.1). While the observed CP El Niño+La Niña value is in the low asymmetry tail, close to the 10^{th} percentile (left dotted line in Fig. 5.1b). As the observed values fall within the range of the members' samples, we

conclude that the model is able to capture the observed ENSO asymmetry and to reproduce other plausible realities, besides the one observed so far.

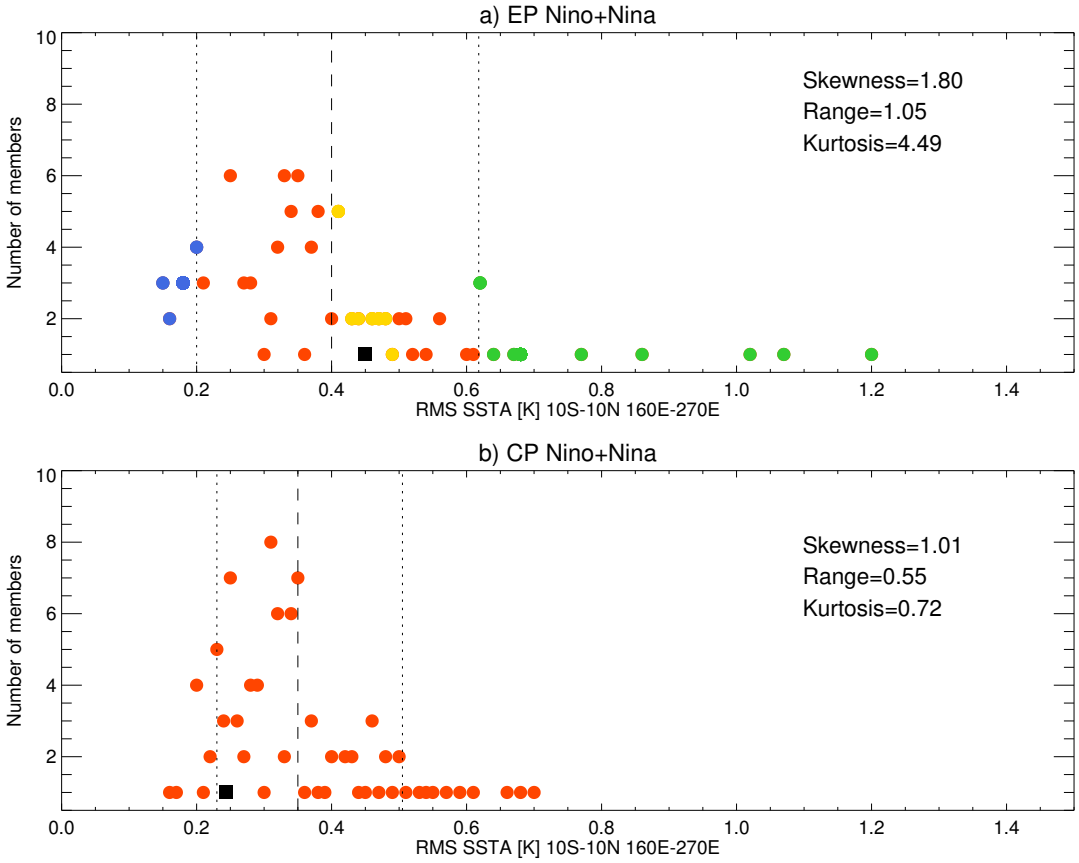

Figure 5.1. Histogram for the NDJF averaged RMS SSTA asymmetry over the Pacific region (160ºE-270ºE, 10ºS-10ºN) for (a) EP El Niño+La Niña and (b) CP El Niño+La Niña. The circles correspond to the 100 members and the black square indicates the RMS asymmetry in HadISST observations. The range, the skewness and the kurtosis for each distribution are shown in each panel. Vertical dashed and dotted lines denote the 10th, the mean and 90th percentiles. For EP El Niño+La Niña, in panel a), members below the 10th percentile (LOWASYM) and above the 90th percentile (HIGHASYM) are noted by blue and green colors respectively. Members with an asymmetry level similar to observations (ASOBS) are indicated by yellow colors (see details in the text).

Table 5.1. (Top) EP El Niño+La Niña diagnostics defined as: the NDJF averaged RMS SSTA over the Pacific equatorial region (160ºE-270ºE, 10ºS-10ºN); the DJF averaged RMS of the eddy geopotential height anomalies (Z'a) at 500hPa over the Pacific region (120ºE-60ºW, 30ºN-75ºN); the JFM averaged RMS of the zonal-mean zonal wind anomalies (Ua) between 10hPa-30hPa and 50ºN-80ºN; and the FM averaged RMS of the SLPa over the NAE region (25ºW-30ºE, 20ºN-90ºN) for the reanalysis and selected members. (Bottom) percentiles of the EP El Niño+La Niña for the above fields as derived from the distribution of the 100 ensemble members.

Composited values

	SSTA (K)	**Z'a (m)**	**Ua (m s^{-1})**	**SLPa (hPa)**
OBS (Reanalysis)	0.45	22.60	4.40	1.32
ASOBS	0.45	24.76	4.12	1.99
LOWASYM	0.18	18.84	3.75	1.98
HIGHASYM	0.82	32.31	5.85	2.70
Equal SSTA intensity	0.33	22.98	3.46	2.19
Stronger EP El Niño	0.91	30.89	7.24	2.71
Stronger La Niña	0.58	24.14	2.42	2.05

Distribution percentiles

	SSTa (K)	**Z'a (m)**	**Ua (m s^{-1})**	**SLPa (hPa)**
10^{th} percentile	0.20	14.21	1.17	1.48
25^{th} percentile	0.28	17.22	1.88	1.65
50^{th} percentile	0.35	21.91	3.05	1.94
75^{th} percentile	0.47	28.03	4.69	2.50
90^{th} percentile	0.62	35.37	6.57	3.00

Given that the grand ensemble shows sample variability in the SSTA asymmetry, we next explore whether the RMS asymmetry of the forcing can be traced up to the atmospheric ENSO response. Figure 5.2 illustrates the relationship between the RMS asymmetries in SSTA and the DJF eddy geopotential height anomalies (Z'a). The RMS asymmetry of Z'a, was also evaluated by Zhang et al. (2014) and the results agree well. For EP El Niño+La Niña (Fig. 5.2a), we found a positive correlation (r=0.51) between the SSTA asymmetry and the Z'a asymmetry, significant at the 95% confidence level, so that a high or low RMS asymmetry in the SSTA forcing leads to a corresponding high or low degree of asymmetry (defined by the RMS) in the tropospheric response. This means that the sample variability in the atmospheric response over the North Pacific is partly driven by the variability on the SSTA asymmetry. Still, internal variability plays a role in mid-latitudes (Hoerling et al. 2001), and indeed the significant correlation shown in Fig. 5.2a is moderate. In contrast, a significant relationship between the RMS asymmetry in the SSTA and the atmospheric response is not found for CP El Niño+La Niña (Fig. 5.2b). The very weak and non-significant correlation could be related to the lack of a robust atmospheric response to CP El Niño (chapter 4). Thereafter, from now on, we focus exclusively on the analysis of EP El Niño+La Niña.

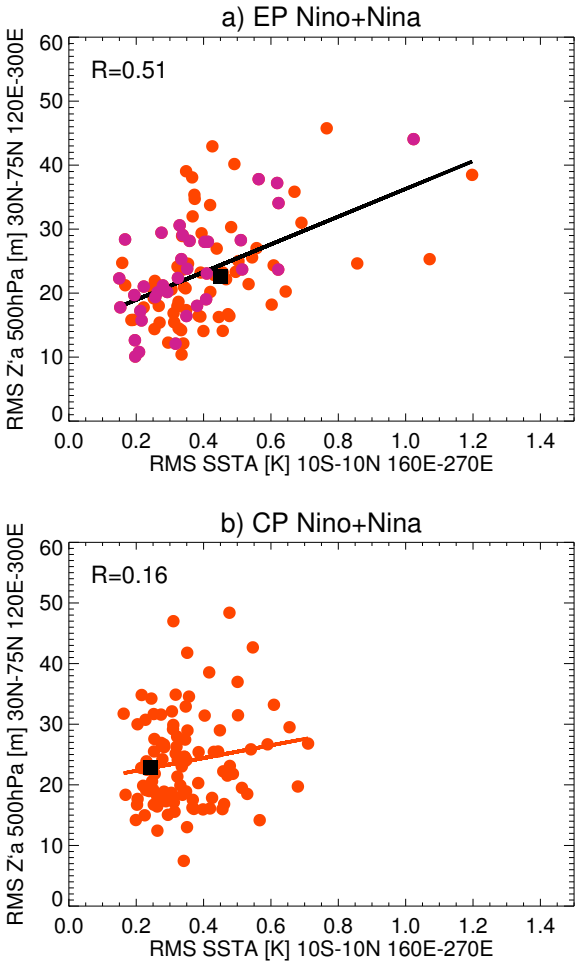

Figure 5.2. Scatter plot of the NDJF averaged RMS asymmetry in SSTA vs. the DJF averaged RMS asymmetry in Z'a for (a) EP El Niño+La Niña and (b) CP El Niño+La Niña. The correlation coefficient is noted in the upper-left corner of each scatter plot. The line indicating the linear fit is colored black (red) for significant (non-significant) correlations at the 95% confidence level. The circles correspond to the 100 members and the black square indicates the reanalysis. In panel a), members with about equal EP El Niño and La Niña SSTA intensity are noted by purple colors. See Table 5.1 for the definition of the different asymmetry diagnostics.

The stratospheric pathway for EP El Niño+La Niña RMS asymmetry is shown in Figure 5.3. The scatter plots for the JFM averaged RMS asymmetry of

the zonal wind anomalies (Ua) vs. RMS asymmetries in SSTA and Z'a are shown in Figs. 3.5a and 3.5b, respectively. The relationship between Ua and February-March (FM) averaged RMS asymmetry of the sea level pressure anomalies over the NAE region (SLPa) is shown in Fig. 3.5c. Sample variability is found in both the stratospheric polar vortex RMS asymmetry, measured by the Ua, and SLPa RMS asymmetry. The asymmetry in the stratospheric response shows a weaker, but still significant relationship with SSTA (r=0.23, Fig. 5.3a) and Z'a (r=0.31, Fig. 5.3b). Thus, other sources of variability contribute to the asymmetry of the RMS zonal wind. A weak, but again significant, correlation is also found between the RMS asymmetry in Ua and SLPa (r=0.34, Fig. 5.3c). Therefore, despite other sources of atmospheric variability are clearly contributing to the range of the RMS asymmetries reported in Fig. 5.3, the weak but significant relationships between the indices of the stratospheric pathway emerging from Fig. 5.3 indicate that the EP El Niño+La Niña asymmetry of the forcing can be traced to the polar stratosphere and to the NAE region, throughout the tropospheric ENSO asymmetry of the Pacific North American region.

5.3 Asymmetry evaluation

5.3.1 Comparison with reanalysis

To compare the modeled anomaly patterns with the reanalysis, we selected a subsample of members with RMS SSTA asymmetry values comparable to the observed one (0.45 K). To do so, and based on Fig. 5.1a, we defined an interval of 0.45±0.50 SD for the distribution of the 100 members' asymmetry. We found 16 members within this interval, noted by yellow colors in Fig. 5.1a and named ASOBS (as observations). The mean RMS asymmetry value of all these members is the same as that for reanalysis (0.45 K). ASOBS can therefore be compared with observations and reanalysis. We also tested other intervals to select ASOBS members and the results are robust to different composite sizes.

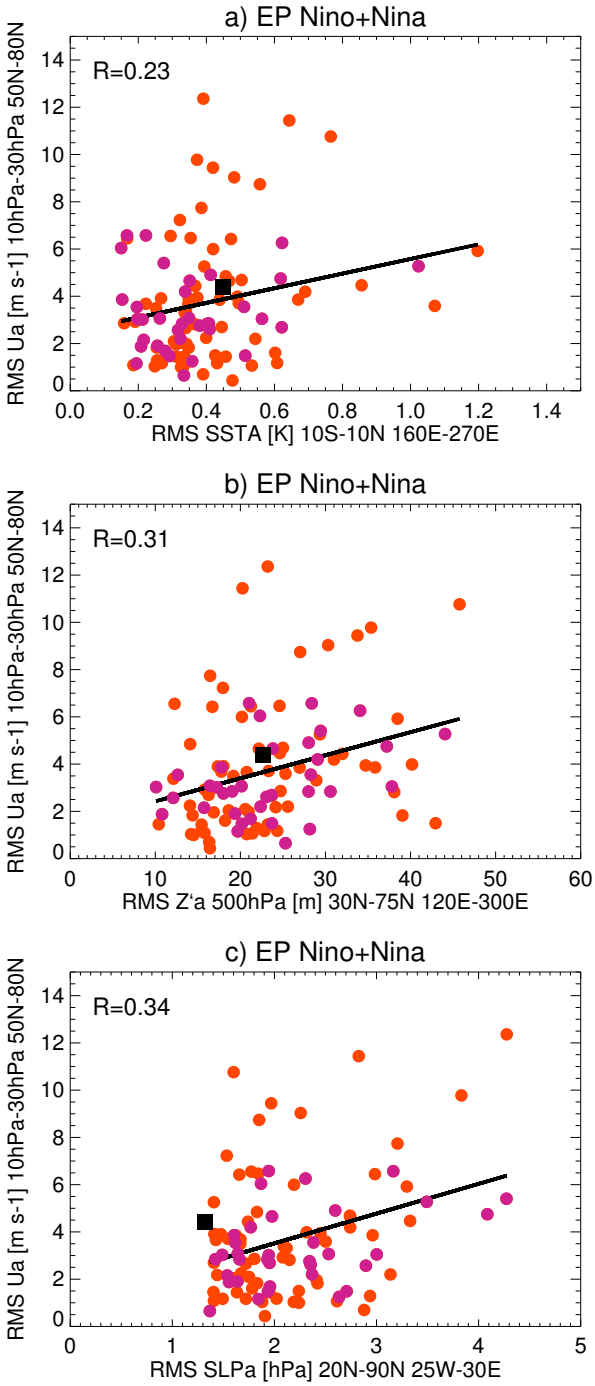

Figure 5.3. As in Fig. 5.2, but for the JFM averaged RMS asymmetry in Ua at the polar stratosphere vs. (a) the NDJF SSTA; (b) the DJF Z'a and (c) the FM SLPa RMS asymmetry for EP El Niño+La Niña.

Figure 5.4 shows the symmetric and asymmetric components between EP El Niño and La Niña in the stratospheric pathway for observations and reanalysis data (denoted as OBS) and ASOBS members. The observed symmetric component computed for HadISST observations (Fig. 5.4a) displays the well-known ENSO SSTA pattern, with positive anomalies along the equatorial Pacific (Hoerling et al. 1997; Zhang et al. 2014). The ASOBS composite (Fig. 5.4b) shows a larger warming around the Date Line, because of the cold bias of the model in the equatorial western Pacific (Jungclaus et al. 2013). For the observed asymmetry (Fig. 5.4c), a significant warming appears in the eastern Pacific region, as a result of the differences in the location of the maximum SSTA between EP El Niño and La Niña, and the larger absolute SSTA for EP El Niño. The ASOBS members' asymmetry is comparable by construction (Fig. 5.4d).

The symmetric components of Z'a (Figs. 5.4e, f) present the characteristic EP El Niño deepening of the Aleutian low, with negative anomalies over the North Pacific Ocean and positive anomalies over North America in both reanalysis and the ASOBS members. The asymmetric components (Figs. 5.4g, h) also show negative anomalies over the Aleutian low region, associated with a stronger EP El Niño signature compared to La Niña, as for SSTA (Figs. 5.4c, d). For the reanalysis, the negative asymmetric center is located north of 45ºN (Fig. 5.4g), whereas the symmetric center (Fig. 5.4e) is located south of 45ºN, owing to the distinct impacts of El Niño and La Niña over the Pacific North American region (Hoerling et al. 1997). The modeled asymmetries are qualitatively similar but weaker than in the reanalysis, probably because of a reduced phase's shift between El Niño and La Niña in the model (Zhang et al. 2014) or because the ensemble mean smooths the signal. However, the composited RMS Z'a asymmetry for ASOBS is similar to that in the reanalysis (24.76 m against 22.60 m, Table 5.1).

In the stratosphere, the symmetric components (Figs. 5.4i, j) show negative anomalies in Ua, as a result of the polar vortex weakening (negative Ua) for EP El Niño and its strengthening (positive Ua) for La Niña (not shown). For the asymmetry (Figs. 5.4k, l), negative Ua indicate stronger anomalies for EP El Niño than for La Niña, in line with the negative Z'a in the troposphere (Figs. 5.4g, h) that prompt enhanced upward wave-activity towards the stratosphere. Again, the modeled anomalies are smaller than for the reanalysis, but the RMS values are still located between the 50th and 75th percentiles of all-members' distribution, as is the reanalysis value (Table 5.1). The lack of a significant stratospheric signature in reanalysis (Fig. 5.4k) might manifest the need of a longer dataset. In fact, as shown in chapter 3, a long reanalysis period is required to obtain a robust response for La Niña. After all, the reanalysis is just one realization.

The stratospheric pathway for EP El Niño and La Niña show anomalies that are translated to the surface in the NAE region. Reanalysis and ASOBS symmetric components reveal a good agreement on the SLPa (Figs. 5.4m,n), characterized by positive anomalies over the Arctic and a negative response over the north Atlantic, displaying a negative NAO-like pattern, associated with the EP El Niño remote teleconnections. For SLPa asymmetric components, only ASOBS displays negative anomalies over the NAE region (Fig. 5.4p). The reanalysis does not show any significant surface response in that region (Fig. 5.4o), in agreement with the lack of a robust signal for the polar stratosphere (Fig. 5.4k). Thus, the reanalysis RMS SLPa asymmetry is located below the 10th percentile, whereas the ASOBS composited value remains between the 50th and 75th percentiles of all-members' distribution (Table 5.1).

In summary, the model results show that for ASOBS members, a moderately high asymmetry, between 50th and 75th percentiles, is maintained throughout the entire stratospheric pathway, characterized by a stronger signature of EP El Niño compared to La Niña, in agreement with observations.

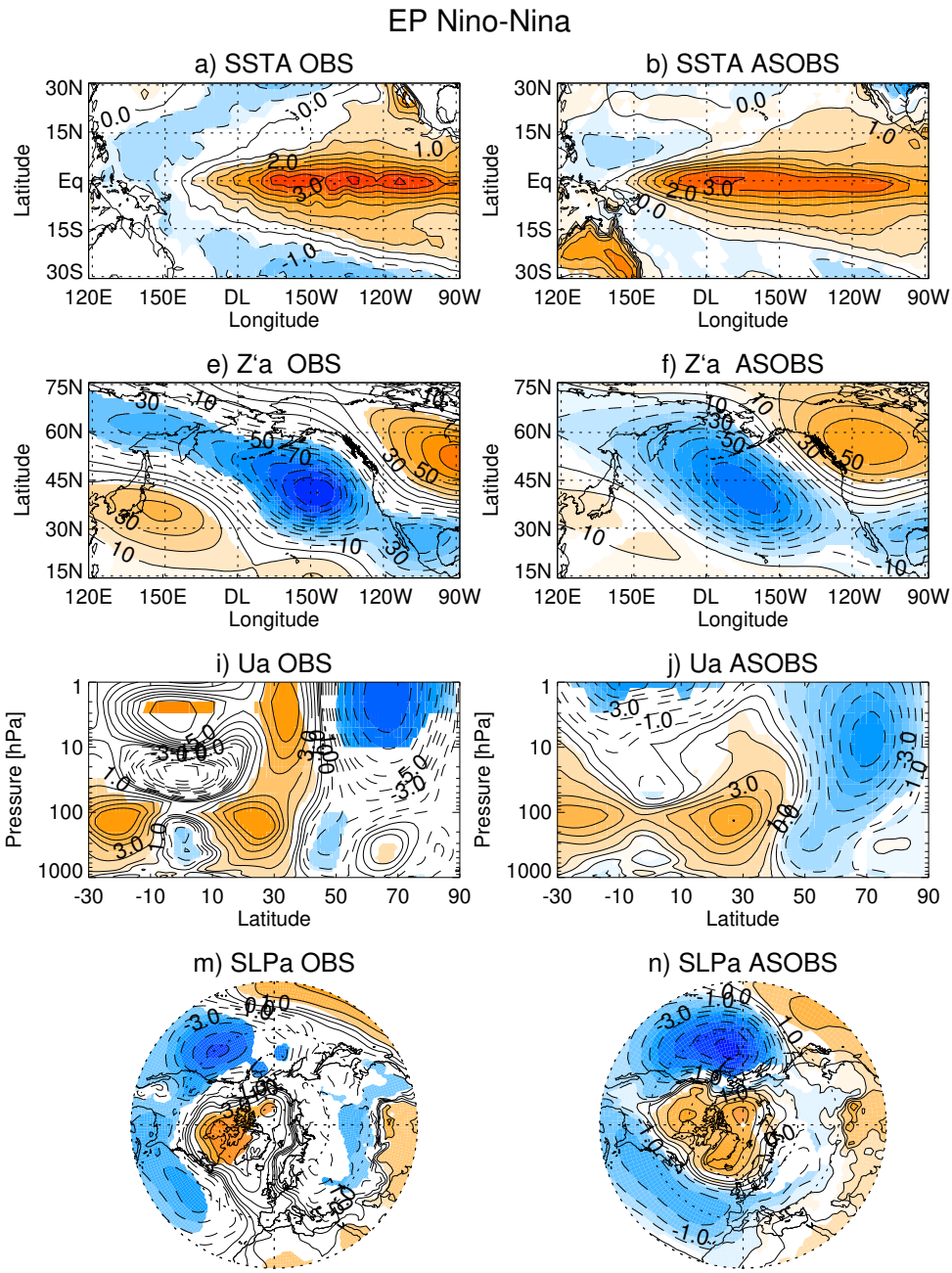

Figure 5.4. Composites of symmetric and asymmetric components of EP El Niño and La Niña for reanalysis (OBS) (1st and 3rd columns) and 16 ASOBS members (2nd and 4rd columns). (a to d) NDJF averaged SSTA (contour interval: ±0.5 K), (e to h) DJF averaged Z'a at 500 hPa (contour interval: ±10 m),

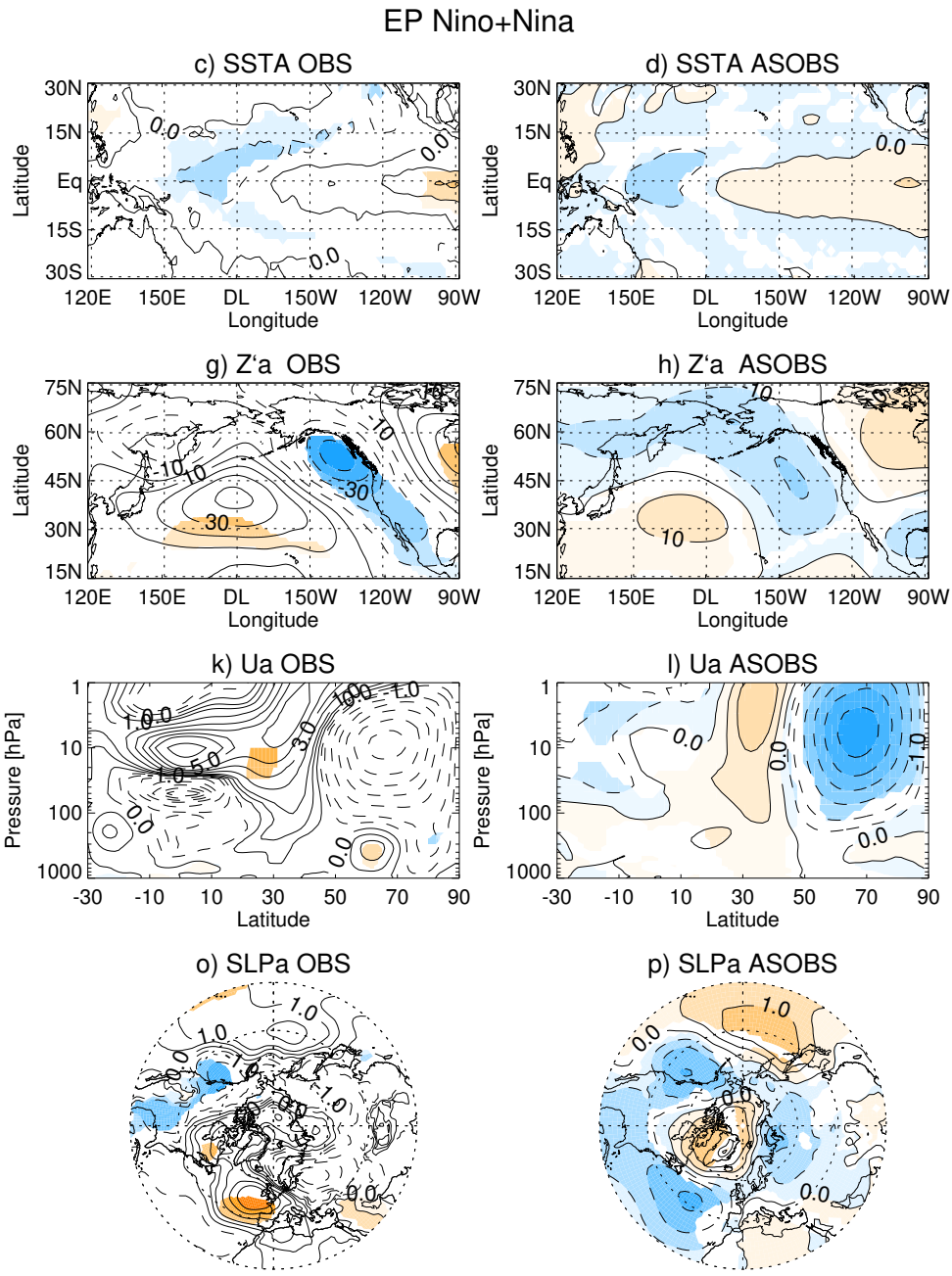

(i to l) JFM averaged latitude–pressure cross sections of Ua (contour intervals: ±0, 0.5, 1, 2, 3, 4, 5, 6 m s^{-1} and every 2 m s^{-1} thereafter) and (m to p) FM averaged SLPa (contour intervals: ±0, 0.5, 1, 2, 3, 4 hPa and every 2 hPa thereafter). Solid (dashed) contours denote positive (negative) anomalies. Shading indicates significant anomalies at the 90% confidence level.

5.3.2 Assessment of extreme asymmetry

In this section, we evaluate the impact of different levels of asymmetry in the stratospheric teleconnection pathway. To do so, based on the level of RMS SSTA asymmetry (Fig. 5.1a) we sub-sampled the members in two groups of members with low and high asymmetry. Members showing values below the 10^{th} percentile are denoted as LOWASYM (low symmetry) members and members with values above the 90^{th} percentile are named as HIGHASYM (high asymmetry) members. The corresponding 10 members are plotted as blue and green dots respectively in Fig. 5.1a.

The stratospheric pathway for low asymmetry (LOWASYM) members is depicted in Figure 5.5. The SSTA do not show any asymmetric signal along the equatorial Pacific (Fig. 5.5a). Accordingly, the corresponding EP El Niño and La Niña SSTA composites (Figs. 5.5b, c) present a highly similar but opposite SSTA forcing. Negligible Z'a asymmetry (Fig. 5.5d) is consistent with the relationship found between SSTA and Z'a in Fig. 5.2a. However, it is striking that the asymmetry in Ua is relatively high and the signature is that of a stronger polar vortex (Fig. 5.5g), with positive Ua. This can be explained by noting that the low SSTA asymmetry is achieved by both similar intensity and location of SSTA for EP El Niño and La Niña (Figs. 5.5b, c). LOWASYM members are characterized by weak EP El Niño events, with large SSTA extended towards west of the Date Line. The study of the CP and EP El Niño signals on chapter 4 showed us that such westward extended El Niño events, close to the CP El Niño type, do not lead to a robust weakening of the stratospheric vortex. Indeed, Z'a asymmetry is not significant over part of the Aleutian low region (Fig. 5.5e) and also, Fig. 5.5h shows a non-significant anomalously strong vortex, an anomaly of the same sign as that for La Niña (Fig. 5.5i). Thus, the longitudinal changes in the location of SSTA with respect the well-known EP El

Niño location can be a conceivable reason for the stronger polar vortex in the stratospheric asymmetric component.

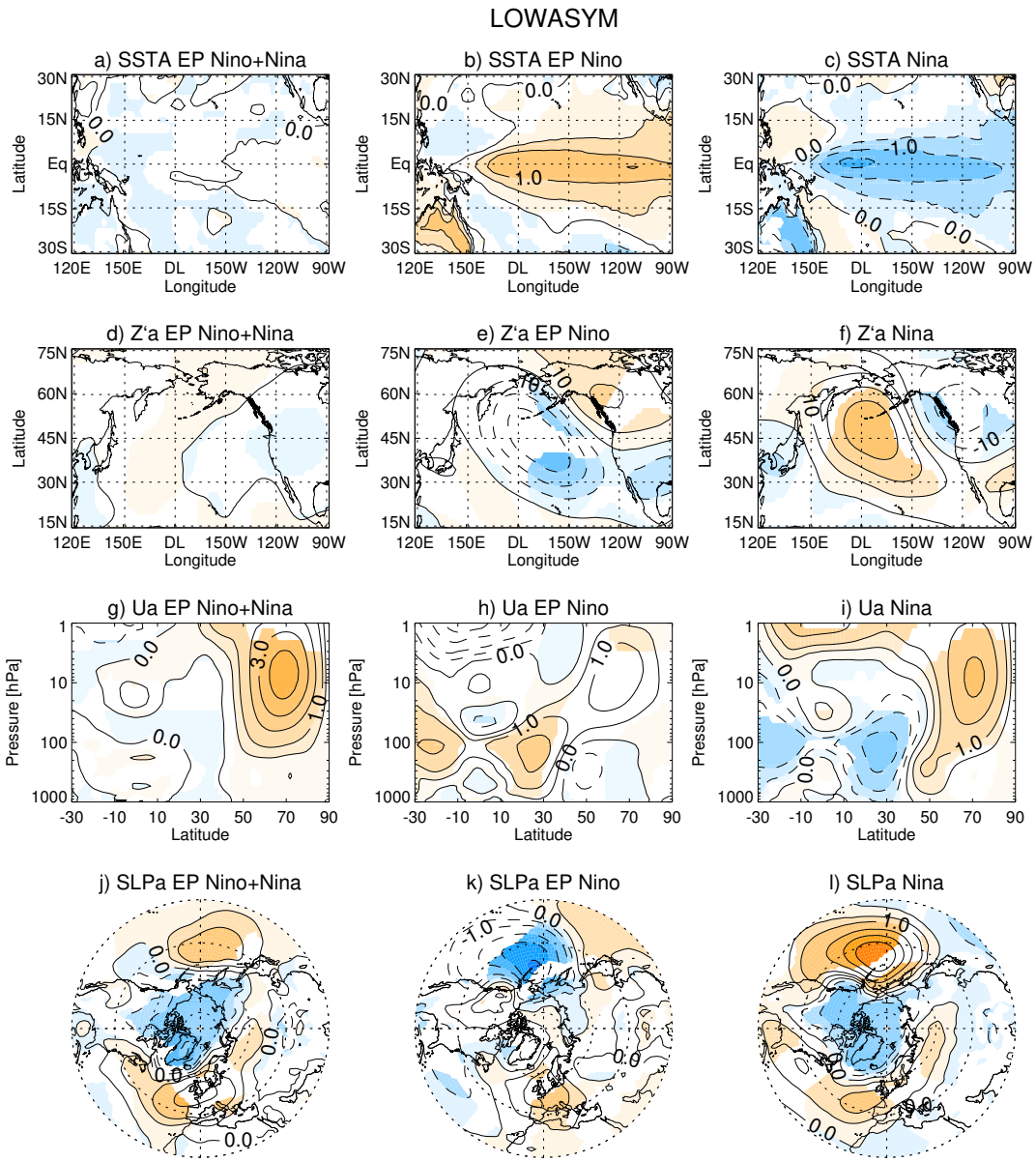

Figure 5.5. Similar to Fig. 5.4, but for the LOWASYM member's composites of (1st column) the asymmetric component of EP El Niño and La Niña, (2nd column) EP El Niño and (3rd column) La Niña.

This interpretation is supported by the weak but positive Z'a asymmetry over the Bering Sea and Alaska region (Fig. 5.5d). This region is known for modulating the upward wave activity flux during the NH wintertime (Nishii et al. 2009). Positive Z'a in this region are related to a suppressed upward wave propagation, which leads to a stronger polar vortex, as in La Niña (Figs. 5.5f,i). Therefore, this means that the main contribution to the stratospheric asymmetry comes from the anomalously strong polar vortex during La Niña winters (Fig. 5.5i). The dominance of La Niña signal is also found in the SLPa asymmetry (Fig. 5.5j), which shows more of a positive NAO-like pattern, as for La Niña (Fig. 5.5l), consistent with a stronger stratospheric vortex. In summary, La Niña signal appears to dominate the stratospheric pathway at low levels of SSTA asymmetry.

Next, we analyze the high asymmetry (HIGHASYM) members in Figure 5.6. In this case, the SSTA asymmetry (Fig. 5.6a) is mainly given by stronger SSTA for EP El Niño (Fig. 5.6b) than for La Niña (Fig. 5.6c). The dominant EP El Niño signal is then carried onto the extra-tropics, in the tropospheric Z'a (Fig. 5.6d), from there into the stratospheric Ua (Fig. 5.6g) and back to the surface in SLPa (Fig. 5.6j). The corresponding composited RMS asymmetry values are located between the 75^{th} and 90^{th} percentiles of all-members' distribution (Table 5.1). Comparing the composites for EP El Niño and La Niña in LOWASYM (Fig. 5.5) and HIGHASYM (Fig. 5.6), it is clear that this change in asymmetry is due to the large spread in the SSTA intensity of EP El Niño, not found in La Niña. For EP El Niño, SSTA and Z'a over the Aleutian low region are doubled from LOWASYM to HIGHASYM (Figs. 5.5b,e vs. 5.6b,e), leading to a weakened polar vortex in HIGHASYM (Fig. 5.6h) together with positive SLPa over the Arctic (Fig. 5.6k), not simulated in LOWASYM. In contrast, La Niña signal is similar in LOWASYM and HIGHASYM sub-groups, presumably because of the comparable SSTA intensity for both La Niña sub-sets (compare Fig. 5.5c vs. Fig. 5.6c). Actually, the maximum SSTA intensity for

LOWASYM and HIGHASYM La Niña composites is similar (1.5 K), whereas for EP El Niño the difference in the maximum SSTA intensity is about 1.5 K.

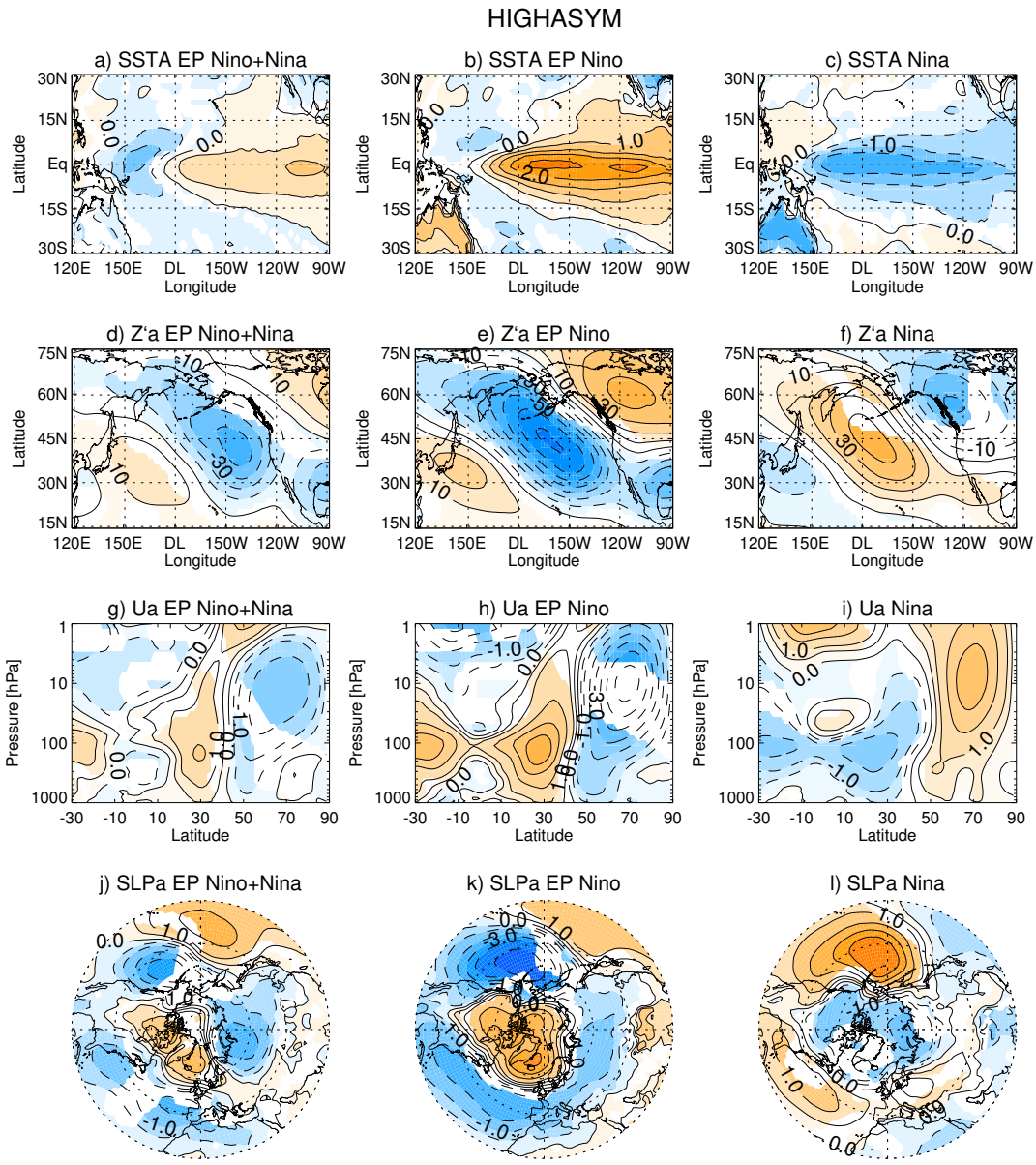

Figure 5.6. As Fig. 5.5, but for the HIGHASYM members.

5.4 Role of the SSTA intensity

Motivated by the large range of SSTA intensities displayed by EP El Niño when comparing HIGHASYM and LOWASYM members (Figs. 5.5 and 5.6), in this section we evaluate the impact of the SSTA intensity on the asymmetry. Figure 5.7 compares EP El Niño and La Niña absolute SSTA intensities, computed over their respective regions. This is different from the classification made in Fig. 5.1, since a larger longitudinal region at the equator is used to compute the RMS SSTA asymmetry in Fig. 5.1. Note that in Fig. 5.7 more than one member can have the equal SSTA. The range of the SSTA, from the minimum to the maximum SSTA value, is 1.8 K for EP El Niño and 1.2 K for La Niña. In other words, in EP El Niño composites the model members display a wider spread on their SSTA intensity, reaching the highest value of 2.6 K, whereas La Niña composites show a narrower spread and the largest absolute value is weaker than for EP El Niño (only one member trespasses -2 K). These results agree with observation from Burgers and Stephenson (1999), but also provide a new insight on the sample variability of the asymmetry, as the EP El Niño SSTA intensity seems to play a key role on the distribution of the degree of asymmetry.

Based on Fig. 5.7, we select members with equal or comparable SSTA intensity for EP El Niño and La Niña, defined as those with absolute differences in SSTA below 0.1 K. The identified 36 members are indicated by purple colors. Note that these members could still be highly asymmetric and thus, show very different asymmetry degrees (purple dots in Figs. 5.2a and 5.3), since the asymmetry level can be also modified by changes in the maximum SSTA location, besides SSTA intensity. The SSTA intensities for EP El Niño and La Niña from observations are shown as well in Fig. 5.7 (black square). The model shows a tendency to have smaller mean intensity events than observed values, for both EP El Niño and El Niña. Nevertheless, among the many model

realities, there are members with larger La Niña SSTA compared to EP El Niño, more frequent (36 members) than those with large EP El Niño SSTA (28 members). Then, our results suggest that realizations with La Niña winters stronger than EP El Niño could occur. Thus, in order to analyze events with either stronger EP El Niño than La Niña SSTA intensity or vice versa, we select the members with the largest differences, above 0.7 K, between EP El Niño and La Niña absolute SSTA intensities. In Fig. 5.7, the five members with the strongest SSTA for EP El Niño compared to La Niña are indicated by gray colors and the three members with the strongest SSTA for La Niña compared to EP El Niño are indicated by blue colors. These samples are named as *stronger* EP El Niño and *stronger* La Niña.

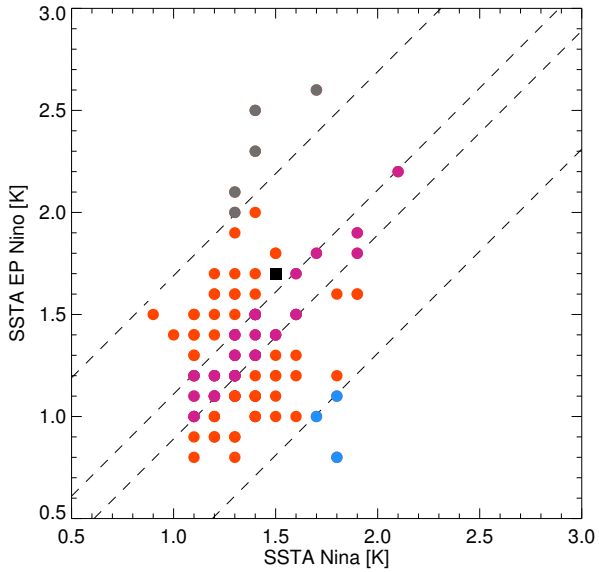

Figure 5.7. Scatter plot of EP El Niño and La Niña absolute NDJF mean SSTA intensities computed over the N3 and N34 regions, respectively. Values are rounded to one decimal. The circles correspond to the 100 members and the black square indicates the observations. Members with equal or comparable (0.1 K absolute difference) SSTA intensity are indicated by purple colors and delimited by dashed lines. *Stronger* EP El Niño and *stronger* La Niña (absolute differences above 0.7 K) are indicated by gray colors (dots above the upper dashed line) and by blue colors (dots below the lower dashed line), respectively.

The asymmetry for members with equal intensity is shown in Figure 5.8 (left panels). The spatial pattern of SSTA (Fig. 5.8a) displays positive and negative anomalies in the east and the west Pacific, respectively. Since the intensity is similar, these values are due to the different location of SSTA in the Pacific during EP El Niño and La Niña winters. The tropospheric Z'a asymmetry center is located at 45ºN, but the asymmetry is negligible over Alaska and the Bering Sea region (Fig. 5.8d), where upward propagating waves can be modulated. Accordingly, the polar stratospheric asymmetry shows null values (Fig. 5.8g). Thus, for EP El Niño and La Niña events of equal SSTA intensity, the stratospheric response is opposite but of the same magnitude. Note that this result is different from that of the LOWASYM case, where EP El Niño displays differences with respect to its canonical location, which leads to weak and insignificant polar stratospheric responses. For the surface impact (Fig. 5.8j) the mirror image for EP El Niño and La Niña is lost. Instead, a node of SLPa appears over the Arctic, with half of the anomaly positive and the other half negative, revealing the existence of opposite non-overlapping responses to EP El Niño and La Niña.

The composited asymmetry for members with *stronger* EP El Niño events (Fig. 5.8b) shows large positive SSTA east to the Date Line. Z'a over the Aleutian low (Fig. 5.8e) and stratospheric Ua (Fig. 5.8h) also show strong responses. They are larger than those reached for HIGHASYM members (Figs. 5.6d, g), which include stronger EP El Niño events compared to La Niña, but also include stronger La Niña events than EP El Niño. Accordingly, the highest level of RMS asymmetry in the stratospheric response is found for the composite of *stronger* EP El Niño members (7.24 m s^{-1}, Table 5.1). For *stronger* La Niña events, large negative anomalies are simulated to the west of the Date Line (Fig. 5.8c), which lead to positive asymmetric Z'a over the Pacific North American region (Fig. 5.8f), related to a stronger polar vortex (Fig. 5.8i),

although, Ua are lower in magnitude than for *stronger* EP El Niño (Fig. 5.8h), in agreement with weaker values in Z'a asymmetry (Fig. 5.8f).

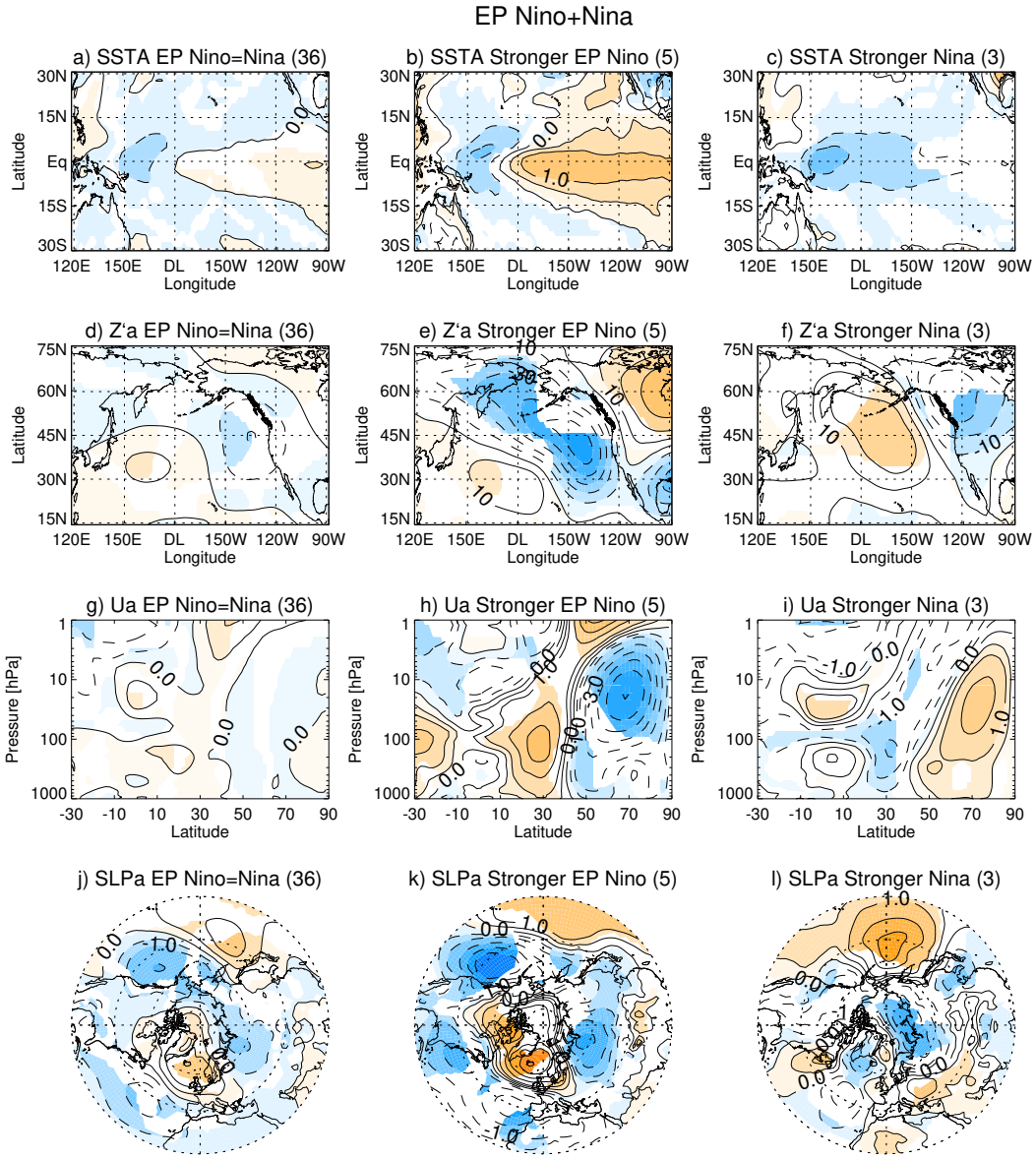

Figure 5.8. Similar to Fig. 5.5, but for EP El Niño+La Niña in (1st column) 36 members with equal SSTA intensity, (2nd column) five members with *stronger* EP El Niño winters and (3rd column) three members with *stronger* La Niña winters (see Fig. 5.7 for the selection of members). Numbers in brackets indicate the number of members in each composite.

The robustness of these results, as indicated by the Monte Carlo test, show that extreme differences on the SSTA between EP El Niño and La Niña can also be traced to the stratospheric pathway. In addition, our results emphasize that the asymmetry can be found in both directions, with larger SSTA anomalies for EP El Niño than for La Niña, but also conversely. Furthermore, we should notice the resemblance in the stratospheric asymmetry between *stronger* La Niña and LOWASYM members (Fig. 5.8i vs. 5.5g). As for the LOWASYM sub-group, *stronger* La Niña are associated with weak SSTA for EP El Niño (around 1 K, Fig 5.7) and they also show the lowest composited Ua asymmetry, between 25th and 50th percentiles (Table 5.1). Thus, while the highest polar stratospheric asymmetry is given by the strongest EP El Niño and hence the largest SSTA differences with La Niña, the lowest asymmetry is reported for weak EP El Niño events, along with stronger La Niña. This link supports the role of the EP El Niño SSTA as modulator of the asymmetry range on the ENSO stratospheric pathway.

5.5 Summary and Discussion

In this chapter, we investigated the ENSO asymmetry and its impact on the stratospheric pathway, by using a grand ensemble of 100 historical simulations from the MPI model. By considering separately the asymmetry of the two types of El Niño (Eastern and Central Pacific), our approach allows us to find the first evidence of large sample variability in the SSTA asymmetry between EP El Niño and La Niña. This is in contrast with results from Zhang et al. (2014), who did not found any variability on the SSTA asymmetry, possibly because they re-sampled the El Niño and La Niña composites of 16 members to create a larger size of 256 asymmetry samples. Instead, our 100 ensemble members of 56-year time-series are independent realizations, each comparable to the reanalysis time-series.

Sampling variability is also present in the tropospheric asymmetric response over the North Pacific. However, whereas for EP El Niño+La Niña the asymmetry in the forcing and in the response are significantly correlated, such relationship is missing for CP El Niño+La Niña, supporting the separation into two El Niño flavors. Therefore, only the variability of EP El Niño and La Niña asymmetry in the SSTA is reported to drive the variability of the tropospheric asymmetry, and can thereafter impact on the stratospheric teleconnections. However, as expected, we also found internal variability in the troposphere-stratosphere coupling which is unrelated to the stratospheric pathway.

Given that the sample variability in SSTA comprehends a large range of asymmetry levels, we have evaluated the impact of extreme asymmetry. Low asymmetry levels are achieved for members with similar SSTA intensity and location for EP El Niño and La Niña. This occurs for weak EP El Niño events with their SSTs extended towards the west. These EP El Niño winters do not impact the polar vortex, so the stratospheric asymmetry is dominated by La Niña signal, i.e., a stronger polar vortex and a positive NAO pattern. In contrast, high asymmetry members are characterized by stronger EP El Niño winters than La Niña. In this case, the asymmetric response reproduces the EP El Niño-like stratospheric pathway signature, with a weaker polar vortex and a negative NAO response. Thus, EP El Niño SSTA drive the level of the asymmetric response. Indeed, while EP El Niño signatures show substantial spread from low to high asymmetry members, La Niña signatures are similar in both sub-groups, evidencing again that the range of stratospheric asymmetry is modulated by EP El Niño SSTA. The dominance of the EP El Niño signal is also found in reanalysis and in members with asymmetry levels similar to observations, whose asymmetry is relatively high according to the spread in the all-members' distribution. However, the MPI model members reveal a plausible

reality not observed yet: realizations with strong La Niña and weak EP El Niño winters that result in a La Niña-like stratospheric asymmetry.

Furthermore, we found that the intensity of both EP El Niño and La Niña SSTA plays a major role on the stratospheric response asymmetry. Extreme differences on the SSTA intensity between EP El Niño and La Niña are translated to the stratospheric pathway. Likewise, almost equal SSTA intensities lead to comparable magnitude but opposite signed stratospheric responses. Rao and Ren (2016a), in a sensitivity study performed with the WACCM model, also found comparable amplitude responses to symmetric SSTA forcings, but this behavior was only reported during strong ENSO events (±2 K threshold), not during moderate winters (defined between ±1 K and ±2 K), as we do (see Fig. 5.7). We need to point out that Rao and Ren (2016a) selected La Niña winters in the N3 region, whereas we consider the N34 region more appropriate to define La Niña winters. This difference could partially account for the discrepancies.

6 Conclusions and outlook

In this thesis, we have addressed several questions that remained open in the literature. In particular, 1) we established a robust stratospheric pathway for La Niña and 2) we resolved the apparent contradiction regarding the stratospheric response to different El Niño flavors. Additionally, based on these results and the availability of an unprecedented grand model ensemble, 3) we revealed novel results regarding the ENSO asymmetry impact on the stratospheric pathway. The main conclusions of each of these topics are summarized next:

La Niña stratospheric signature

1. A NH stratospheric pathway is established during La Niña events in boreal winter, based on reanalysis data. During strong La Niña events, those defined below -1 SD, a robust stronger and colder polar vortex is observed. The significant stratospheric wind anomalies reach the troposphere and impact on the NAE region, leading to a surface response characterized by a positive NAO phase.

2. Dynamical analysis reveals that the stronger polar stratospheric vortex observed during La Niña winters is due to reduced upward planetary wave activity into the stratosphere. This finding is the result of destructive interference between the climatological and the anomalous La Niña stationary eddies over the Pacific–North American region.

3. The lack of a robust stratospheric signature during La Niña winters reported in previous studies is explained here in relation to the lower thresholds previously used to detect the events. We showed that the weaker signal obtained with less restrictive thresholds is more prone to be obscured by the influence of other sources of variability. In particular, the occurrence of SSWs, partly linked to the phase of the QBO, modulates the observed stratospheric signal.

4. Our results highlight the importance of using a relatively restrictive threshold to define La Niña events in order to obtain a robust stratospheric response and consequently, a robust surface response in the NAE region through the stratosphere. We claim that a threshold of -1 SD is needed. In the case of less restrictive thresholds, a robust stratospheric cooling is only found in the absence of SSWs. These results are relevant to improve seasonal predictability over Europe.

Controversy on the NH response to El Niño flavors

5. We show that the CP El Niño response is modulated by the prominent role of SSWs, whose signal modulates the polar stratospheric response to CP El Niño. This also explains previous contradictory results that concluded that the CP El Niño stratospheric signal depended on the composite size and index used to identify the events.

6. The CP El Niño polar stratospheric signature is robust when the events are classified according to the occurrence of SSWs, with opposite responses in winters with and without SSWs. In CP El Niño winters with SSWs, a significant warmer and weaker vortex appears reflecting the behavior of the SSW. In

contrast, CP El Niño winters without SSWs exhibit a significant cooling and a stronger polar vortex.

7. Polar stratospheric responses to CP and EP El Niño are clearly distinguishable in the absence of SSWs in early winter, from November to January, with differences over the Aleutian low region and the following upward wave activity. On the other hand, during CP El Niño winters with SSWs, EP and CP El Niño responses are similar in the middle stratosphere.

8. Our results are robust regardless of the CP El Niño definition and demonstrate that the occurrence of SSWs needs to be taken into account when studying the stratospheric response to CP El Niño.

The asymmetry between El Niño and La Niña

9. For the first time, large sample variability is found in the SSTA asymmetry between El Niño and La Niña, evaluated in a grand ensemble of 100 members of historical experiments made with the MPI-ESM-LR model.

10. The sample variability of the SSTA forcing asymmetry between EP El Niño and La Niña drives part of the tropospheric and stratospheric asymmetric responses. This relationship is not simulated in the case of CP El Niño and La Niña.

11. The asymmetry between EP El Niño and La Niña exhibits a range of sample variability. Low asymmetry levels are characterized by weak EP El Niño winters with their largest SSTA extended westward, and a stronger La Niña signature on the stratospheric asymmetry, a feature not observed to date. In contrast, high asymmetry levels are related to strong EP El Niño winters that dominate the asymmetric stratospheric pathway. This means that the level of asymmetry is mainly modulated by EP El Niño, which presents a larger spread of SSTA than the less variable La Niña.

12. SSTA intensity plays a major role on the asymmetry of the ENSO stratospheric pathway. EP El Niño and La Niña winters with about equal SSTA

intensities lead to comparable in magnitude but opposite signed stratospheric responses.

As said above, several questions have been answered in this thesis but still, several topics deserve further investigation. Throughout this manuscript we highlighted that the ENSO stratospheric response might be modulated by the occurrence of SSWs and the QBO phases, but the observational record is too short to analyze separately the impact of both sources of variability. In this regard, simulations with an internally-simulated QBO would allow evaluating interactions among SSWs and the QBO phases and their modulation on the NAE La Niña teleconnections. In addition, long simulations with such models would allow investigating the role of the QBO on the EP and CP El Niño polar stratospheric responses.

Regarding the SSW occurrence during ENSO winters, the possible role of the North Pacific SSTs as a precursor of SSWs during CP El Niño remains an open question. At the same time, further analysis is also needed on the delayed SSW occurrence during strong La Niña winters. Finally, the potential of La Niña to improve the seasonal prediction skill can be within the scope of future studies and it should be tested in model simulations with seasonal prediction systems.

References

Aceituno, P., 1988: On the Functioning of the Southern Oscillation in the South American Sector. Part I: Surface Climate. *Mon. Wea. Rev.*, **116**, 505–524, doi:10.1175/1520-0493(1988)116<0505:OTFOTS>2.0.CO;2.

Alexander, M. A., I. Bladé, M. Newman, J. R. Lanzante, N. C. Lau, and J. D. Scott, 2002: The atmospheric bridge: The influence of ENSO teleconnections on air-sea interaction over the global oceans. *J. Climate*, **15**, 2205–2231, doi:10.1175/1520-0442(2002)015<2205:TABTIO>2.0.CO;2.

An, S. Il, and F. F. Jin, 2004: Nonlinearity and asymmetry of ENSO. *J. Climate*, **17**, 2399–2412, doi:10.1175/1520-0442(2004)017<2399:NAAOE>2.0.CO;2.

Andrews, D. G., J. R. Holton, and C. B. Leovy, 1987: Middle Atmosphere Dynamics. *International Geophysics Series, Academic Press*, Vol. 40 of, p. 489.

Ashok, K., S. K. Behera, S. A. Rao, H. Weng, and T. Yamagata, 2007: El Niño Modoki and its possible teleconnection. *J. Geophys. Res.*, **112**, C11007, doi:10.1029/2006JC003798.

Baldwin, M. P., and T. J. Dunkerton, 1998: Quasi-biennial modulation of the southern hemisphere stratospheric polar vortex. *Geophys. Res. Lett.*, **25**,

3343–3346.

——, and ——, 1999: Propagation of the Arctic Oscillation from the stratosphere to the troposphere. *J. Geophys. Res.*, **104**, 937–946.

——, and ——, 2001: Stratospheric harbingers of anomalous weather regimes. *Science*, **294**, 581–584, doi:10.1126/science.1063315.

——, and Coauthors, 2001: The quasi-biennial oscillation. *Reviews of Geophysics*, **39**, 179–229.

Barriopedro, D., and N. Calvo, 2014: On the relationship between ENSO, Stratospheric Sudden Warmings, and Blocking. *J. Climate*, **27**, 4704–4720, doi:10.1175/JCLI-D-13-00770.1.

Barsugli, J. J., and P. D. Sardeshmukh, 2002: Global atmospheric sensitivity to tropical SST anomalies throughout the Indo-Pacific basin. *J. Climate*, **15**, 3427–3442, doi:10.1175/1520-0442(2002)015<3427:GASTTS>2.0.CO;2.

Bell, C. J., L. J. Gray, A. J. Charlton-Perez, M. M. Joshi, and A. A. Scaife, 2009: Stratospheric communication of El Niño teleconnections to European winter. *J. Climate*, **22**, 4083–4096, doi:10.1175/2009JCLI2717.1.

Bjerknes, J., 1969: Atmospheric Teleconnections From The Equatorial Pacific. *Mon. Wea. Rev.*, **97**, 163–172, doi:10.1175/1520-0493(1969)097<0163:ATFTEP>2.3.CO;2.

Brönnimann, S., 2007: Impact of El Niño–Southern Oscillation on European climate. *Reviews of Geophysics*, **45**, doi:10.1029/2006RG000199.

Burgers, G., and D. B. Stephenson, 1999: The "Normality" of El Niño. *Geophys. Res. Lett.*, **26**, 1027–1030.

Butler, A. H., and L. M. Polvani, 2011: El Niño, La Niña, and stratospheric sudden warmings: A reevaluation in light of the observational record. *Geophys. Res. Lett.*, **38**, L13807, doi:10.1029/2011GL048084.

——, ——, and C. Deser, 2014: Separating the stratospheric and tropospheric pathways of El Niño–Southern Oscillation teleconnections. *Environ. Res. Lett.*, **9**, 24014, doi:10.1088/1748-9326/9/2/024014.

——, and Coauthors, 2016: The Climate-system Historical Forecasting Project: Do stratosphere-resolving models make better seasonal climate predictions in boreal winter? *Q. J. Roy. Meteor. Soc*, **142**, 1413–1427.

——, J. P. Sjoberg, D. J. Seidel, and K. H. Rosenlof, 2017: A sudden stratospheric warming compendium. *Earth Syst. Sci. Data*, **9**, 63–76, doi:10.7289/V5NS0RWP.

Cagnazzo, C., and E. Manzini, 2009: Impact of the stratosphere on the winter tropospheric teleconnections between ENSO and the North Atlantic and European region. *J. Climate*, **22**, 1223–1238, doi:10.1175/2008JCLI2549.1.

Calvo, N., M. A. Giorgetta, R. Garcia-Herrera, and E. Manzini, 2009: Nonlinearity of the combined warm ENSO and QBO effects on the Northern Hemisphere polar vortex in MAECHAM5 simulations. *J. Geophys. Res.*, **114**, D13109, doi:10.1029/2008JD011445.

——, R. R. Garcia, W. J. Randel, and D. R. Marsh, 2010: Dynamical mechanism for the increase in tropical ipwelling in the lowermost tropical stratosphere during warm ENSO events. *Journal of the Atmospheric Sciences*, **67**, 2331–2340, doi:10.1175/2010JAS3433.1.

——, and Coauthors, 2017: Northern Hemisphere Stratospheric Pathway of Different El Niño Flavors in Stratosphere-Resolving CMIP5 Models. *J. Climate*, **30**, 4351–4371, doi:10.1175/JCLI-D-16-0132.1.

Camp, C. D., and K. K. Tung, 2007: Stratospheric polar warming by ENSO in winter: A statistical study. *Geophys. Res. Lett.*, **34**, 2–5, doi:10.1029/2006GL028521.

Capotondi, A., and Coauthors, 2015: Understanding ENSO Diversity. *Bulletin of the American Meteorological Society*, **96**, 921–938, doi:10.1175/BAMS-D-13-00117.1.

Charlton, A. J., and L. M. Polvani, 2007: A new look at stratospheric sudden warmings. Part I: Climatology and modeling benchmarks. *J. Climate*, **20**, 449–469, doi:10.1175/JCLI3996.1.

Charlton-Perez, A. J., and Coauthors, 2013: On the lack of stratospheric dynamical variability in low-top versions of the CMIP5 models. *J. Geophys. Res. Atmos.*, **118**, 1–12, doi:10.1002/jgrd.50125.

Charney, J. G., and P. G. Drazin, 1961: Propagation of Planetary-Scale Disturbances from the Lower into the Upper Atmosphere. *J. Geophys. Res.*, **66**, 83–109.

Chiodi, A. M., and D. E. Harrison, 2013: El Niño impacts on seasonal U.S. Atmospheric Circulation, Temperature, and Precipitation Anomalies: The OLR-Event Perspective*. *J. Climate*, **26**, 822–837, doi:10.1175/JCLI-D-12-00097.1.

Chiodo, G., D. R. Marsh, R. Garcia-Herrera, N. Calvo, and J. A. García, 2014: On the detection of the solar signal in the tropical stratosphere. *Atmospheric Chemistry and Physics*, **14**, 5251–5269, doi:10.5194/acp-14-5251-2014.

Compo, G. P., and Coauthors, 2011: The Twentieth Century Reanalysis Project. *Quart. J. Roy. Meteor. Soc.*, **137**, 1–28, doi:10.1002/qj.776.

Coughlin, K., and K. Tung, 2001: QBO signal found at the extratropical surface through northern annular modes. *Geophys. Res. Lett.*, **28**, 4563–4566, doi:10.1029/2001GL013565.

Crooks, S. A., and L. J. Gray, 2005: Characterization of the 11-year solar signal using a multiple regression analysis of the ERA-40 dataset. *J. Climate*, **18**, 996–1015, doi:10.1175/JCLI-3308.1.

Dee, D. P., and Coauthors, 2011: The ERA-Interim reanalysis: configuration and performance of the data assimilation system. *Quart. J. Roy. Meteor. Soc.*, **137**, 553–597, doi:10.1002/qj.828.

Domeisen, D. I. V., A. H. Butler, K. Fröhlich, M. Bittner, W. A. Müller, and J. Baehr, 2015: Seasonal Predictability over Europe arising from El Niño and Stratospheric Variability in the MPI-ESM Seasonal Prediction System. *J. Climate*, **28**, 256–271, doi:10.1175/JCLI-D-14-00207.1.

Dunkerton, T. J., D. P. Delisi, and M. P. Baldwin, 1988: Distribution of Major

Stratospheric Warmings in Relation to the Quasi-Biennial Oscillation. *Geophysical Monograph Series*, **15**, 136–139.

Ebita, A., and Coauthors, 2011: The Japanese 55-year Reanalysis "JRA-55": An Interim Report. *Sola*, **7**, 149–152, doi:10.2151/sola.2011-038.

Edmon, H. J., B. J. Hoskins, and M. E. McIntyre, 1980: Eliassen-Palm Cross Sections for the Troposphere. *Journal of the Atmospheric Sciences*, **37**, 2600–2616, doi:10.1175/1520-0469(1980)037<2600:EPCSFT>2.0.CO;2.

Eliassen, A., and E. Palm, 1961: On the Transfer of Energy in Stationary Mountain Waves. *Geofysiske Publikasjoner*, **22**, 1–23, doi:10.1098/rstl.1884.0016.

Fletcher, C. G., and P. J. Kushner, 2011: The role of linear interference in the annular mode response to tropical SST forcing. *J. Climate*, **24**, 778–794, doi:10.1175/2010JCLI3735.1.

Free, M., and D. J. Seidel, 2009: Observed El Niño–Southern Oscillation temperature signal in the stratosphere. *J. Geophys. Res.*, **114**, D23108, doi:10.1029/2009JD012420.

Fueglistaler, S., B. Legras, A. Beljaars, J.-J. Morcrette, A. Simmons, A. M. Tompkins, and S. Uppala, 2009: The diabatic heat budget of the upper troposphere and lower/mid stratosphere in ECMWF reanalysis. *Quart. J. Roy. Meteor. Soc.*, **135**, 21–37, doi:10.1002/qj.361.

Fujiwara, M., and Coauthors, 2017: Introduction to the SPARC Reanalysis Intercomparison Project (S-RIP) and overview of the reanalysis systems. *Atmospheric Chemistry and Physics*, **17**, 1417–1452, doi:10.5194/acp-17-1417-2017.

García-Herrera, R., N. Calvo, R. R. Garcia, and M. A. Giorgetta, 2006: Propagation of ENSO temperature signals into the middle atmosphere: A comparison of two general circulation models and ERA-40 reanalysis data. *J. Geophys. Res.*, **111**, D06101, doi:10.1029/2005JD006061.

Garfinkel, C. I., and D. L. Hartmann, 2007: Effects of the El Niño–Southern

Oscillation and the Quasi-Biennial Oscillation on polar temperatures in the stratosphere. *J. Geophys. Res.*, **112**, D19112, doi:10.1029/2007JD008481.

——, and ——, 2008: Different ENSO teleconnections and their effects on the stratospheric polar vortex. *J. Geophys. Res.*, **113**, D18114, doi:10.1029/2008JD009920.

——, a. H. Butler, D. W. Waugh, M. M. Hurwitz, and L. M. Polvani, 2012: Why might stratospheric sudden warmings occur with similar frequency in El Niño and La Niña winters? *J. Geophys. Res. Atmos.*, **117**, D19106, doi:10.1029/2012JD017777.

——, M. M. Hurwitz, D. W. Waugh, and A. H. Butler, 2013: Are the teleconnections of Central Pacific and Eastern Pacific El Niño distinct in boreal wintertime? *Climate Dyn.*, **41**, 1835–1852, doi:10.1007/s00382-012-1570-2.

Gerber, E. P., C. Orbe, and L. M. Polvani, 2009: Stratospheric influence on the tropospheric circulation revealed by idealized ensemble forecasts. *Geophys. Res. Lett.*, **36**, L24801, doi:10.1029/2009GL040913.

——, and Coauthors, 2012: Assessing and understanding the impact of stratospheric dynamics and variability on the earth system. *Bull. Amer. Meteor. Soc*, **93**, 845–859, doi:10.1175/bAms-d-11-00145.1.

Gill, A. E., 1980: Some simple solutions for heat-induced tropical circulation. *Quart. J. Roy. Meteor. Soc.*, **106**, 447–462, doi:10.1002/qj.49710644905.

Giorgetta, M. a., and Coauthors, 2013: Climate and carbon cycle changes from 1850 to 2100 in MPI-ESM simulations for the Coupled Model Intercomparison Project phase 5. *Journal of Advances in Modeling Earth Systems*, **5**, 572–597, doi:10.1002/jame.20038.

Gorgas García, J., N. Cardiel López, and J. Zamorano Calvo, 2011: *Estadística Basica para estudiantes de ciencias*. Universidad Complutense de Madrid. 258 pp.

Graf, H.-F., and D. Zanchettin, 2012: Central Pacific El Niño, the "subtropical

bridge," and Eurasian climate. *J. Geophys. Res.*, **117**, D01102, doi:10.1029/2011JD016493.

Halpert, M. S., and C. F. Ropelewski, 1992: Surface Temperature Patterns Associated with the Southern Oscillation. *J Climate*, **5**, 577–593, doi:10.1175/1520-0442(1992)005<0577:STPAWT>2.0.CO;2.

Hamilton, K., 1993: An Examination of Observed Southern Oscillation Effects in the Northern Hemisphere Stratosphere. *Journal of Atmospheric Sciences*, **50**, 3468–3473.

Hansen, F., K. Matthes, and S. Wahl, 2016: Tropospheric QBO-ENSO interactions and differences between the atlantic and pacific. *J. Climate*, **29**, 1353–1368, doi:10.1175/JCLI-D-15-0164.1.

Harada, Y., and Coauthors, 2016: The JRA-55 Reanalysis: Representation of Atmospheric Circulation and Climate Variability. *Journal of the Meteorological Society of Japan. Ser. II*, **94**, 269–302, doi:10.2151/jmsj.2016-015.

Harris, I., P. D. D. Jones, T. J. J. Osborn, and D. H. H. Lister, 2014: Updated high-resolution grids of monthly climatic observations - the CRU TS3.10 Dataset. *International Journal of Climatology*, **34**, 623–642, doi:10.1002/joc.3711.

Hegyi, B. M., and Y. Deng, 2011: A dynamical fingerprint of tropical Pacific sea surface temperatures on the decadal-scale variability of cool-season Arctic precipitation. *J. Geophys. Res.*, **116**, D20121, doi:10.1029/2011JD016001.

Hoerling, M. P., and A. Kumar, 2001: Atmospheric Response Patterns Associated with Tropical Forcing. *J. Climate*, **15**, 2184–2203, doi:10.1175/1520-0442(2002)015<2184:arpawt>2.0.co;2.

——, ——, and M. Zhong, 1997: El Niño, La Niña, and the nonlinearity of their teleconnections. *J. Climate*, **10**, 1769–1786.

——, ——, and T. Xu, 2001: Robustness of the nonlinear climate response to ENSO's extreme phases. *J. Climate*, **14**, 1277–1293, doi:10.1175/1520-0442(2001)014<1277:ROTNCR>2.0.CO;2.

Holton, J. R., and H. C. Tan, 1980: The influence of the equatorial quasi-biennial oscillation on the global circulation at 50 mb. *Journal of the Atmospheric Sciences*, **37**, 2200–2208.

——, P. H. Haynes, M. E. McIntyre, A. R. Douglass, R. B. Rood, and L. Pfister, 1995: Stratosphere-troposphere exchange. *Reviews of Geophysics*, **33**, 403, doi:10.1029/95RG02097.

Horel, J. D., and J. M. Wallace, 1981: Planetary-scale atmospheric phenomena associated with the Southern Oscillation. *Mon. Wea. Rev.*, **109**, 813–829.

Hoskins, B. J., and D. J. Karoly, 1981: The steady linear response of a spherical atmosphere to thermal and orographic forcing. *Journal of the Atmospheric Sciences*, **38**, 1179–1196.

Huang, B., and Coauthors, 2015: Extended reconstructed sea surface temperature version 4 (ERSST.v4). Part I: Upgrades and intercomparisons. *J. Climate*, **28**, 911–930, doi:10.1175/JCLI-D-14-00006.1.

Hurrell, J. W., 1996: Influence of variations in extratropical wintertime teleconnections on northern hemisphere temperature. *Geophys. Res. Lett.*, **23**, 665–668, doi:10.1029/96GL00459.

——, Y. Kushnir, and M. Visbeck, 2001: The North Atlantic Oscillation. *Science*, **291**, 603–605, doi:10.1126/science.1058761.

Hurwitz, M. M., P. A. Newman, L. D. Oman, and A. M. Molod, 2011: Response of the Antarctic Stratosphere to Two Types of El Niño Events. *J. Atmos. Sci.*, **68**, 812–822, doi:10.1175/2011JAS3606.1.

——, ——, and C. I. Garfinkel, 2012: On the influence of North Pacific sea surface temperature on the Arctic winter climate. *J. Geophys. Res. Atmos.*, **117**, D19110, doi:10.1029/2012JD017819.

——, N. Calvo, C. I. Garfinkel, A. H. Butler, S. Ineson, C. Cagnazzo, E. Manzini, and C. Peña-Ortiz, 2014: Extra-tropical atmospheric response to ENSO in the CMIP5 models. *Climate Dyn.*, **43**, doi:10.1007/s00382-014-2110-z.

Ilyina, T., K. D. Six, J. Segschneider, E. Maier-Reimer, H. Li, and I. Núñez-Riboni, 2013: Global ocean biogeochemistry model HAMOCC: Model architecture and performance as component of the MPI-Earth system model in different CMIP5 experimental realizations. *Journal of Advances in Modeling Earth Systems*, **5**, 287–315, doi:10.1029/2012MS000178.

Ineson, S., and A. A. Scaife, 2009: The role of the stratosphere in the European climate response to El Niño. *Nature Geoscience*, **2**, 32–36, doi:10.1038/ngeo381.

Iza, M., and N. Calvo, 2015: Role of Stratospheric Sudden Warmings on the response to Central Pacific El Niño. *Geophys. Res. Lett.*, **42**, 2482–2489, doi:10.1002/2014GL062935.

——, ——, and E. Manzini, 2016: The Stratospheric Pathway of La Niña. *J. Climate*, **29**, 8899–8914, doi:10.1175/JCLI-D-16-0230.1.

——, E. Manzini, N. Calvo, D. Barriopedro, and L. Kornblueh, 2017: El Niño and La Niña Asymmetry: Its impact on the Stratospheric Pathway in a Model Grand Ensemble. *Submitted to J. Climate.*

Jungclaus, J. H., and Coauthors, 2013: Characteristics of the ocean simulations in the Max Planck Institute Ocean Model (MPIOM) the ocean component of the MPI-Earth system model. *Journal of Advances in Modeling Earth Systems*, **5**, 422–446, doi:10.1002/jame.20023.

Kalnay, E., and Coauthors, 1996: The NCEP/NCAR 40-year reanalysis project. *Bulletin of the American Meteorological Society*, **77**, 437–471.

Kanamitsu, M., W. Ebisuzaki, J. Woollen, S. K. Yang, J. J. Hnilo, M. Fiorino, and G. L. Potter, 2002: NCEP-DOE AMIP-II reanalysis (R-2). *Bulletin of the American Meteorological Society*, **83**, 1631–1643+1559, doi:10.1175/BAMS-83-11-1631.

Kang, I. S., and J. S. Kug, 2002: EI Niño and la Niña sea surface temperature anomalies: Asymmetry characteristics associated with their wind stress anomalies. *Journal of Geophysical Research Atmospheres*, **107**, 1–10,

doi:10.1029/2001JD000393.

Kao, H.-Y., and J.-Y. Yu, 2009: Contrasting eastern-Pacific and central-Pacific types of ENSO. *J. Climate*, **22**, 615–632, doi:10.1175/2008JCLI2309.1.

Kidston, J., A. a. Scaife, S. C. Hardiman, D. M. Mitchell, N. Butchart, M. P. Baldwin, and L. J. Gray, 2015: Stratospheric influence on tropospheric jet streams, storm tracks and surface weather. *Nature Geoscience*, **8**, 433–440, doi:10.1038/ngeo2424.

Kiladis, G. N., and H. van Loon, 1988: The Southern Oscillation. Part VII: Meteorological Anomalies over the Indian and Pacific Sectors Associated with the Extremes of the Oscillation. *Mon. Wea. Rev.*, **116**, 120–136, doi:10.1175/1520-0493(1988)116<0120:TSOPVM>2.0.CO;2.

——, and H. F. Diaz, 1989: Global Climatic Anomalies Associated with Extremes in the Southern Oscillation. *J. Climate*, **2**, 1069–1090, doi:10.1175/1520-0442(1989)002<1069:GCAAWE>2.0.CO;2.

Kim, S. T., and J.-Y. Yu, 2012: The two types of ENSO in CMIP5 models. *Geophys. Res. Lett.*, **39**, L11704, doi:10.1029/2012GL052006.

Kistler, R., and Coauthors, 2001: The NCEP-NCAR 50-year reanalysis: Monthly means CD-ROM and documentation. *Bulletin of the American Meteorological Society*, **82**, 247–267, doi:10.1175/1520-0477(2001)082<0247:TNNYRM>2.3.CO;2.

Kobayashi, S., and Coauthors, 2015: The JRA-55 Reanalysis: General Specifications and Basic Characteristics. *Journal of the Meteorological Society of Japan. Ser. II*, **93**, 5–48, doi:10.2151/jmsj.2015-001.

Kug, J.-S., and Y.-G. Ham, 2011: Are there two types of la Niña? *Geophys. Res. Lett.*, **38**, 2–7, doi:10.1029/2011GL048237.

——, F.-F. Jin, and S.-I. An, 2009: Two types of El Niño events: Cold tongue El Niño and warm pool El Niño. *J. Climate*, **22**, 1499–1515, doi:10.1175/2008JCLI2624.1.

L'Heureux, M. L., and Coauthors, 2016: Observing and Predicting the 2015-16

El Niño. *Bulletin of the American Meteorological Society*, BAMS-D-16-0009.1, doi:10.1175/BAMS-D-16-0009.1.

Larkin, N. K., and D. E. Harrison, 2002: ENSO warm (El Niño) and cold (La Niña) event life cycles: Ocean surface anomaly patterns, their symmetries, asymmetries, and implications. *J. Climate*, **15**, 1118–1140, doi:10.1175/1520-0442(2002)015<1118:EWENOA>2.0.CO;2.

——, and ——, 2005: Global seasonal temperature and precipitation anomalies during El Niño autumn and winter. *Geophys. Res. Lett.*, **32**, L16705, doi:10.1029/2005GL022860.

Lee, T., and M. J. McPhaden, 2010: Increasing intensity of El Niño in the central-equatorial Pacific. *Geophys. Res. Lett.*, **37**, 1–5, doi:10.1029/2010GL044007.

Li, Y., and N.-C. C. Lau, 2013: Influences of ENSO on Stratospheric Variability, and the Descent of Stratospheric Perturbations into the Lower troposphere. *J. Climate*, **26**, 4725–4748, doi:10.1175/JCLI-D-12-00581.1.

Limpasuvan, V., D. W. J. Thompson, and D. L. Hartmann, 2004: The life cycle of the Northern Hemisphere sudden stratospheric warmings. *J. Climate*, **17**, 2584–2596, doi:10.1175/1520-0442(2004)017<2584:TLCOTN>2.0.CO;2.

Liu, W., and Coauthors, 2015: Extended reconstructed sea surface temperature version 4 (ERSST.v4): Part II. Parametric and structural uncertainty estimations. *J. Climate*, **28**, 931–951, doi:10.1175/JCLI-D-14-00007.1.

Lloyd-Hughes, B., and M. A. Saunders, 2002: Seasonal prediction of European spring precipitation from El Niño-Southern Oscillation and local sea-surface temperatures. *International Journal of Climatology*, **22**, 1–14, doi:10.1002/joc.723.

van Loon, H., and K. Labitzke, 1987: The Southern Oscillation. Part V: The Anomalies in the Lower Stratosphere of the Northern Hemisphere in Winter and a Comparison with the Quasi-Biennial Oscillation. *Mon. Wea. Rev.*, **115**, 357–369, doi:10.1175/1520-

0493(1987)115%3C0357:TSOPVT%3E2.0.CO;2.

Lu, H., M. P. Baldwin, L. J. Gray, and M. J. Jarvis, 2008: Decadal-scale changes in the effect of the QBO on the northern stratospheric polar vortex. *J. Geophys. Res.*, **113**, D10114, doi:10.1029/2007JD009647.

Manzini, E., 2009: Atmospheric science: ENSO and the stratosphere. *Nature Geoscience*, **2**, 749–750, doi:10.1038/ngeo677.

——, M. A. Giorgetta, M. Esch, L. Kornblueh, and E. Roeckner, 2006: The influence of sea surface temperatures on the Northern winter stratosphere: Ensemble simulations with the MAECHAM5 Model. *J. Climate*, **19**, 3863–3882, doi:10.1175/JCLI3826.1.

Marshall, A. G., and A. a. Scaife, 2009: Impact of the QBO on surface winter climate. *J. Geophys. Res.*, **114**, D18110, doi:10.1029/2009JD011737.

Matsuno, T., 1966: Quasi-geostrophic motions in the equatorial area. *Journal of the Meteorological Society of Japan*, **44**, 25–43, doi:10.1002/qj.49710644905.

——, 1971: A Dynamical Model of the Stratospheric Sudden Warming. *Journal of the Atmospheric Sciences*, **28**, 1479–1494, doi:10.1175/1520-0469(1971)028<1479:ADMOTS>2.0.CO;2.

Mcinturff, R. M., 1978: Stratospheric Warmings: Synoptic, Dynamic and General-Circulation aspects. *NASA Reference Publication*, Vol. 1017 of, p. 19.

McIntyre, M. E., and T. N. Palmer, 1983: Breaking planetary waves in the stratosphere. *Nature*, **305**, 593–600, doi:10.1038/305593a0.

McPhaden, M. J., S. E. Zebiak, and M. H. Glantz, 2006: ENSO as an Integrating Concept in Earth Science. *Science*, **314**, 1740–1745, doi:10.1126/science.1132588.

Mitchell, D. M., L. J. Gray, and a. J. Charlton-Perez, 2011: The structure and evolution of the stratospheric vortex in response to natural forcings. *J. Geophys. Res. Atmos.*, **116**, D15110, doi:10.1029/2011JD015788.

——, and Coauthors, 2015: Signatures of naturally induced variability in the atmosphere using multiple reanalysis datasets. *Quart. J. Roy. Meteor. Soc.*, **141**,

2011–2031, doi:10.1002/qj.2492.

Monahan, A. H., 2001: Nonlinear Principal Component Analysis: Tropical Indo–Pacific Sea Surface Temperature and Sea Level Pressure. *J. Climate*, **14**, 219–233, doi:10.1175/1520-0442(2001)013<0219:NPCATI>2.0.CO;2.

Moron, V., and I. Gouirand, 2003: Seasonal modulation of the El Niño-southern oscillation relationship with sea level pressure anomalies over the North Atlantic in October-March 1873-1996. *International Journal of Climatology*, **23**, 143–155, doi:10.1002/joc.868.

——, and G. Plaut, 2003: The impact of El Niño-southern oscillation upon weather regimes over Europe and the North Atlantic during boreal winter. *International Journal of Climatology*, **23**, 363–379, doi:10.1002/joc.890.

Newman, P. A., E. R. Nash, and Rosenfield Joan E., 2001: What controls the temperature of the Arctic stratosphere during the spring? *J. Geophys. Res.*, **106**, 19999–20010.

Nishii, K., H. Nakamura, and T. Miyasaka, 2009: Modulations in the planetary wave field induced by upward-propagating Rossby wave packets prior to stratospheric sudden warming events: A case-study. *Quart. J. Roy. Meteor. Soc.*, **135**, 39–52, doi:10.1002/qj.

——, ——, and Y. J. Orsolini, 2011: Geographical dependence observed in blocking high influence on the stratospheric variability through enhancement and suppression of upward planetary-wave propagation. *J. Climate*, **24**, 6408–6423, doi:10.1175/JCLI-D-10-05021.1.

O'Sullivan, D., and M. L. Salby, 1990: Coupling of the Quasi-biennial Oscillation and the Extratropical Circulation in the Stratosphere through Planetary Wave transport. *Journal of Atmospheric Sciences*, **47**, 650–673.

Okumura, Y. M., and C. Deser, 2010: Asymmetry in the duration of El Niño and la Niña. *J. Climate*, **23**, 5826–5843, doi:10.1175/2010JCLI3592.1.

Onogi, K., and Coauthors, 2007: The JRA-25 Reanalysis. *Journal of the Meteorological Society of Japan*, **85**, 369–432, doi:10.2151/jmsj.85.369.

Palmeiro, F. M., D. Barriopedro, R. García-Herrera, and N. Calvo, 2015: Comparing Sudden Stratospheric Warming Definitions in Reanalysis Data. *J. Climate*, **28**, 6823–6840, doi:10.1175/JCLI-D-15-0004.1.

——, M. Iza, D. Barriopedro, N. Calvo, and R. García-Herrera, 2017: The complex behavior of El Niño winter 2015–2016. *Geophys. Res. Lett.*, **44**, 2902–2910, doi:10.1002/2017GL072920.

Philander, S. G. H., 1985: El Niño and La Niña. *Journal of the Atmospheric Sciences*, **42**, 2652–2662, doi:10.1175/1520-0469(1985)042<2652:ENALN>2.0.CO;2.

Polvani, L. M., and D. W. Waugh, 2004: Upward wave activity flux as a precursor to extreme stratospheric events and subsequent anomalous surface weather regimes. *J. Climate*, **17**, 3548–3554.

——, L. Sun, A. H. Butler, J. H. Richter, and C. Deser, 2017: Distinguishing stratospheric sudden warmings from ENSO as key drivers of wintertime climate variability over the North Atlantic and Eurasia. *J. Climate*, **30**, 1959–1969, doi:10.1175/JCLI-D-16-0277.1.

Pozo-Vázquez, D., S. R. Gámiz-Fortis, J. Tovar-Pescador, M. J. Esteban-Parra, and Y. Castro-Díez, 2005: El Niño-southern oscillation events and associated European winter precipitation anomalies. *International Journal of Climatology*, **25**, 17–31, doi:10.1002/joc.1097.

Randel, W. J., R. R. Garcia, N. Calvo, and D. Marsh, 2009: ENSO influence on zonal mean temperature and ozone in the tropical lower stratosphere. *Geophys. Res. Lett.*, **36**, 1–5, doi:10.1029/2009GL039343.

Rao, J., and R. Ren, 2016a: Asymmetry and nonlinearity of the influence of ENSO on the northern winter stratosphere: 2. Model study with WACCM. *J. Geophys. Res. Atmos.*, **121**, 9017–9032, doi:10.1002/2015JD024520.

——, and ——, 2016b: Asymmetry and nonlinearity of the influence of ENSO on the northern winter stratosphere: 1. Observations. *J. Geophys. Res. Atmos.*, **121**, 9000–9016, doi:10.1002/2015JD024520.

Rasmusson, E. M., and T. H. Carpenter, 1982: Variations in Tropical Sea Surface Temperature and Surface Wind Fields Associated with the Southern Oscillation/El Niño. *Mon. Wea. Rev.*, **110**, 354–384, doi:10.1175/1520-0493(1982)110<0354:VITSST>2.0.CO;2.

Rayner, N. A., D. E. Parker, E. B. Horton, C. K. Folland, L. V. Alexander, D. P. Rowell, E. C. Kent, and A. Kaplan, 2003: Global analyses of sea surface temperature, sea ice, and night marine air temperature since the late nineteenth century. *J. Geophys. Res.*, **108**, 4407, doi:10.1029/2002JD002670.

Reick, C. H., T. Raddatz, V. Brovkin, and V. Gayler, 2013: Representation of natural and anthropogenic land cover change in MPI-ESM. *Journal of Advances in Modeling Earth Systems*, **5**, 459–482, doi:10.1002/jame.20022.

Reiter, E. R., 1978: Long-term wind variability in the tropical Pacific, its possible causes and effects. *Mon. Weather Rev.*, **106**, 324–330.

Richter, J. H., C. Deser, and L. Sun, 2015: Effects of stratospheric variability on El Niño teleconnections. *Environ. Res. Lett.*, **10**, 124021, doi:10.1088/1748-9326/10/12/124021.

Rienecker, M. M., and Coauthors, 2011: MERRA: NASA's modern-era retrospective analysis for research and applications. *J. Climate*, **24**, 3624–3648, doi:10.1175/JCLI-D-11-00015.1.

Robock, A., 2000: Volcanic Eruptions and climate. *Reviews of Geophysics*, 191–219.

Roeckner, E., and Coauthors, 2006: Sensitivity of simulated climate to horizontal and vertical resolution in the ECHAM5 atmosphere model. *J. Climate*, **19**, 3771–3791, doi:10.1175/JCLI3824.1.

Ropelewski, C. F., and M. S. Halpert, 1987: Global and Regional Scale Precipitation Patterns Associated with the El Niño/Southern Oscillation. *Mon. Wea. Rev.*, **115**, 1606–1626, doi:10.1175/1520-0493(1987)115<1606:GARSPP>2.0.CO;2.

——, and ——, 1989: Precipitation Patterns Associated with the High Index Phase of the Southern Oscillation. *J. Climate*, **2**, 268–284,

doi:10.1175/1520-0442(1989)002<0268:PPAWTH>2.0.CO;2.

Saha, S., and Coauthors, 2010: The NCEP climate forecast system reanalysis. *Bulletin of the American Meteorological Society*, **91**, 1015–1057, doi:10.1175/2010BAMS3001.1.

Sardeshmukh, P. D., and B. J. Hoskins, 1988: The Generation of Global Rotational Flow by Steady Idealized Tropical Divergence. *Journal of the Atmospheric Sciences*, **45**, 1228–1251, doi:10.1175/1520-0469(1988)045<1228:TGOGRF>2.0.CO;2.

Sassi, F., D. Kinnison, B. A. Boville, R. R. Garcia, and R. Roble, 2004: Effect of El Niño–Southern Oscillation on the dynamical, thermal, and chemical structure of the middle atmosphere. *J. Geophys. Res.*, **109**, D17108, doi:10.1029/2003JD004434.

Scaife, A. A., and Coauthors, 2016: Seasonal winter forecasts and the stratosphere. *Atmospheric Science Letters*, **17**, 51–56, doi:10.1002/asl.598.

Scherhag, R., 1952: Die explosionsartige Stratosphärenerwarmung des Spätwinters 1951/52. *Ber. Deut. Wetterdieuste*, **38**, 51–63.

Shepherd, T. G., 2000: The middle atmosphere. *Journal of Atmospheric and Solar-Terrestrial Physics*, **62**, 1587–1601, doi:10.1016/S1364-6826(00)00114-0.

Shukla, J., and J. M. Wallace, 1983: Numerical-Simulation of the Atmosphric Response to Equatorial Pacific Sea Surface Temperature Anomalies. *Journal of the Atmospheric Sciences*, **40**, 1613–1630, doi:10.1175/1520-0469(1983)040<1613:nsotar>2.0.co;2.

Sigmond, M., J. F. Scinocca, V. V. Kharin, and T. G. Shepherd, 2013: Enhanced seasonal forecast skill following stratospheric sudden warmings. *Nature Geoscience*, **6**, 98–102, doi:doi:10.1038/ngeo1698.

Singh, A., T. Delcroix, and S. Cravatte, 2011: Contrasting the flavors of El Niño-Southern Oscillation using sea surface salinity observations. *Journal of Geophysical Research: Oceans*, **116**, 1–16, doi:10.1029/2010JC006862.

Smith, K. L., and P. J. Kushner, 2012: Linear interference and the initiation of

extratropical stratosphere-troposphere interactions. *J. Geophys. Res. Atmos.*, **117**, 1–16, doi:10.1029/2012JD017587,2012.

Stevens, B., and Coauthors, 2013: Atmospheric component of the MPI-M earth system model: ECHAM6. *Journal of Advances in Modeling Earth Systems*, **5**, 146–172, doi:10.1002/jame.20015.

Sung, M.-K., B.-M. Kim, and S.-I. An, 2014: Altered atmospheric responses to eastern Pacific and central Pacific El Niños over the North Atlantic region due to stratospheric interference. *Climate Dyn.*, **42**, 159–170, doi:10.1007/s00382-012-1661-0.

Taguchi, M., 2010: Observed connection of the stratospheric quasi-biennial oscillation with El Niño-Southern Oscillation in radiosonde data. *Journal of Geophysical Research Atmospheres*, **115**, 1–12, doi:10.1029/2010JD014325.

——, 2015: Connection of predictability of major stratospheric sudden warmings to polar vortex geometry. *Atmospheric Science Letters*, **17**, 33–38, doi:10.1002/asl.595.

——, and D. L. Hartmann, 2006: Increased occurrence of stratospheric sudden warmings during El Niño as simulated by WACCM. *J. Climate*, **19**, 324–332, doi:10.1175/JCLI3655.1.

Taylor, K. E., 2001: Summarizing multiple aspects of model performance in a single diagram. *J. Geophys. Res.*, **106**, 7183, doi:10.1029/2000JD900719.

——, R. J. Stouffer, and G. A. Meehl, 2012: An Overview of CMIP5 and The Experiment Design. *Bull. Amer. Meteor. Soc.*, **3**, 485–498, doi:10.1175/BAMS-D-11-00094.1.

Trenberth, K. E., 1997: The Definition of El Niño. *Bulletin of the American Meteorological Society*, **78**, 2771–2777, doi:10.1175/1520-0477(1997)078<2771:TDOENO>2.0.CO;2.

——, and D. P. Stepaniak, 2001: Indices of El Niño evolution. *J. Climate*, **14**, 1697–1701, doi:0.1175/1520-0442(2001)014h1697:LIOENOi2.0.CO;2.

——, G. W. Branstator, D. Karoly, A. Kumar, N. C. Lau, and C. Ropelewski,

1998: Progress during TOGA in understanding and modeling global teleconnections associated with tropical sea surface temperatures. *Journal of Geophysical Research-Oceans*, **103**, 14291–14324, doi:10.1029/97jc01444.

Uppala, S. M., and Coauthors, 2005: The ERA-40 re-analysis. *Quart. J. Roy. Meteor. Soc.*, **131**, 2961–3012, doi:10.1256/qj.04.176.

Walker, G. T., 1923: Correlation in seasonal variations of weather, VIII: A preliminary study of world weather. *Mem. Ind. Meteor. Dept. (Poona)*, **24**, 275–310.

——, 1924: Correlation In Seasonal Variations Of Weather IX - A Further Study of World Weather. *Memoirs of the India Meteorological Department*, **24**, 275–333, doi:10.1175/1520-0493(1925)53<252:CISVOW>2.0.CO;2.

——, and E. W. Bliss, 1932: World Weather V - NAO. *Memoirs of the Royal Meteorological Society*, **IV**, 54–84, doi:10.1002/qj.49705422601.

Wallace, J. M., and D. S. Gutzler, 1981: Teleconnections in the Geopotential Height Field during the Northen Hemisphere Winter. *Mon. Wea. Rev.*, **109**, 784–812.

Waugh, D. W., and L. M. Polvani, 2010: The Stratosphere: Dynamics, Transport, and Chemistry - Stratospheric Polar Vortices. *Geophysical Monograph Series*, **190**, 43–58, doi:10.1029/2009GM000887.

Weng, H., K. Ashok, S. K. Behera, S. A. Rao, and T. Yamagata, 2007: Impacts of recent El Niño Modoki on dry/wet conditions in the Pacific rim during boreal summer. *Climate Dyn.*, **29**, 113–129, doi:10.1007/s00382-007-0234-0.

——, S. K. Behera, and T. Yamagata, 2009: Anomalous winter climate conditions in the Pacific rim during recent El Niño Modoki and El Niño events. *Climate Dyn.*, **32**, 663–674, doi:10.1007/s00382-008-0394-6.

Wu, B., T. Li, and T. Zhou, 2010: Asymmetry of atmospheric circulation anomalies over the western north Pacific between El Niño and La Niña. *J. Climate*, **23**, 4807–4822, doi:10.1175/2010JCLI3222.1.

Yeh, S.-W., J.-S. Kug, B. Dewitte, M.-H. Kwon, B. P. Kirtman, and F.-F. Jin,

2009: El Niño in a changing climate. *Nature*, **461**, 511–514, doi:10.1038/nature08316.

Yu, J.-Y., and S. T. Kim, 2010: Identification of Central - Pacific and Eastern - Pacific types of ENSO in CMIP3 models. **37**, 1–7, doi:10.1029/2010GL044082.

——, and Y. Zou, 2013: The enhanced drying effect of Central-Pacific El Niño on US winter. *Environ. Res. Lett.*, **8**, 14019, doi:10.1088/1748-9326/8/1/014019.

——, H. Y. Kao, T. Lee, and S. T. Kim, 2011: Subsurface ocean temperature indices for Central-Pacific and Eastern-Pacific types of El Niño and La Niña events. *Theoretical and Applied Climatology*, **103**, 337–344, doi:10.1007/s00704-010-0307-6.

——, Y. Zou, S. T. Kim, and T. Lee, 2012: The changing impact of El Niño on US winter temperatures. *Geophys. Res. Lett.*, **39**, doi:10.1029/2012GL052483.

Yuan, W., M. A. Geller, and P. T. Love, 2014: ENSO influence on QBO modulations of the tropical tropopause. *Quart. J. Roy. Meteor. Soc.*, **140**, 1670–1676, doi:10.1002/qj.2247.

Zhang, T., J. Perlwitz, and M. P. Hoerling, 2014: What is responsible for the strong observed asymmetry in teleconnections between El Niño and La Niña? *Geophys. Res. Lett.*, **41**, 1019–1025, doi:10.1002/2013GL058964.

Zou, Y., J.-Y. Yu, T. Lee, M.-M. Lu, and S. T. Kim, 2014: CMIP5 model simulations of the impacts of the two types of El Niño on the US winter temperature. *Journal of Geophysical Research Atmospheres*, **119**, 3076–3092, doi:10.1002/2013JD021064.

Zubiaurre, I., and N. Calvo, 2012: The El Niño-Southern Oscillation (ENSO) Modoki signal in the stratosphere. *J. Geophys. Res.*, **117**, D04104, doi:10.1029/2011JD016690.

Acronyms

AO: Arctic Oscillation

ASOBS: as Observations members

ATSM: anomalías de temperatura superficial del mar

CAMS: Climate Anomaly Monitoring System

CMIP5: Coupled Model Intercomparison Project phase 5

COADS: Comprehensive Ocean-Atmosphere Data Set

CP El Niño: Central Pacific El Niño

CPC: Climate Prediction Center

CRU TS: Climatic Research Unit time series

CSEs: Calentamientos Súbitos Estratosféricos

DJF: December-January-February

E: East

ECHAM: European Centre Hamburg model

ECMWF: European Centre for Medium-Range Weather Forecasts

EMI: El Niño Modoki index

ENSO: El Niño-Southern Oscillation

EOF: empirical orthogonal function

EP El Niño: East Pacific El Niño

EP flux: Eliassen-Palm flux

EQBO: East phase of the QBO

ERA-40: 40 year ECMWF reanalysis

ERA-Interim: ECMWF Interim reanalysis

ERSST: Extended Reconstruction Sea Surface Temperature

ESM: Earth System Model

FM: February-March

GTS: Global Telecommunications System

HadISST: Hadley Centre Sea Ice and Sea Surface Temperature

HAMOCC: Hamburg ocean carbon cycle model

HIGHASYM: High asymmetry members

HN: hemisferio norte

ICOADS: International Comprehensive Ocean–Atmosphere Data Set

JFM: January-February-March

JRA-25: Japanese 25-year Reanalysis

JRA-55: Japanese 55-year Reanalysis

LOWASYM: Low asymmetry members

LR: Low Resolution

MDB: Met Office Marine Data Bank

MEI: Multivariate ENSO Index

MERRA: Modern Era Retrospective-Analysis for Research and Applications

MPI: Max Planck Institute

MPIOM: Max Planck Institute Ocean Model

N: North

NAE: North Atlantic European

NAM: Northern Annular Mode

NAO: North Atlantic Oscillation

NCAR: National Center for Atmospheric Research

NCDC: National Climatic Data Center

NCEP: National Centers for Environmental Prediction

NDJF: November-December-January-February

NH: North Hemisphere

NOAA: National Oceanic and Atmospheric Administration

ND: November-December

OCB: Oscilación Cuasi-Bienal

OLR: outgoing longwave radiation

PCA: Principal Component Analysis

PNA: Pacific-North American

QBO: quasi-bieannial oscillation

r: pearson correlation coeffient

RMS: root-mean square

S: South

SD: standard deviations

SLP: sea level pressure

SLPa: SLP anomalies

SPARC: Stratosphere-troposphere Processes And their Role in Climate

S-RIP: SPARC Reanalysis Intercomparison Project

SST: sea surface temperature

SSTA: sea surface temperature anomalies

SSWs: Stratospheric Sudden Warmings

TEM: transformed Eulerian mean

Ua: zonal-mean zonal wind anomalies

US: United States

UTC: Coordinated Universal Time

W: West

WACCM: Whole Atmosphere Community Climate Model

WMO: World Meteorological Organization

WQBO: West phase of the QBO

Z'a: eddy geopotential height anomalies